SCUOLA DI DOTTORATO
UNIVERSITÀ DEGLI STUDI DI MILANO-BICOCCA

Department of Biotechnology and Biosciences

PhD program in Converging Technologies for Biomolecular Systems (TeCSBi)
Cycle XXXV

Functions and regulation of the MRX and Ku protein complexes at DNA ends

Rinaldi Carlo
780425

Tutor and supervisor: Prof. Longhese Maria Pia

Coordinator: Prof. Branduardi Paola

ACADEMIC YEAR 2021/2022

INDEX

ABSTRACT

Genome instability is one of the hallmarks of cancer cells and can be caused by DNA repair defects. Among different types of DNA damage, DNA double-strand breaks (DSBs) are highly cytotoxic lesions that can form accidentally during DNA replication or upon exposure to genotoxic agents. DSBs must be repaired in order to avoid loss of genetic information or chromosome rearrangements. Eukaryotic cells activate a cellular response, named DNA damage response (DDR), that promotes repair of DSBs by two main mechanisms: non-homologous end joining (NHEJ), which directly religates the two broken ends, and homologous recombination (HR), which uses sister chromatids or homologous chromosomes as a template to repair the DNA break. The key process in determining which pathway is used to repair DSBs is the initial processing of the DSB ends. While NHEJ requires little or no DNA end processing, HR is initiated by nucleolytic degradation of the 5′ terminated strands at both DNA ends to generate 3′-ended single-stranded DNA that catalyses homologous pairing and strand invasion.

The cellular response to DNA double-strand breaks is initiated by the evolutionarily conserved Ku70-Ku80 (Ku) and MRX/MRN complexes, which are rapidly recruited to DNA ends. The Ku complex protects the DNA ends from nucleolytic degradation and acts as a hub for the recruitment of downstream NHEJ components. The MRX/MRN complex, which comprises Mre11, Rad50, and Xrs2/NBS1 subunits, maintains the DSB ends in close proximity and initiates DSB resection. Furthermore, it recruits to DSBs Tel1/ATM, which is one of the apical kinases involved in the DNA damage checkpoint, a surveillance mechanism that couples DSB repair with cell-cycle progression. Tel1, once loaded to DNA by the MRX complex, promotes and stabilizes MRX association at both DSBs and telomeres in a positive feedback loop.

Ku, MRX/MRN, and Tel1/ATM are also required to maintain the length of telomeres, specialized nucleoprotein complexes at the ends of eukaryotic

chromosomes. Telomeric DNA is distinguished from intrachromosomal DNA double-strand break ends by different protein complexes, which are recruited to telomeres and prevent DDR activation, degradation, fusions, and recombination events.

In *Saccharomyces cerevisiae*, Rap1 is one of protein that composes these protein complexes. Rap1 binds telomeres through two tandem Myb-like domains, and recruits Rif2 to them. Both Rap1 and Rif2 counteract Tel1 activation, nucleolytic degradation, and NHEJ at telomeres. Rif2 appears to exert all these functions through inhibition of MRX association with telomeric DNA by two different mechanisms. In fact, first Rif2 competes with Tel1 for MRX interaction, thus antagonizing Tel1-mediated stabilization of MRX association with DNA ends. Second, Rif2 decreases MRX DNA binding activity by promoting ATP hydrolysis by Rad50 and therefore by decreasing the time spent by MRX complex in its ATP-bound state. However, how Rap1 negatively controls MRX activity at DNA ends remained to be determined.

In the first part of my thesis, I contributed to show that Rif2 counteracts MRX association at both DSBs and telomeres in a manner dependent on Rap1. Rap1 in turn can inhibit MRX functions in a Rif2-dependent and independent manner. In fact, the generation and characterization of Rap1 mutant variants that increase or decrease Myb affinity to DNA has allowed to show that Rap1 binding to DNA through both Myb-like domains results in the formation of Rap1-DNA complexes that control MRX functions primarily through Rif2. By contrast, the transition to a binding mode where a single Myb-like domain is bound to DNA, leads to Rap1-DNA complexes that inhibit MRX function at telomeres mostly in a Rif2-independent manner. Thus, Rap1 functions at DNA ends are influenced by its DNA binding mode, highlighting the structural plasticity of this protein.

An important issue in NHEJ is the maintenance of the DSB ends in close proximity to allow their correct and efficient religation. This function is called

end-tethering and involves both the MRX/MRN complex and the Sae2/CtIP protein. Although some data in *Escherichia coli* suggested an involvement of the Ku complex in maintaining the DSB ends close to each other, whether Ku has a role in this control mechanism remained to be determined.

In the second part of my thesis, I investigated this issue by using a Ku70 mutant variant that increases Ku persistence at DSBs. The characterization of the *ku70-C85Y* allele, that was identified by searching for *ku70* mutations that were able to restore resistance of *sae2*Δ cells to phleomycin, has allowed to show that the Ku complex promotes DSB end-tethering and the C85Y mutation enhances this bridging function by increasing Ku retention very close to the DSB ends. The function of Ku in DSB end-tethering occurs independently of MRX complex, and it is regulated by the checkpoint kinase Tel1/ATM.

Tel1/ATM antagonizes Ku function in DSB end-tethering by limiting Ku persistence at the DSB ends. In fact, Tel1 kinase promotes both the nucleosome removal around DSBs and Ku sliding inwards. As the presence of Ku at the DSB ends prevents the access of resection nucleases, the Tel1-mediated regulation of Ku association with the DSB ends provides an important layer of control in the choice between NHEJ and HR, suggesting a new function of Tel1 in the DNA damage response.

All the findings reported in this thesis contributed to elucidate the molecular mechanisms that modulate DNA repair and maintain genome stability in response to DSBs, with a specific focus on the functions and regulation of MRX and Ku complexes.

RIASSUNTO

L'instabilità del genoma è una delle caratteristiche riscontrabili nelle cellule tumorali e può essere causata da difetti nella riparazione dei danni al DNA. Tra le diverse tipologie di danno al DNA, le rotture del doppio filamento del DNA (DNA *double-strand breaks*, DSBs) costituiscono lesioni altamente citotossiche che possono formarsi accidentalmente durante la replicazione del DNA o in seguito all'esposizione ad agenti genotossici. I DSBs devono essere correttamente ed efficacemente riparati da parte della cellula al fine di evitare la perdita di informazioni genetiche o il verificarsi di riarrangiamenti cromosomici aberranti.
Per far fronte a queste lesioni del DNA, le cellule eucariotiche attivano una complessa risposta cellulare, denominata risposta al danno del DNA (DDR), che innesca e promuove la riparazione dei DSBs.
I due principali meccanismi di riparazione che la cellula può mettere in atto sono l'unione terminale non omologa (*non-homologous end joining*, NHEJ), che rilega direttamente le due estremità rotte, e la ricombinazione omologa (*homologous recombination*, HR), che utilizza il cromatide fratello o il cromosoma omologo come templato per ripristinare le informazioni genetiche perse nel sito di rottura del DNA.
La scelta di quale tra questi due percorsi di riparazione debba essere utilizzato per riparare i DSBs è determinata dal processamento delle estremità del DSB. Infatti, mentre l'unione terminale non omologa (NHEJ) richiede un processamento minimo dell'estremità del DNA, la ricombinazione omologa (HR) necessita che le estremità rotte subiscano una degradazione nucleolitica, allo scopo di generare estremità a singolo filamento in 3' che catalizzano l'invasione dell'elica.
Sia nel NHEJ sia nella ricombinazione omologa, la risposta cellulare alle rotture del doppio filamento di DNA è avviata dai complessi proteici evolutivamente conservati Ku70-Ku80 (Ku) e MRX/MRN, i quali sono rapidamente reclutati alle estremità del DNA.

Il complesso Ku, formato dall'associazione delle due subunità Ku70 e Ku80, si lega alle estremità del DNA e le protegge dalla degradazione nucleolitica, permettendo inoltre il reclutamento delle proteine necessarie per le fasi successive della rilegatura mediata dal NHEJ. Il complesso MRX/MRN, composto dalle subunità Mre11, Rad50 e Xrs2/NBS1, consente di mantenere le estremità del DSB vicine tra loro e avvia il processo di degradazione nucleolitica del DSB. Inoltre, MRX/MRN recluta ai DSBs la proteina Tel1/ATM, una delle principali chinasi coinvolte nel *checkpoint* del danno al DNA, un meccanismo di sorveglianza che consente di accoppiare la riparazione dei DSBs con la progressione del ciclo cellulare. Tel1, una volta caricato sul DNA dal complesso MRX, promuove e stabilizza l'associazione di MRX alle estremità del DNA, in un meccanismo a feedback positivo.

Ku, MRX/MRN e Tel1/ATM sono tuttavia richiesti anche per mantenere correttamente la lunghezza dei telomeri, complessi nucleoproteici specializzati presenti alle estremità dei cromosomi eucariotici. Poiché le estremità telomeriche risultano essere strutturalmente simili alle estremità del DNA che si originano dopo la rottura della doppia elica, occorre che vi sia una distinzione tra esse. Tale distinzione è consentita da diversi complessi proteici, i quali sono reclutati ai telomeri allo scopo di prevenire l'attivazione della DDR ed evitare eventi di degradazione, fusione e ricombinazione.

Nel lievito *Saccharomyces cerevisiae*, la proteina Rap1 è uno dei principali componenti di questi complessi nucleoproteici. Rap1, infatti, si lega direttamente al DNA telomerico attraverso i suoi due domini Myb-like. Successivamente, Rap1 recluta la proteina Rif2. Ai telomeri, sia Rif2 che Rap1 contrastano l'attivazione di Tel1, la degradazione nucleolitica e l'unione terminale non omologa (NHEJ).

In merito a Rif2, questa proteina sembra svolgere tutte queste funzioni attraverso l'inibizione dell'associazione del complesso MRX al DNA telomerico. Tale

inibizione avviene mediante due diversi meccanismi: (i) Rif2 compete con Tel1 per l'interazione con MRX, contrastando la stabilizzazione dell'associazione di MRX alle estremità del DNA mediata da Tel1: (ii) Rif2 stimola l'idrolisi dell'ATP da parte della subunità Rad50, innescando un cambio conformazionale del complesso MRX che ne causa una ridotta associazione al DNA. Tuttavia, in merito a Rap1, restavano ancora da chiarire le modalità con cui questa proteina regola negativamente l'attività del complesso MRX alle estremità del DNA.

Nella prima parte della mia tesi, ho contribuito a dimostrare che la proteina Rif2 contrasta l'associazione del complesso MRX sia ai DSBs che ai telomeri in un modo dipendente da Rap1. Rap1, a sua volta, può inibire le funzioni del complesso MRX sia in modo dipendente che indipendente da Rif2. Infatti, la generazione e la caratterizzazione di varianti mutanti di Rap1 in grado di aumentare o diminuire l'affinità del dominio Myb-like per il DNA, ha permesso di dimostrare che il legame di Rap1 al DNA tramite entrambi i suoi domini Myb-like provoca la formazione di complessi Rap1-DNA capaci di controllare le funzioni di MRX alle estremità del DNA principalmente attraverso Rif2. Al contrario, il passaggio a una modalità di legame in cui un singolo dominio Myb-like di Rap1 è legato al DNA, porta alla formazione di complessi Rap1-DNA che inibiscono la funzione di MRX ai telomeri in modo indipendente da Rif2. Pertanto, le funzioni di Rap1 alle estremità del DNA sono fortemente influenzate dalla modalità con cui lega il DNA, evidenziando la plasticità strutturale di questa proteina.

Un aspetto importante inerente al NHEJ è la comprensione del meccanismo deputato al mantenimento in stretta vicinanza fra loro delle due estremità rotte, funzione necessaria per consentire la corretta ed efficiente riparazione di un DSB. Tale funzione è chiamata *end-tethering* e coinvolge sia il complesso MRX/MRN che la proteina Sae2/CtIP. Sebbene alcuni dati ottenuti in *Escherichia coli* suggeriscano anche un coinvolgimento del complesso Ku nel mantenere

vicine le estremità di un DSB, restava ancora da comprendere il suo effettivo ruolo in questo meccanismo.

Nella seconda parte della mia tesi, ho quindi studiato questo possibile coinvolgimento di Ku utilizzando una variante mutante di Ku70 che aumenta la persistenza del complesso Ku alle estremità di un DSB. Attraverso la ricerca di mutazioni nel gene *KU70* in grado di sopprimere la sensibilità di cellule *sae2*Δ all'agente genotossico fleomicina, è stato possibile identificare l'allele *ku70-C85Y*. La successiva caratterizzazione di questo allele ha permesso di dimostrare che il complesso Ku promuove l'*end-tethering* delle estremità dei DBSs e che la mutazione C85Y migliora tale funzione aumentando la persistenza di Ku alle due estremità rotte del DNA. Inoltre, la funzione svolta dal complesso Ku nel *tethering* delle estremità dei DBSs è risultata essere indipendente dal complesso MRX e regolata dalla chinasi di *checkpoint* Tel1/ATM. Infatti, Tel1/ATM antagonizza la funzione svolta dal complesso Ku nel *tethering* delle estremità dei DBSs limitandone la persistenza alle estremità rotte del DNA, promuovendo sia la rimozione del nucleosoma attorno ai DSBs sia il conseguente scorrimento di Ku sul DNA. Poiché la presenza di Ku alle estremità del DSB impedisce l'accesso delle nucleasi necessarie per il processo di resezione, la regolazione dell'associazione di Ku alle estremità di un DSB mediata da Tel1 fornisce un importante livello di controllo nella scelta di quale percorso di riparazione debba essere utilizzato tra NHEJ e HR, suggerendo quindi una nuova funzione di Tel1 nella risposta al danno al DNA.

I risultati riportati in questa tesi hanno contribuito a chiarire i meccanismi molecolari che modulano la riparazione del DNA e che consentono il mantenimento della stabilità genomica in risposta ai DSBs, con un focus specifico sulle funzioni e sulla regolazione dei complessi MRX e Ku da parte di altre proteine coinvolte nella risposta al danno del DNA.

PUBLICATIONS

1. **Rinaldi C.**, Pizzul P., Casari E., Tisi R., Longhese M.P. *"The Ku complex promotes DNA end-bridging and this function is antagonized by Tel1/ATM kinase"*. Nucleic Acids Research - Under review

2. Casari E., Gnugnoli M., **Rinaldi C.**, Pizzul P., Colombo C.V., Bonetti D., Longhese M.P. *"To fix or not to fix: maintenance of chromosome ends versus repair of DNA double-strand breaks"*. Cells, 2022 11, 3224

3. Pizzul P., Casari E., Gnugnoli M., **Rinaldi C.**, Corallo F., Longhese M.P. *"The DNA damage checkpoint: a tale from budding yeast"*. Frontiers in Genetics, 2022 13, 995163

4. **Rinaldi C.**, Pizzul P., Longhese M.P., Bonetti D. *"Sensing R-loop-associated DNA damage to safeguard genome stability"* Frontiers in Cell and Developmental Biology, 2021 8, 618157

5. Bonetti D., **Rinaldi C.**, Vertemara J., Notaro M., Pizzul P., Tisi R., Zampella G., Longhese M.P. *"DNA binding modes influence Rap1 activity in the regulation of telomere length and MRX functions at DNA ends"*. Nucleic Acids Research, 2020 48, 2424-2441

INTRODUCTION

The DNA damage response: maintaining genomic stability to prevent cancer

Cancer is one of the major causes of human death and its incidence is constantly increasing. It has been estimated that one in five people will develop a form of cancer in their lifetime. In 2020, there were about 19.3 million new cases of cancer worldwide and about 10 million deaths from the disease. In 2040, there will be 28.4 million new cancer cases worldwide, an increase of 47% compared to 2020 [Sung *et al*., 2021]. For this reason, biological, clinical, and medical research has focused on tumors with the aim of better understanding the mechanisms underlying the onset of cancer in order to obtain specific, targeted, and effective treatments.

It had long been known that DNA lesions cause mutations that can lead to carcinogenesis [Negrini *et al.*, 2010; Jeggo *et al.*, 2016]. Several hereditary cancer predispositions result from mutations in genes involved in DNA damage repair. Furthermore, malignant cells frequently acquire loss-of-function mutations in DNA repair genes which favour disease progression and/or therapy resistance. These data have led to the definition of genomic instability as one of the most prominent hallmarks of cancer cells [Hanahan, 2022] (Figure 1). Although DNA repair defects are clearly causative of cancer, the increased DNA damage sensitivity of cancer cells has been exploited therapeutically through the use of radio- and chemo-therapies that force their DNA damage-induced death [Gavande *et al.*, 2016; Bhattacharya and Asaithamby, 2017].

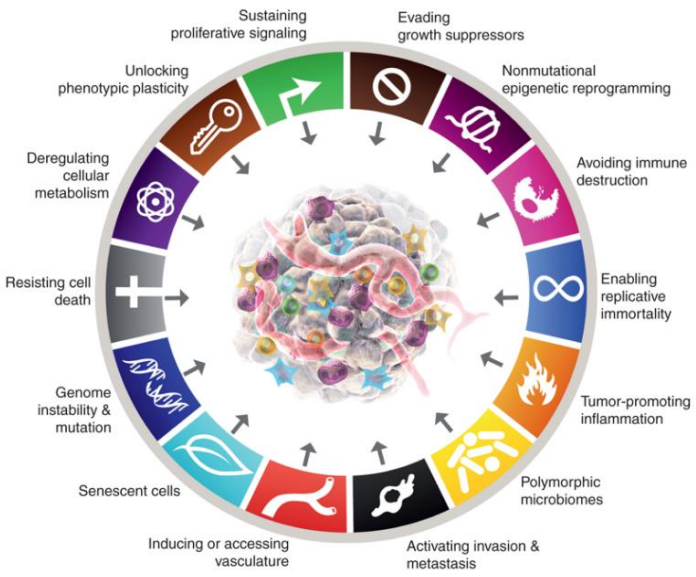

Figure 1. Schematic representation of the hallmarks of cancer [Hanahan, 2022].

DNA damage can occur spontaneously during DNA metabolism or can be induced by environmental agents [Roos *et al*., 2016]. Spontaneous DNA alterations can be due to deoxyribonucleoside triphosphate (dNTP) or ribonucleoside triphosphate (rNTP) misincorporation during DNA replication, modification of DNA bases by alkylation, loss of DNA bases by depurination, interconversion between DNA bases by deamination, head-on or co-directional transcription/replication collisions, and production of reactive oxygen species (ROS) that can oxidize DNA bases leading to DNA breaks.

Exogenous DNA damage can be produced either by chemicals, such as base analogues and alkylating/hydroxylating agents, or by ultraviolet (UV) and ionizing (IR) radiations [Friedberg *et al.*, 2005]. These DNA damaging agents can induce different types of DNA lesions such as base modifications, mismatches, stalled replication forks, DNA crosslinks, and single-strand breaks (SSBs) or double-

strand breaks (DSBs) (Figure 2). DNA lesions can compromise cell survival by blocking DNA transcription and replication, and lesions that are either not repaired or unproperly repaired can lead to genomic instability by causing mutations or genome aberrations.

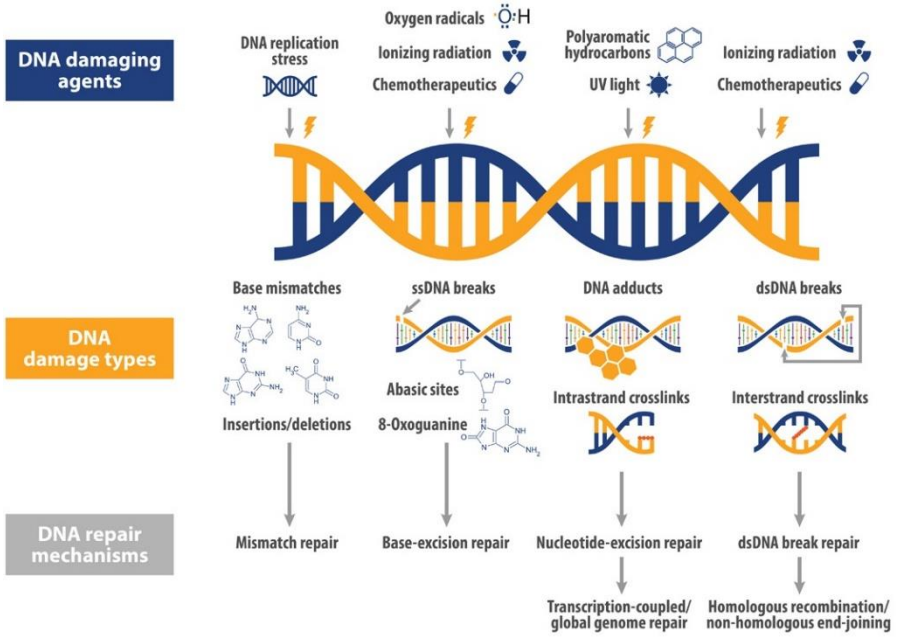

Figure 2. Different endogenous and exogenous DNA lesions and possible DNA repair mechanisms [Adapted from Helena *et al.*, 2018].
Several DNA damaging agents can cause a wide and different types of DNA lesions. According to the type of lesions, specific DNA repair mechanisms are involved in their fixing.

It is important to point out that viral infections also cause the onset of tumors. It is now estimated that approximately 10% of worldwide cancers are attributable to viral infections. Oncogenic viruses include various classes of DNA and RNA viruses that induce cancer by a variety of mechanisms. The viruses associated

with the greatest number of cancer cases are the human papillomaviruses (HPVs) and the hepatitis viruses HBV and HCV. Other oncoviruses include Epstein-Barr virus (EBV), Kaposi's sarcoma-associated herpes virus (KSHV), human T-cell leukemia virus (HTLV-I), and Merkel cell polyomavirus (MCPyV) [Schiller and Lowy, 2014].

To counteract threats posed by DNA damage, cells have evolved conserved mechanisms, collectively termed DNA damage response (DDR), which is a spatiotemporally regulated process, where several proteins are assembled at the sites of DNA damage in a sequential and co-ordinated manner in order to detect DNA lesions, signal their presence, and promote their repair [Jackson and Bartek, 2009]. DNA damage signalling by the DDR is carried out by the DNA damage checkpoint, which is a network of signalling pathways that are able to recognize the presence of DNA lesions or aberrant DNA structures and transmit a signal throughout transducers to a set of effectors that participate in a broad range of cellular processes [Elledge, 1996]. These processes include the slowing down of cell-cycle progression, promotion of DNA repair, inhibition of origin firing, protection and stability of replication forks, regulation of deoxyribonucleotide (dNTP) production, induction of transcription, initiation of apoptosis or autophagy [Lanz *et al.*, 2019].

Main DNA repair mechanisms include: mismatch repair (MMR), which is devoted to excise mispaired bases; base excision repair (BER), which excises uracil and other inappropriate bases from the DNA; and nucleotide excision repair (NER), which excises a variety of helix-distorting DNA lesions as an oligonucleotide fragment. Moreover, in case cells suffer breakage of both DNA chains, this type of DNA lesion is repaired by mechanisms that, based on their homology requirements, can be mainly divided into non-homologous end joining (NHEJ) and homologous recombination (HR) [Mehta and Haber, 2014] (Figure 2).

The DDR is crucial for human health: hereditary defects in the DDR cause a variety of diseases that are associated with cancer predisposition, infertility, developmental defects, neurological degeneration, immune deficiency, and premature ageing [Hoeijmakers, 2009; Taylor *et al.*, 2019;]. Since there is a close connection between genomic stability and the correct functioning of the DDR, it is important to fully understand the mechanisms underlying this cellular response in order to discover new therapeutic targets useful against cancer and other genetic diseases. As most of the proteins involved in the DDR are highly conserved, the yeast *Saccharomyces cerevisiae* represents an excellent model system for the study of the molecular mechanisms underlying genome integrity pathways. In fact, *S. cerevisiae* combines precise and easy genetic manipulability with a high level of evolutive conservation of the DDR pathways [O'Neil *et al.*, 2017].

DNA Double-Strand Breaks

DNA double-strand breaks (DSBs) are among the most deleterious types of DNA damage as failure to repair them can result in loss of genetic information or cell death, whereas inaccurate repair can lead to chromosome rearrangements [Casari *et al.*, 2019]. DSBs are generated when the phosphor-sugar backbones on both DNA strands are broken in the same position or in close proximity allowing the physical dissociation of the DNA double helix into two molecules. They can arise accidentally during DNA replication and transcription or upon exposure to genotoxic agents, such as specific chemotherapeutic drugs or ionizing radiation (IR) [Sturzenegger *et al.*, 2014]. However, the major source of DSBs in proliferating cells is represented by the DNA replication process itself, that can be impaired by a transient slowing or stalling of replication forks due to damaged DNA, unusual DNA structures, repetitive sequences or nucleotide depletion leading to generate DNA intermediates that are fragile and susceptible to breakage [Berti and Vindigni, 2016].

Transcription has also been implicated as one of the leading causes of DSBs through the generation of stable RNA-DNA hybrid intermediates that can cause the arrest of the replication forks. When a RNA-DNA hybrid results in the displacement of the second DNA strand in the double helix, three-stranded structures, called R-loops, are generated and might promote DSB formation in case their homeostasis is altered [Rinaldi *et al.*, 2021]. DSBs are also generated during cellular metabolism, when a high reactive class of molecules called reactive oxygen species (ROS) react with DNA causing its oxidation [Srinivas *et al.*, 2019].

Nevertheless, it should be noted that DSBs can be also normal intermediates during physiological processes, such V(D)J recombination that produces T-cell receptors and immunoglobulin antigen receptors during lymphoid cell development, and meiotic recombination that is important not only to ensure

exchange of genetic information between homologous chromosomes and therefore genetic variability, but also to allow correct chromosome segregation during the first meiotic division [Bassing *et al.*, 2004; Longhese *et al.*, 2009; Manfrini *et al.*, 2010].

As cancer cells are more sensitive to DSB inducing agents than normal cells, chemical agents that can induce DSBs are often used as chemotherapeutic drugs. A few examples include: cross-linking agents, such as cisplatin and psoralens, that covalently crosslink bases of the same strand (intra-strand) or of complementary strands (inter-strand); radiomimetic agents, such as phleomycin (phleo) and bleomycin (bleo), that introduce DSBs by mimicking the action of ionizing radiation; base alkylating agents, such as methyl methanesulfonate (MMS), that cause the stalling of replication forks; DNA topoisomerase inhibitors, such as camptothecin (CPT), irinotecan, and topotecan, that block Topoisomerase 1 on DNA and create a physical barrier to replication fork progression; ribonucleotide reductase inhibitors, such as hydroxyurea (HU), that deplete the deoxyribonucleotides pool [Aguilera and Garcia-Muse, 2013].

In addition to cancer predisposition, defects in the cellular response to DSBs also lead to the onset and development of different inheritable human diseases including cancer, neurological defects, immunodeficiencies, and genetic syndromes such as ataxia telangiectasia, ataxia telangiectasia-like disorder, Nijmegen breakage syndrome, severe combined immunodeficiency (SCID), LIG4-syndrome, ATR-Seckel syndrome, and Fanconi anemia [O'Driscoll *et al.*, 2006; McKinnon, 2012].

Resection and homologous recombination

A DNA DSB can be repaired by homologous recombination (HR), which is a highly conserved error-free repair pathway that uses DNA information stored in a homologous double-stranded DNA as template to restore the genetic information lost at the break site [Mehta and Haber, 2014; Kowalczykowski, 2015]. HR is initiated by nucleolytic degradation of the 5′ terminated strands at both DNA ends by a concerted action of nucleases in a process termed DNA end resection [Bonetti *et al.*, 2018]. The preferential degradation of the 5′-terminated strands results in formation of 3′-ended single-stranded DNA (ssDNA) ends that are first coated by a heterotrimeric complex called Replication Protein A (RPA). RPA is subsequently replaced by the strand exchange protein Rad51 to form a nucleoprotein filament that is used to search for a homologous dsDNA sequence [Symington and Gautier, 2011; Kowalczykowski, 2015].

The mechanism of resection and most of the involved proteins are highly conserved from yeast to humans, and similar pathways have also been found in prokaryotes [Cejka, 2015]. Genetic studies in *S. cerevisiae* identified at least three distinct nucleases involved in end-resection: the MRX (Mre11-Rad50-Xrs2 in yeast; MRE11-RAD50-NBS1 in mammals) complex, Dna2, and Exo1 (DNA2 and EXO1 in mammals, respectively). In particular, the Mre11 subunit of MRX complex has five conserved phosphoesterase motifs that are required for 3′-5′ double-strand DNA (dsDNA) exonuclease and ssDNA endonuclease activities of the protein [Bressan *et al.*, 1998; Paull and Gellert, 1998; Trujillo *et al.*, 1998; Usui *et al.*, 1998]. Rad50 is characterized by Walker A and B ATP binding cassettes located at the amino- and carboxy-terminal regions of the protein. The ATP-bound state of Rad50 inhibits the Mre11 nuclease activity by masking the active site of Mre11 from contacting DNA [Lim *et al.*, 2011]. ATP hydrolysis induces conformational changes of both Rad50 and Mre11 subunits that allow the Mre11 nuclease domain to access the DSB ends and to be engaged in DSB

resection [Lammens *et al.*, 2011; Lim *et al.*, 2011; Williams *et al.*, 2011; Möckel *et al.*, 2012; Deshpande *et al.*, 2014].

The current model for DSB resection posits that the MRX/MRN complex is recruited to the DSB ends to catalyze an endonucleolytic cleavage of the 5'-terminated DNA strands [Lisby *et al*., 2004]. This cleavage requires the Sae2/CtIP protein that promotes the endonuclease activity of the Mre11 nuclease [Clerici *et al*., 2005; Sartori *et al.*, 2007; Cannavo and Cejka, 2014]. Then, the MRX complex removes nucleotides from the 5'-termini of the break, generating short 3'-ended ssDNA tails. These tails are subjected to extensive processing by either Exo1 or the combined activities of the Sgs1 helicase and the Dna2 nuclease, which are capable of resecting thousands of nucleotides in length in the 5′-3′ direction [Mimitou and Symington, 2008; Zhu *et al.*, 2008] (Figure 3).

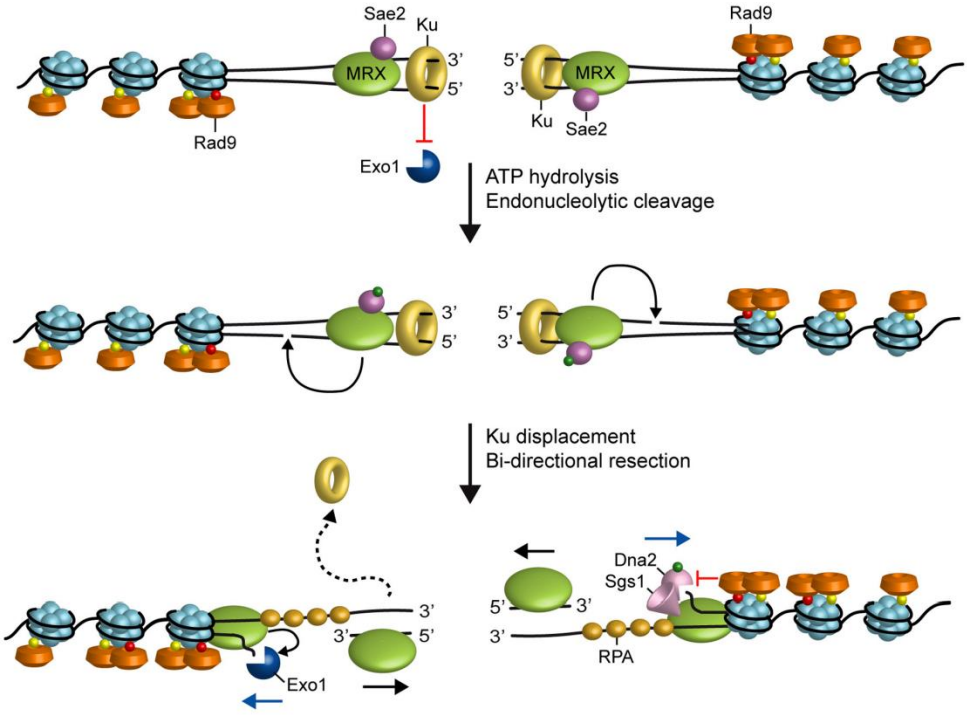

Figure 3. Model for resection of DNA double-strand breaks [Adapted from Bonetti *et al.*, 2018].
The first proteins recruited to the DSB are MRX, Sae2, and Ku. Ku inhibits Exo1 access to DNA ends, while Rad50, in its ATP-bound state, blocks the Mre11 nuclease activity. After ATP hydrolysis by Rad50, Mre11 catalyses the endonucleolytic cleavage of the 5'-strands of the DSB. Mre11-dependent processing is promoted by Sae2. The first incision by MRX-Sae2 creates an entry site for Exo1 and Sgs1-Dna2 nucleases, that process DNA in the 5'-3' direction from the nick (blue arrows), while MRX degrades in the 3'-5' direction toward the DSB ends (black arrows). Rad9 inhibits their resection activity.

DSB resection is negatively controlled to prevent excessive generation of ssDNA. In particular, the Ku complex (hereafter referred to Ku), composed of the two Ku70 and Ku80 subunits, which form a heterodimer that adopts a quasi-symmetric ring structure that encircles the dsDNA with a particular high affinity, competes with MRX complex for DSB binding [Mimori and Hardin, 1986; Griffith *et al.*, 1992; Blier *et al.*, 1993; Yaneva *et al.*, 1997; Walker *et al.*, 2001].

The association of Ku to the DSB ends restricts formation of ssDNA by impairing the association and/or the activity of the Exo1 nuclease.

Long-range resection is inhibited by the checkpoint protein Rad9, which acts as a barrier for the long-range resection nucleases Exo1 and Sgs1/Dna2 [Lee *et al.*, 1998; Lazzaro *et al.*, 2008].

Extension of DSB resection is influenced also by histone H2A modifications. In fact, one way to recruit Rad9 at the sites of damage depends on Rad9 interaction with histone H2A phosphorylated on Ser129 (γH2A) [Shroff *et al.*, 2004; Javaheri *et al.*, 2006; Toh *et al.*, 2006; Hammet *et al.*, 2007].

Different mechanisms exist to conclude HR. In the canonical HR pathway, the 3'-ended ssDNA tail at one of the DSB ends invades an intact duplex homologous, forming a D-loop structure that primes DNA synthesis. The displaced ssDNA can then anneal with the complementary sequence on the other side of the DSB to generate a double Holliday junction, whose random cleavage yield to noncrossover and crossover products [San Filippo *et al.*, 2008; Krejci *et al.*, 2012]. Alternatively, if the newly synthesized strand is displaced by the D-loop, its annealing with the 3' ssDNA end at the other end of the DSB leads to the generation of noncrossover products. This mechanism is called synthesis-dependent strand-annealing (SDSA) and is used in mitotically growing cells.

DSBs can be repaired also by other recombination pathways that do not involve strand invasion. One of them is the Single-Strand Annealing (SSA), which occurs when the DSB is flanked by two direct repeats that, once resected, can anneal to each other. This repair mechanism leads to the deletion of the DNA between the direct repeats and one of the repeats [Krejci *et al.*, 2012].

The DNA damage checkpoint

Generation of ssDNA at the DSB ends triggers activation of the DNA damage checkpoint, which is an elaborate signaling network that regulates a variety of cellular processes such as DNA replication, DNA repair, and cell-cycle transitions [Ciccia and Elledge, 2010]. In *S. cerevisiae*, three different DNA damage checkpoints have been described: G1/S, intra-S phase, and G2/M checkpoint. The G1/S checkpoint slows down the G1/S transition by delaying bud emergence, spindle pole body duplication, and S-phase entry in order to provide time for the cell to repair DNA lesions before initiation of DNA replication. The intra-S phase checkpoint controls origin firing and stabilises the replisome machinery on damaged DNA to ensure an efficient recovery of DNA replication after the repair of DNA lesions. The G2/M checkpoint slows down the transition from metaphase to anaphase, thus avoiding segregation of damaged sister chromatids [Ciccia and Elledge, 2010].

The mammalian proteins ATM (Ataxia-Telangiectasia-Mutated) and ATR (ATM- and Rad3-related), as well as their *S. cerevisiae* orthologs Tel1 and Mec1, respectively, are the most upstream checkpoint kinases that directly recognize aberrant DNA structures and activate the checkpoint cascade. They are both activated by DNA damage. However, while Tel1/ATM responds primarily to DSBs, Mec1/ATR is activated by a much wider range of genotoxic lesions whose processing generates ssDNA intermediates [Ciccia and Elledge, 2010]. The apical kinases Tel1/ATM and Mec1/ATR are members of the PIKK family that comprises large proteins of 270-450 kDa, characterized by N-terminal HEAT repeat domains followed by kinase domains in C-terminus [Bosotti *et al.*, 2000; Lempiäinen and Halazonetis, 2009]. In humans, biallelic mutations in ATM lead to the syndrome ataxia telangiectasia (AT), whose clinical phenotypes include neurodegeneration, immunodeficiency, radiosensitivity, premature ageing, and predisposition to cancer [Savitsky *et al.*, 1995; Lee and Paull, 2021].

Furthermore, mutations that reduce ATR protein levels lead to the Seckel syndrome, a hereditary form of microcephalic dwarfism [O'Driscoll *et al.*, 2003]. In both yeast and mammals, Tel1/ATM recruitment and activation require the MRX/MRN complex through a poorly understood mechanism. In fact, Tel1/ATM interacts with the Xrs2/NBS1 subunit of MRX/MRN complex, and this interaction mediates Tel1/ATM association to DSBs [Nakada *et al.*, 2003; You *et al.*, 2005]. *In vitro*, Tel1/ATM activation requires ATP binding by the MRX/MRN complex but not ATP hydrolysis, suggesting that MRX/MRN needs to be bound to ATP to stimulate Tel1/ATM activation [Lee *et al.*, 2013; Hailemariam *et al.*, 2019]. The presence of Tel1/ATM bound to DNA ends in turn has a structural role in stabilizing MRX association with DNA ends. This stabilization is important to allow a proper MRX-DNA binding that is necessary to sustain DSB repair [Cassani *et al.*, 2016]. In human, full activation of ATM is also determined by its autophosphorylation of different serine residues; in particular autophosphorylation of Ser1981 leads to the dissociation of the two ATM dimers into active monomers [Bakkenist *et al.*, 2003].

Instead, Mec1/ATR recognizes and is activated by ssDNA tracs that are coated by the Replication Protein A (RPA) complex [Zou and Elledge, 2003]. Mec1 activation during S phase requires higher levels of RPA-coated ssDNA than those necessary to activate the checkpoint in G1 or in G2, suggesting the existence of a threshold for checkpoint activation during DNA replication. This threshold ensures that the ssDNA, that is normally generated at functional replication forks, is not enough to induce a checkpoint response [Shimada *et al.*, 2002; Tercero *et al.*, 2003].

ssDNA recognition by Mec1/ATR is mediated by Ddc2 (human ATRIP), which forms a constitutive complex with Mec1/ATR and promotes its activation [Rouse and Jackson, 2002]. Loss of Ddc2/ATRIP causes the same phenotypes as loss of Mec1/ATR, indicating that Ddc2/ATRIP is required for full Mec1/ATR activity

[Paciotti *et al.*, 1998]. However, localization of Mec1-Ddc2 to the sites of DNA damage is not sufficient to convert it into a catalytically active complex. Specific sensors transduce the DNA damage response signal to Mec1 and stimulate its kinase activity. In budding yeast, Mec1 kinase activation depends on the binding to Mec1 of at least three different activator proteins: the ATP-dependent helicase/nuclease Dna2, the checkpoint protein Ddc1 (RAD9 in humans), and the multi-BRCT domain protein Dpb11 (TOPBP1 in humans). Dpb11 is recruited to DNA lesions by the 9-1-1 complex, which is an heterotrimer with a ring-shaped structure composed of Ddc1, Mec3, and Rad17 proteins (RAD9-RAD1-HUS1 in humans). The 9-1-1 complex is recruited to DNA in a Mec1-Ddc2-independent manner by the Replication factor C (RFC)-like clamp loader Rad24-Rfc2-5 (RAD17-RFC2-5 in humans) [Kondo *et al.*, 2001; Melo *et al.*, 2001; Majka *et al.*, 2006; Navadgi-Patil and Burgers, 2009].

The current model for checkpoint activation posits that MRX, which is rapidly recruited to DSBs, promotes Tel1 association to DNA ends and its activation. Tel1, in turn, once bound to DSBs supports the activity of the MRX complex by structurally stabilizing it on DNA. DSB processing by Exo1 and Dna2-Sgs1 nucleases generate ssDNA that is coated by RPA. RPA-coated ssDNA allows the recruitment of Mec1-Ddc2 and a switch from Tel1- to Mec1-mediated signalling mechanism. Once activated, Tel1/ATM and Mec1/ATR apical kinases phosphorylate and activate the downstream checkpoint kinases Rad53 (human CHK2) and Chk1 (human CHK1), which control two parallel branches of the checkpoint phosphorylate. While Rad53 is the principal effector kinase that mediates checkpoint activation in response to DNA damage in all the cell-cycle phases, Chk1 contributes to activating only the G2/M checkpoint [Sanchez *et al.*, 1999]. Rad53 can also inhibit Exo1 activity and restrict the access to the DSB of Sgs1-Dna2 [Morin *et al.*, 2008] (Figure 4).

Activation of Rad53 and Chk1 downstream checkpoint kinases requires the

mediator proteins Rad9 (human 53BP1) and Mrc1 (human Claspin). In particular, Rad9 allows Rad53 phosphorylation and checkpoint activation in response to DNA damage in the G1 and G2 phases, whereas Mrc1, which is a component of the replisome, promotes Rad53 activation during S phase [Bacal *et al.*, 2018]. Once phosphorylated by Mec1 or Tel1, Rad9 acts first as adaptor to induce Mec1-Rad53 interaction and Mec1-mediated Rad53 phosphorylation at the sites of DNA lesions. Then, Rad9 acts as a scaffold to bring Rad53 molecules in close proximity to allow Rad53 in-trans activation [Gilbert *et al.*, 2001; Pellicioli *et al.*, 1999; Toh and Lowndes, 2003]. Fully activated Rad53 molecules are then released from phosphorylated Rad9 in an ATP-dependent manner [Gilbert *et al.*, 2001].

In the absence of DNA damage, Rad9 is already present on DNA *via* an interaction between its Tudor domain and histone H3 methylated on lysine 79, a modification that is catalyzed by the methyltransferase Dot1 (van Leeuwen *et al.*, 2002; Giannattasio *et al.*, 2005; Wysocki *et al.*, 2005; Toh *et al.*, 2006; Grenon *et al.*, 2007). Rad9 association with sites of damage is induced by an interaction between its BRCT domain and histone H2A (H2AX in humans) that has been phosphorylated at serine 129 (γH2A/γH2AX) by Mec1 and Tel1 [Downs *et al.*, 2000; Shroff *et al.*, 2004; Toh *et al.*, 2006; Hammet *et al.*, 2007]. Finally, Rad9 recruitment to DNA lesions depends also on Dpb11, which acts as a scaffold that brings Rad9, Mec1-Ddc2, and 9-1-1 complex in close proximity to facilitate Rad9 phosphorylation by Mec1 [Granata *et al.*, 2010; Pfander and Diffley, 2011]. Dpb11-Rad9 interaction requires Rad9 phosphorylation on the S462 and T474 residues by the Cdk1-Clb complexes [Granata *et al.*, 2010; Pfander and Diffley, 2011].

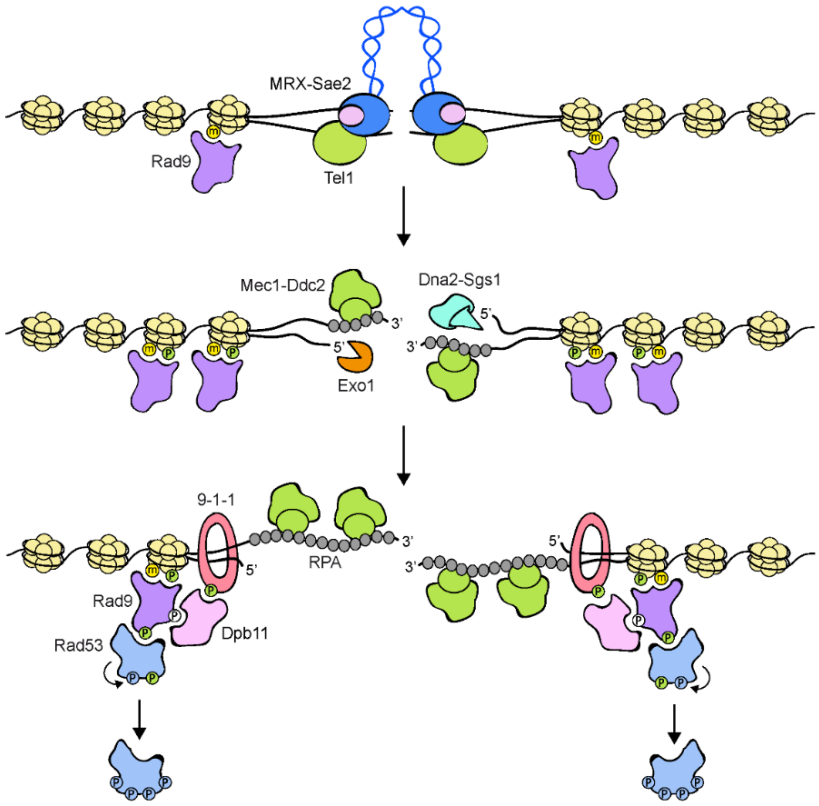

Figure 4. Checkpoint activation in response to DSBs [Adapted from Pizzul *et al.*, 2022].

The MRX-Sae2 complex is rapidly recruited to DNA ends. Rad9 is already bound to chromatin *via* interaction with methylated histone H3 (yellow dots). MRX bound to DNA ends recruits and activates Tel1, which in turn phosphorylates histone H2A on S129 (green dots), an event that leads to a further enrichment of Rad9 at DSBs. DSB end processing by Exo1 and Dna2-Sgs1 nucleases generates ssDNA that is coated by RPA. RPA-coated ssDNA allows the recruitment of Mec1-Ddc2 and a switch from Tel1 to Mec1 signaling. The 9-1-1 clamp loader recruits the 9-1-1 complex at the 5′ recessed end of the ssDNA-dsDNA junction. Mec1 in turn phosphorylates the Ddc1 subunit of the 9-1-1 complex (green dots), thus creating a docking site for Dpb11 binding. Rad9, once phosphorylated by Cdk1 (white dots), can also bind to Dpb11 that acts as a scaffold to promote Rad9-Mec1 interaction and therefore Rad9 phosphorylation by Mec1. Phosphorylated Rad9 first acts as an adaptor to bring Rad53 into close proximity to Mec1 to allow Mec1-dependent Rad53 phosphorylation. Then, Rad9 promotes Rad53 in trans-autophosphorylation (light blue dots) by increasing the local concentration of Rad53 molecules. Fully activated Rad53 molecules are then released from the Rad9 complex.

Non-homologous end joining

Double-strand breaks can be repaired also by a DNA repair pathway that re-ligates directly the two broken ends with little or no DNA-end processing in a process called canonical non-homologous end joining (c-NHEJ) [Chang *et al.*, 2017]. This repair pathway is conserved from prokaryotes to humans and is the main pathway to repair DSBs in vertebrates, although it can introduce mutations at the repair junction [Lieber, 2010]. NHEJ recognizes and ligates the DNA ends in a flexible manner by using different proteins depending on whether the DNA ends are blunt or contain DNA hairpins, 5' or 3' overhangs at their ends. This flexibility allows this pathway to function on a wide range of DNA-end configurations.

In general, the NHEJ repair mechanism comprises three main steps: binding of specific proteins to DSBs, processing of the broken DNA strands, and re-ligation. In both yeast to mammals, the DSB is first recognized by the Ku70-Ku80 heterodimer, which protects the DSB ends from degradation and it acts as a hub to directly or indirectly recruit downstream NHEJ components, including the DNA Ligase IV (Dnl4/Lig4 in *S. cerevisiae* and DNL4 in mammals) [Dudášová *et al.*, 2004; Hefferin *et al.*, 2005; Clerici *et al.*, 2008; Zierhut and Diffley 2008; Chang *et al.*, 2017; Zahid *et al.*, 2021].

The DNA Ligase IV is an ATP-dependent ligase with an extended C-terminus. In yeast, this enzyme interacts with its cofactor Lif1 (XRCC4 in mammals) that stimulates the ligase activity [Grawunder *et al.*, 1997]. Lig4-Lif1 recruitment to DSBs also requires Ku70, whereas Lif1 association to DSBs requires the presence of the Nej1 protein (XLF in mammals) [Hefferin *et al.*, 2005; Daley *et al.*, 2005]. In mammals, XLF has structural similarity to XRCC4 and XLF N-terminal head domain interacts with the N-terminal head domain of XRCC4 [Ahnesorg *et al.*, 2006]. The XRCC4-XLF complex forms a sleeve-like structure

around a DNA duplex that has been proposed to stabilize the positioning of the ends before covalent ligation [Brouwer *et al.*, 2016].

In mammals, NHEJ relies also on the DNA-dependent protein kinase (DNA-PKcs), which is a Ser/Thr kinase belonging to the phosphoinositide 3-kinase related protein kinase (PI3KK) family that also includes mTOR, ATM, and ATR. DNA-PKcs has an N-terminal domain with a helical domain and distinct phosphorylation clusters, a FAT domain, and a catalytic domain [Sharif *et al.*, 2017]. DNA-PKcs forms a complex with Ku and the DNA, called DNA-PK, which can phosphorylate both itself and other repair factors [Meek *et al.*, 2008]. Furthermore, this complex keeps the broken ends together and recruits to DSB downstream NHEJ components through phosphorylation events [Williams *et al.*, 2014]. Formation of these structural assemblies occurs in a two-step mechanism: initially the DNA ends are held together in a long-range synaptic complex composed by Ku, DNA-PKcs, DNA Ligase IV, XRCC4, and XLF. Then, upon dissociation of DNA-PKcs, a short-range synaptic complex is formed where the DNA ends bound to Ku are aligned for processing and final ligation [Graham *et al.*, 2016; Chaplin *et al.*, 2021; Chen *et al.*, 2021].

In addition, the Ku complex also directly recruits a specific group of DNA polymerases in order to fill possible loss of DNA at the repair junction. In mammals, the DNA polymerase μ (POLμ) and the DNA polymerase λ (POLλ) can fill gaps created during NHEJ repair. These DNA polymerases, which can incorporate either dNTPs or rNTPs in a template-dependent or a template-independent manner [Bertocci *et al.*, 2006], are members of the Pol X family of nucleotidyl transferases and interact with Ku through their N-terminal domains [Chang *et al*., 2017]. In yeast, Pol4 plays a similar role and interacts directly with the DNA ligase IV. This interaction stimulates the DNA synthesis activity of Pol4 in order to couple gap-filling and ligation [Tseng and Tomkinson 2002; Dudášová *et al*., 2004].

In mammals, processing of the DNA ends to make them ligatable by NHEJ involves Artemis, which possesses exo- and endo-nuclease activities and is activated in complex with DNA-PKcs [Goodarzi *et al.*, 2006; Gu *et al.*, 2010]. The Artemis-DNA-PKcs complex uses its endonucleolytic activity to remove 5' and 3' DNA overhangs in order to create DNA ends that can be religated by the XRCC4-DNA Ligase IV complex [Dudášová *et al.*, 2004; Poinsignon *et al.*, 2004] (Figure 5). Other proteins, like WRN helicase, FEN1 endonuclease, and EXO1 exonuclease have been involved in the processing of DSB ends during NHEJ [Pannunzio *et al.*, 2018]. In yeast, the ortholog of FEN1 is Rad27, a structure-specific nuclease that possesses flap endonuclease and 5′ to 3′ exonuclease activities, and it represents the most studied NHEJ endonuclease [Harrington and Lieber, 1994].

NHEJ dysfunctions can lead to different human genetic diseases even if spontaneous mutations in NHEJ proteins are exceedingly rare in humans. Artemis mutations can lead to deficiency in antibody production and a severe combined immunodeficiency (SCID) caused by V(D)J recombination defects [de Villartay, 2015; Volk *et al.*, 2015]. Rare mutations in Lig4 gene cause the Lig4-syndrome, characterized by immune deficiency, microcephaly, and delay in development [Davis and Chen, 2013]. Mutations in other components of the ligase IV complex, such as XRCC4 and XLF, can lead to similar pathologies [de Villartay, 2015; IJspeert *et al.*, 2016]. Finally, a reduced NHEJ efficiency is one of a possible cause of genomic instability and subsequent tumoral transformation [Hefferin and Tomkinson, 2005; Lieber, 2010].

When c-NHEJ is compromised, cells can repair DSBs by using an imprecise end-joining pathway that is commonly referred to as microhomology-mediated end-joining (MMEJ) [Emerson *et al.*, 2016]. MMEJ is used when the DSB are held together by very short homologous complementary sequences that are often less than 10 bases. Ligation of these DSB ends by MMEJ leads to deletion of the

intervening sequence between the microhomologies [Ma *et al*., 2003; Daley and Wilson, 2005] and, for this reason, it is considered an error-prone pathway.
In both yeast and mammals, MMEJ requires the MRX/MRN complex, but not Ku and the recombinase Rad52 [Ma *et al.*, 2003]. In addition, partial reduction of MMEJ in *dnl4*Δ mutants suggests a role for the DNA ligase IV [Ma *et al.*, 2003]. Recent studies suggest that Srs2 helicase, Sae2/CtIP nuclease, Tel1/ATM kinase, and Pol4/Rev3/Pol32 DNA polymerases are important for MMEJ in yeast [Lee and Lee; 2007]. In mammals, MMEJ depends on Mre11, CtIP, DNA ligase III, and PARP1 [Audebert *et al.*, 2004; Wang *et al.*, 2005; Bennardo *et al.*, 2008; Dinkelmann *et al.*, 2009; Rass *et al.*, 2009; Xie *et al.*, 2009]. Since MMEJ is highly mutagenic, it can be responsible for gross chromosomal rearrangements observed in yeast mutants with a compromised DNA damage response [Kolodner *et al.*, 2002]. Finally, this backup pathway contributes to genome instability of cancer cells. In fact, MMEJ is commonly upregulated in cancers, especially in homologous recombination-deficient cancer cells [Patterson-Fortin and D'Andrea, 2020]. Furthermore, the similarity between MMEJ repair junctional sequences and the junctional sequences of chromosomal translocations causing human tumors highlights a role of MMEJ in oncogenic chromosome rearrangements [Yu and Gabriel, 2003].

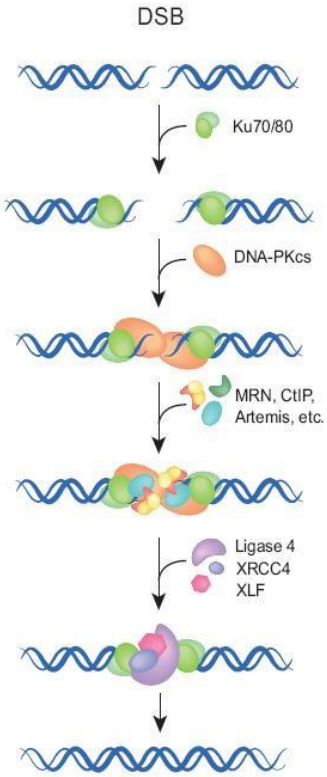

Figure 5. NHEJ repair mechanism in higher eukaryotes [Adapted from Dueva *et al.*, 2013].
After DSB formation, Ku complex is rapidly recruited at the DNA broken ends where it protects them from degradation and acts as a hub to recruit NHEJ components like DNA-PKcs, XRCC4, and XLF. The broken ends are kept together and DNA Ligase IV rilegates them. The DNA lesion is repaired but some mutations could have been inserted at joined site by NHEJ repair mechanism.

DSB end-tethering

One of the most important questions in the NHEJ mechanism concerns how the two DNA ends resulting from a DSB are held in close physical proximity for repair. This function, which is called end-tethering, refers to the ability to maintain the DSB ends closed to each other, and it is a relevant event to allow an accurate and efficient repair of a DSB by NHEJ.

In *S. cerevisiae*, both the MRX complex and Sae2 are involved in end-tethering [Kaye *et al.*, 2004; Lobachev *et al.*, 2004; Lee *et al.*, 2008; Clerici *et al.*, 2005; Nakai *et al.*, 2001]. The Rad50 subunit is characterized by an ATP binding domain at both its N- and C-terminal regions. Between these two outer regions, there are two long coiled-coil domains that interact with each other through a Zn-hook to form intra-linked complexes that maintain the DSB ends tethered to each other [Casari *et al.*, 2019]. Moreover, the conformational state of the ATP nucleotide binding domain, generated by the association of two ATPase motifs, is crucial to regulate the MRX end-tethering function. In fact, upon ATP binding, Rad50 closes into a rigid conformation, in which the N- and C-terminal domains interact with each other and form a central groove that can accommodate dsDNA. This closed ATP-bound state of Rad50 favours DNA binding, end-tethering, and NHEJ [Deshpande *et al.*, 2014], suggesting that MRX exerts these functions when it is present in the ATP-bound state. By contrast, in the ATP-hydrolyzed state, the Rad50 ATPase subunits are more flexible and open, making DNA accessible to the Mre11 nuclease active sites and favouring the first steps of homologous recombination [Lammens *et al.*, 2011; Lim *et al.*, 2011; Williams *et al.*, 2011; Möckel *et al.*, 2012; Deshpande *et al.*, 2014]. Thus, these ATP-driven transitions regulate the balance between two different MRX functions: (i) end-tethering and NHEJ, which require ATP binding, and (ii) end-resection and HR, which require ATP hydrolysis (Figure 6).

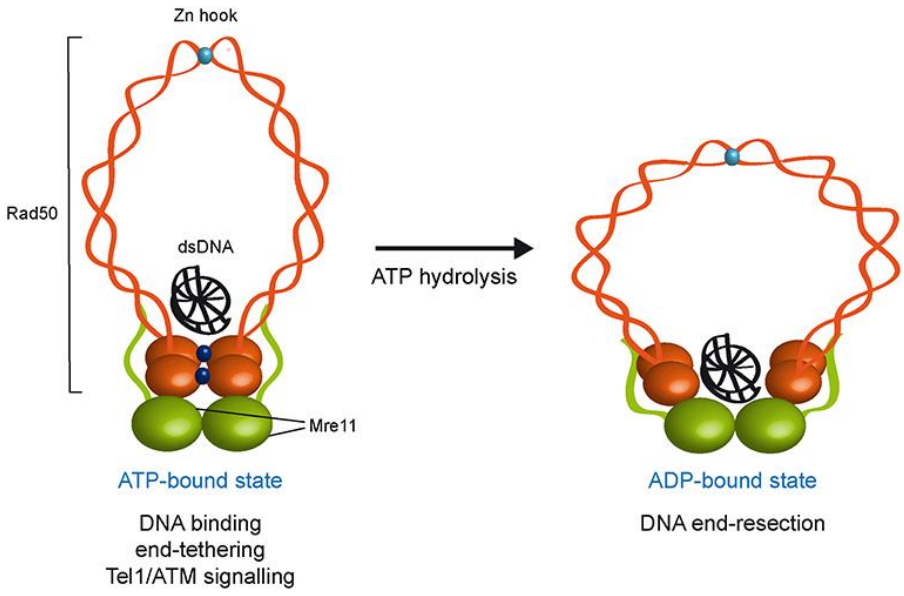

Figure 6. End-tethering function releated to the ATP- and ADP-bound state of the MRX complex [Adapted from Casari *et al.*, 2019].
The Mre11 dimer (green) is bound to Rad50 dimer (orange) with a double-stranded DNA molecule located on the top surface of Rad50. The ATP-bound state of Rad50 supports DNA binding, end-tethering, and Tel1/ATM signalling, whereas it renders the dsDNA inaccessible to the Mre11 nuclease active sites and therefore negatively regulates Mre11 nuclease activity. ATP hydrolysis by Rad50 opens the complex to allow the Mre11 active sites to access DNA. Whether the ADP-bound state maintains an interlinked assembly is unknown. ATP molecules are indicated as blue dots. Zn^{2+} atoms are indicated as light blue dots.

Through its Xrs2 subunit, the MRX complex also recruits and activates the checkpoint protein Tel1 to coordinate DSB repair with cell-cycle progression [Villa *et al.*, 2016]. Once Tel1 is recruited to DSBs by MRX, it plays a structural role in stabilizing the association of MRX to the DSB ends in a manner independently of its kinase activity. This Tel1-mediated regulation of MRX retention on DNA ends is important to allow proper MRX-DNA binding that is needed for end-tethering, highlighting a role of Tel1 in the first steps of NHEJ repair pathway [Cassani *et al.*, 2016; Casari *et al.*, 2019].

In mammals, several studies have shown that the DNA-PKcs by itself is responsible for keeping the DNA ends together [DeFazio *et al.*, 2002], although other studies have attributed the main bridging activity to the DNA-PK holoenzyme, composed of Ku and DNA-PKcs [Weterings *et al.*, 2003; Spagnolo *et al.*, 2006; Wang *et al.*, 2018]. However, in other studies, DNA-PKcs was not found to be necessary for DSB end-tethering, which required Ku together with XRCC4-DNA ligase IV [Reid *et al.*, 2015; Chang *et al.*, 2016; Zhao *et al.*, 2019], suggesting that Ku could play a role in the formation of a molecular DSB bridge. Consistent with this hypothesis, early atomic force and electron microscopy experiments have shown that recombinant Ku was capable to mediate DNA looping and to coprecipitate two labelled DNA molecules [Cary *et al.*, 1997; Ramsden and Gellert, 1998]. Furthermore, a single molecule study of bacterial NHEJ, a mechanism relying on a homodimeric Ku and Ligase D, revealed that the Ku dimer alone is sufficient to form DNA bridges that are stabilized upon addition of Ligase D [Öz *et al.*, 2021]. This situation is similar to the NHEJ mechanism found in yeast cells, which do not possess DNA-PKcs.

The two Ku subunits have three structural domains: an N-terminal von Willebrand A (vWA)-like domain, a central β-barrel domain, and an α-helical C-terminal arm. The C-terminal halves of both Ku70 and Ku80 are required for DNA binding [Wu and Lieber, 1996], while the central region of Ku80 is required for its interaction with Ku70 [Cary *et al.*, 1998]. Ku binds DNA ends asymmetrically, with the Ku70 vWA-like domain outward-facing in close proximity to the DNA end and the Ku80 vWA-like domain inward-facing [Ribes-Zamora *et al.*, 2007] (Figure 7). The overall structure of Ku complex appears to provide a possible scaffold for end-to-end fusion, raising the possibility that Ku could be also an alignment factor of DNA broken ends, increasing the association between two DNA molecules [Ramsden and Gellert, 1998; Cary *et al.*, 1997].

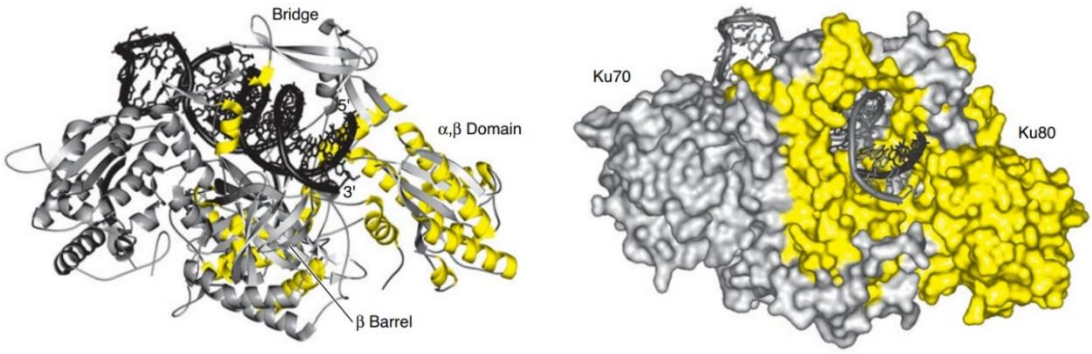

Figure 7. The Ku complex: secondary and tertiary structure [Adapted from Friedberg *et al.*, 2006].
The Ku complex is composed by Ku70 and Ku80 subunits that form a quasi-symmetric structure with a ring that encircles the duplex DNA.

Telomeres

MRX, Tel1, and Ku are also required to maintain the length of telomeres, which are specialized nucleoprotein structures at the ends of eukaryotic linear chromosomes. Telomere basic structure is conserved among eukaryotes and consists of several short tandem DNA repeats, which are G-rich in the strand containing the 3' end. In *S. cerevisiae*, these short tandem DNA repeats are long about 300 +/-75 bp with $C_{1-3}A/TG_{1-3}$ repeats, followed by sub-telomeric regions with repeated elements called X and Y' that are closer to centromere [Wellinger and Zakian, 2012].

The main functions of telomeres are to allow replication of chromosomal extremities and to distinguish them from an intrachromosomal DNA double-strand break [Jain and Cooper, 2010]. Telomere length is maintained by the action of a specialized reverse transcriptase called telomerase, which in *S. cerevisiaie* is composed of Est1, Est2, and Est3 subunits together with the TLC1 RNA [Lundblad and Szostak, 1989; Singer and Gottschling, 1994; Lin and Zakian, 1995; Lingner *et al.*, 1997; Morris and Lundblad, 1997; Hughes *et al.*, 2000; Wellinger and Zakian, 2012]. Telomerase uses its own RNA component TLC1 as a template for the extension of 3'-ended guanine rich strand (G-tail) [Larrivéè *et al.*, 2004], whereas the complementary strand is extended by the polα-primase complex.

Telomeric DNA is distinguished from intrachromosomal DNA double-strand break ends by different protein complexes, which are recruited to telomeres and prevent DDR activation, degradation, fusions, and recombination events. Several studies have established that suppression of DNA repair and DNA damage checkpoint at telomeres, referred to as capping, relies on proteins specifically present or enriched at single-stranded and double-stranded telomeric DNA. These proteins in budding yeast include CST, Ku, and the Rap1-Rif1-Rif2 complexes.

The CST complex, which is composed of Cdc13, Stn1, and Ten1 subunits, is also present in mammalian cells and comprises the CTC1, STN1, and TEN1 subunits [Miyake *et al.*, 2009; Chen *et al.*, 2009; Wu *et al.*, 2012] (Figure 8). The CST complex binds the telomeric 3′ G-overhang (G-tail) and is essential for chromosome capping and telomere replication [Nugent *et al.*, 1996; Churikov *et al.*, 2013].

The Ku complex encircles the telomeric dsDNA and protects telomeres especially from Exo1-mediated nucleolytic degradation, as it does at DSBs [Bonetti *et al.*, 2010]. Furthermore, Ku contributes to maintain telomere length by interacting with the telomerase subunits Est1 and Est2, and with the telomerase RNA TLC1 [Peterson *et al.*, 2001; Fisher *et al.*, 2004; Chan *et al.*, 2008]. Ku-TLC1 association is required for TLC1 nuclear retention, suggesting an involvement of Ku in the nuclear-cytoplasmic trafficking of telomerase. However, Ku recruitment at telomeres is independent of TLC1 and occurs throughout the cell cycle [Peterson *et al.*, 2001; Stellwagen *et al.*, 2003; Fisher *et al.*, 2004, 2005; Chan *et al.*, 2008; Gallardo *et al.*, 2008, 2011].

The other protein complex with capping function is composed of Rap1, Rif1, and Rif2 proteins. This protein complex functionally recapitulates the human shelterin complex that comprises TRF1, TRF2, RAP1, TIN2, TPP1, and POT1 subunits [de Lange *et al.*, 2018] (Figure 8). In *S. cerevisiae*, Rap1 and Rif2, and to a much lesser extent Rif1, repress telomere-telomere fusions by NHEJ, telomere degradation, and checkpoint activation [Marcand *et al.*, 2008; Bonetti *et al.*, 2010; Vodenicharov *et al.*, 2010]. Rif2 also inhibits activation of Tel1, which is known to promote telomerase-mediated telomere elongation [Ritchie and Petes, 2000]. By contrast, Rif1, but not Rif2, is important to support viability in cells where Cdc13 is dysfunctional [Anbalagan *et al.*, 2011]. Thus, Rap1 and its interactors Rif1 and Rif2 have capping activities, with Rif1 and Rif2 making specific and separable contributions to this capping.

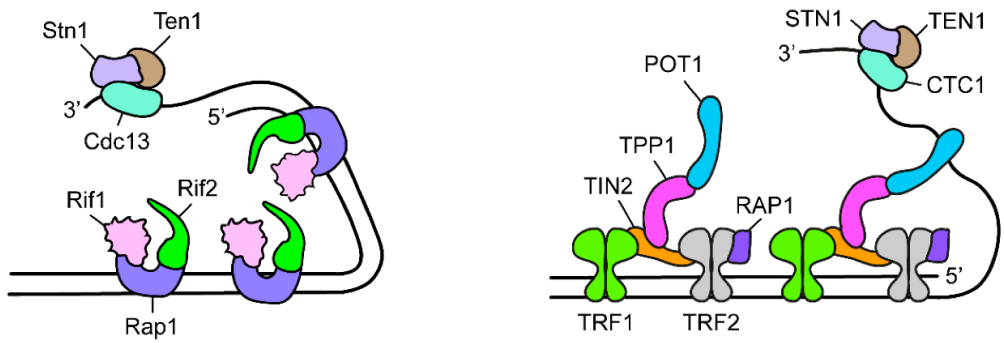

Figure 8. Schematic representations of telomeric structure and capping proteins in yeast and mammals [Adapted from Casari *et al.*, 2022].
In yeast, telomeres are protected by the Rap1-Rif1-Rif2 and the CST (Cdc1-Stn1-Ten1 subunits) complexes. In mammals, telomeric protection functions are ensured by shelterin complex composed of TRF1, TRF2, TIN2, RAP1, TPP1, and POT1 subunits, and by the CST complex (CTC1-STN1-TEN1 subunits).

Rap1 is a DNA binding protein with an 827 amino acids sequence that was identified as a generic transcriptional activator/repressor [Shore and Nasmyth, 1987; Tornow *et al.*, 1993; Lieb *et al.*, 2001; Zhao *et al.*, 2006]. At telomeres, Rap1 negatively regulates telomere length, represses transcription, and inhibits telomeric fusions by NHEJ [Conrad *et al.*, 1990; Lustig *et al.*, 1990; Kurtz and Shore, 1991; Sussel and Shore, 1991; Kyrion *et al.*, 1993; Moretti and Shore, 2001; Pardo and Marcand, 2005; Marcand *et al.*, 2008; Kabir *et al.*, 2010; Chen *et al.*, 2011; Azad and Tomar, 2016].

Rap1 consists of three conserved domains: a BRCT domain in the N-terminal region, a centrally located DNA binding domain, and a C-terminal domain called RCT. The RCT domain is sufficient for Rap1 interaction with Rif2 and Rif1, as well as with Sir3 and Sir4, two factors involved in gene silencing [Wotton and Shore, 1997; Moretti and Shore, 2001]. The lack of this domain causes both an increase in telomere length, that is similar to that observed when Rif1 and Rif2 are concomitantly lacking [Kyrion *et al.*, 1992; Wotton and Shore, 1997], and

loss of mating-type and telomeric silencing similar to that observed when Sir3 or Sir4 is deleted [Liu *et al.*, 1994; Moretti *et al.*, 1994].

The Rap1 DNA binding domain binds telomere repeat DNA in a sequence-specific manner through both its Myb-like motifs, which make contact with the two half-sites of a recognition sequence consisting of two direct repeats spaced by 1 or 3 bp [Graham and Chambers, 1994; Konig *et al.*, 1996; Taylor *et al.*, 2000; Matot *et al.*, 2012]. Immediately after the C-terminal Myb-like domain, a wrapping loop folds back and interacts with the N-terminal Myb-like motif to form a closed complex on DNA. Interestingly, Rap1 was shown to form *in vitro* higher stoichiometry complexes, where a single Myb-like domain is bound to both telomeric and non-telomeric double-stranded DNA with lower affinity. This transition is thought to be due to a transient opening of the C-terminal wrapping loop that leads to a destabilization of the clamped structure [Del Vescovo *et al.*, 2004; Feldmann and Galletto, 2004; Feldmann *et al.*, 2015].

A Rap1 ortholog with similar domain structure is present in humans. However, unlike budding yeast Rap1, which directly binds to telomeric DNA, mammalian Rap1 associates with telomeres through its interaction with the telomeric protein TRF2, which shares the DNA binding domain with *S. cerevisiae* Rap1 [Li *et al.*, 2000; de Lange, 2018].

Rap1 dysfunction causes MRX-mediated telomere degradation [Bonetti *et al.*, 2010; Vodenicharov *et al.*, 2010], suggesting that Rap1 inhibits MRX activity at least at telomeres. The lack of $Rap1^{RCT}$ domain was shown to increase the association of MRX at telomeres, suggesting that Rap1 acts through Rif2 to negatively regulate MRX association at telomeres [Bonetti *et al.*, 2010]. In *S. cerevisiae*, Rap1 physically interacts with Rif2, which binds telomeres through a direct interaction with the C-terminal region of Rap1 ($Rap1^{RCT}$), as demonstrated in two-hybrid experiments [Hardy *et al.*, 1992; Wotton and Shore, 1997].

Instead, Rif2 is a member of ATPase associated with diverse cellular activities

(AAA+) protein family. The Rif2^{AAA+} domain is formed by association of the ASCE motif, an α bundle, and an N-terminal domain called Rif2^{RBM} [Shi *et al.*, 2013]. In the Rif2-Rap1 complex structure, each Rif2 molecule binds to two different Rap1^{RCT} molecules through two independent interfaces: the Rif2^{AAA+} domain and the Rif2^{RBM}. Thus, one single Rap1 molecule, through its RCT domain, binds simultaneously to two Rif2 molecules in a non-overlapping manner [Shi *et al.*, 2013].

Rif2 negatively regulates telomere elongation and counteracts Tel1 activation, nucleolytic degradation, and NHEJ at telomeres [Hardy *et al.*, 1992; Wotton and Shore, 1997; Marcand *et al.*, 2008; Bonetti *et al.*, 2010; Bonetti *et al.*, 2010]. All these abilities appear to rely on inhibition of MRX activity at telomeres. Since Rif2 interacts with the C-terminus of Xrs2, subunit of MRX, within the same region as Tel1 [Hirano *et al.*, 2009], Rif2 was initially proposed to inhibit MRX association/persistence to telomeric DNA ends by competing with Tel1 for Xrs2 binding, therefore antagonizing Tel1-mediated stabilization of MRX association with DNA ends. However, the finding that Rif2 interacts *in vitro* with Rad50 and can inhibit MRX-dependent stimulation of Tel1 kinase activity independently of Xrs2 [Cassani *et al.*, 2016; Hailemariam *et al.*, 2019], suggests that Rif2 can act directly on Rad50 to control MRX activity at telomeres. Interestingly, Rif2 was shown to stimulate ATP hydrolysis by Rad50 in an Xrs2-independent manner [Cassani *et al.*, 2016; Hailemariam *et al.*, 2019]. As MRX binding to DNA, as well as its ability to stimulate Tel1 activation, and NHEJ requires that Rad50 is bound to ATP [Lammens *et al.*, 2011; Williams *et al.*, 2011; Liu *et al.*, 2016; Seifert *et al.*, 2016; Hailemariam *et al.*, 2019], Rif2 can inhibit all these MRX functions by discharging the MRX ATP-bound conformation through stimulation of Rad50 ATPase.

RESULTS AND DISCUSSION

Nucleic Acids Research

2020 Mar 18; 48(5):2424-2441

doi: 10.1093/nar/gkz1203

DNA binding modes influence Rap1 activity in the regulation of telomere length and MRX functions at DNA ends

Diego Bonetti[1], **Carlo Rinaldi**[1], Jacopo Vertemara[1], Marco Notaro, Paolo Pizzul[1], Renata Tisi[1], Giuseppe Zampella[1], Maria Pia Longhese[1*]

[*] Corresponding Author

[1] Dipartimento di Biotecnologie e Bioscienze, Università degli Studi di Milano-Bicocca, Milano, 20126, Italy

Chromosomal DNA double-strand breaks (DSBs) are highly cytotoxic lesions that can occur spontaneously during normal cell metabolism or can be induced upon exposure of cells to ionizing radiation or chemicals. Two major pathways are used for repairing DSBs: non-homologous end joining (NHEJ), which directly religates the two broken ends [Chang *et al.*, 2017], and homologous recombination (HR), which uses undamaged homologous duplex DNA as template for repair [Metha *et al.*, 2014; Kowalczykowski, 2015]. HR is initiated by nucleolytic degradation (resection) of the 5′ terminated strands at both DNA ends to generate 3′-ended single-stranded DNA (ssDNA) ends that catalyze homologous pairing and strand invasion [Bonetti *et al.*, 2018].

The evolutionarily conserved Mre11-Rad50-Xrs2/NBS1 complex (MRX in *S. cerevisiae*, MRN in humans) is rapidly recruited to DSBs, where it maintains the DSB ends in close proximity, initiates DSB resection, and activates the checkpoint protein kinase Tel1 (ATM in mammals) [Gobbini *et al.*, 2016; Syed and Tainer, 2018]. The Mre11 subunit is a dimer that possesses both 3′-to-5′ exonuclease and ssDNA endonuclease activities [Paull and Gellert, 1998; Trujillo *et al.*, 1998]. Mre11 initiates resection by catalyzing an endonucleolytic cleavage of the 5′-terminated strands at both DSB DNA ends with the support of the Sae2 protein [Cannavo and Cejka, 2014; Mimitou and Symington, 2008; Zhu *et al.*, 2008; Shibata *et al.*, 2014; Reginato *et al.*, 2017; Wang *et al.*, 2017]. This MRX-mediated DNA cleavage generates an entry site for the nucleases Exo1 and Dna2, which degrade DNA in a 5′-3′ direction, coupled with Mre11 exonuclease that degrades back toward the DNA end in a 3′-5′ direction [Mimitou and Symington, 2008; Zhu *et al.*, 2088; Shibata *et al.*, 2014; Reginato *et al.*, 2017; Wang *et al.*, 2017]. The Rad50 subunit binds ATP and possesses ATPase activity [Gobbini *et al.*, 2016; Syed and Tainer, 2018]. The characterization of Rad50 mutant variants that either stabilize or destabilize the ATP-bound conformation has shown that the ATP-bound state of MRX promotes DNA binding, end-

tethering, and Tel1 activation, whereas ATP hydrolysis by Rad50 leads to MRX engagement in DSB resection by allowing the access to DNA of the Mre11 nuclease active site [Deshpande *et al.*, 2014; Cassani *et al.*, 2019].

Both MRX and Tel1 are also required to maintain the length of telomeres, specialized nucleoprotein complexes at the ends of eukaryotic chromosomes [Ritchie and Petes, 2000; Bi *et al.*, 2004; Larrivée *et al.*, 2004; Chai *et al.*, 2006]. MRX recruits Tel1 to both DSBs and telomeres through direct interaction between Tel1 and the Xrs2 subunit [Nakada *et al.*, 2003; Falck *et al.*, 2005; Lee and Paull, 2005; You *et al.*, 2005]. Tel1, once loaded to DNA by the MRX complex, promotes/stabilizes MRX association to both DSBs and telomeres in a positive feedback loop [Hirano *et al.*, 2009; Martina *et al.*, 2012; Cassani *et al.*, 2016]. This Tel1-mediated control of MRX persistence to DNA ends is particularly important to support DNA damage resistance when MRX accumulation at DSBs is reduced, such as in the presence of the Rad50 V1269M mutation in the C-terminal ATPase domain. The *rad50-V1269M* (*rad50-VM*) allele, which was identified by searching for *S. cerevisiae* mutants that require Tel1 to survive to genotoxic treatments [Cassani *et al.*, 2016], causes a reduction of Rad50 association at DNA ends that leads to defects in keeping the DSB ends tethered to each other [Cassani *et al.*, 2016]. The lack of Tel1 exacerbates both the DNA damage hypersensitivity and the end-tethering defect of *rad50-VM* cells by further reducing the amount of $MR^{VM}X$ bound at DSBs [Cassani *et al.*, 2016]. This finding suggests that this Tel1-mediated regulation of MRX retention at DNA ends is particularly important for maintaining the broken ends tethered together.

Interestingly, both the DNA damage hypersensitivity and the end-tethering defects of *rad50-VM* cells are suppressed by the lack of Rif2 [Cassani *et al.*, 2016], which acts together with Rap1 and Rif1 as negative regulator of telomere length [Wotton and Shore, 1997]. This restored DNA damage resistance and end-

tethering of *rad50-VM* cells is possibly due to the lack of Rif2-mediated inhibition of MRX association at DSBs. Rif2 plays a dual function in repressing MRX retention at DNA ends. First, it decreases MRX persistence to both DSBs and telomeres in a Tel1-dependent manner [Hirano *et al.*, 2009; Martina *et al.*, 2012; Cassani *et al.*, 2016]. This finding, together with the observation that Rif2 competes with Tel1 for MRX interaction [Hirano *et al.*, 2009], suggests that Rif2 inhibits MRX persistence at DSBs by counteracting Tel1-mediated stabilization of MRX association at DNA ends. Second, Rif2 enhances the ATP hydrolysis activity by Rad50 [Cassani *et al.*, 2016; Wotton and Shore, 1997; Hailemariam *et al.*, 2019], suggesting that Rif2 lowers MRX association at DNA ends by decreasing the time spent by MRX in the ATP-bound conformation that supports the DNA binding activity of the complex [Deshpande *et al.*, 2014; Cassani *et al.*, 2019]. Consistently with this hypothesis, *rif2*Δ cells show increased efficiency of both end-tethering and NHEJ compared to wild-type cells [Cassani *et al.*, 2016]. Rif2 directly binds to Rap1 [Wotton and Shore, 1997; Hailemariam *et al.*, 2019; Shi *et al.*, 2013], which is a DNA binding protein that negatively regulates telomere length, activates transcription at promoters, represses transcription at the silent mating-type loci and at telomeres, and inhibits telomeric fusions by NHEJ [Azad and Tomar, 2016]. Rap1 is essential for cell viability and its partial dysfunction can lead to loss of silencing [Kurtz and Shore, 1991; Sussel and Shore, 1991; Kyrion *et al.*, 1993], telomere lengthening [Sussel and Shore, 1991; Kyrion *et al.*, 1993; Lustig *et al.*, 1990], and telomere fusions [Pardo and Marcand, 2005; Marcand *et al.*, 2008]. Rap1 consists of three conserved domains: a BRCT domain in the N-terminal region, a centrally located DNA binding domain (DBD) with two Myb-like folds, and a C-terminal domain called RCT. The RCT domain is sufficient for Rap1 interaction with Rif2 and Rif1, as well as with Sir3 and Sir4, two nucleosome-binding factors involved in gene silencing [Wotton and Shore, 1997; Moretti and Shore, 2001]. The lack of this domain

causes both an increase in telomere length that is similar to that observed when Rif1 and Rif2 are concomitantly lacking [Wotton and Shore, 1997; Kyrion *et al.*, 1992], and loss of mating-type and telomeric silencing similar to that observed when Sir3 or Sir4 is deleted [Liu *et al.*, 1994; Moretti *et al.*, 1994].

While there are no obvious Rif2 orthologs in mammals, a Rap1 ortholog harbouring similar domain structure is present in both fission yeast and humans. However, unlike budding yeast Rap1, which directly binds to telomeric DNA, both mammalian and fission yeast Rap1 associate with telomeres through their interaction with the telomeric protein TRF2 [Li *et al.*, 2000]. In mammals, Rap1 and TRF2 interact with TRF1, TIN2, POT1, and TPP1 to form a protein complex called shelterin that maintains telomere identity [de Lange, 2018]. While TIN2, TPP1, and POT1 have no obvious *S. cerevisiae* orthologs, both human TRF1 and TRF2 share the DNA binding domain with *S. cerevisiae* Rap1 [de Lange, 2018]. Crystal structures have shown that $Rap1^{DBD}$ binds telomere repeat DNA in a sequence-specific fashion through both the Myb-like motifs, which make contact with the two half-sites of a recognition sequence consisting of two direct repeats spaced by 1 or 3 bp [Graham *et al.*, 1994; Konig *et al.*, 1996; Taylor *et al.*, 2000; Matot *et al.*, 2012]. Immediately after the C-terminal Myb-like domain, a wrapping loop folds back and interacts with the N-terminal Myb-like motif to form a closed complex on DNA. Interestingly, Rap1 was shown to form *in vitro* higher stoichiometry complexes, where a single Myb-like domain is bound to both telomeric and non-telomeric double-stranded DNA (dsDNA) with lower affinity [Del Vescono *et al.*, 2004; Feldmann and Galletto, 2014; Feldmann *et al.*, 2015]. This transition is thought to be due to a transient opening of the C-terminal wrapping loop that leads to a destabilization of the clamped structure [Feldmann and Galletto, 2014; Feldmann *et al.*, 2015].

Rap1 dysfunction was shown to cause MRX-mediated telomere degradation [Bonetti *et al.*, 2010; Vodenicharov *et al.*, 201], suggesting that Rap1 inhibits

MRX activity at least at telomeres. However, whether Rap1 exerts this function through Rif2 is unclear. On one hand, the lack of Rap1^{RCT} was shown to increase the association of MRX at telomeres [Bonetti *et al.*, 2010], suggesting that Rap1 acts through Rif2 to negatively regulate MRX association at telomeres. On the other hand, MRX fails to associate to long telomeric DNA sequences and this effect requires Rap1 but not Rif2 or Rap1^{RCT} [Negrini *et al.*, 2007]. Furthermore, artificial tethering of Rap1 molecules adjacent to non-telomeric DNA ends needs Rif2 to decrease MRX accumulation at nearby DNA ends only when Tel1 is absent [Hirano *et al.*, 2009]. In any case, whether Rap1 represses MRX association at DSBs is unknown.

Here, we show that Rif2 counteracts MRX association to DNA ends in a manner dependent on Rap1, which binds to DSBs and promotes Rif2 association to them. In fact, *rif2* or *rap1* alleles specifically impaired in Rap1 or Rif2 interaction, respectively, suppress the DNA damage hypersensitivity, and the end-tethering defect caused by the *rad50-VM* allele by increasing MRX association to DSBs. Rap1 in turn can inhibit MRX functions in a Rif2-dependent and independent manners. In fact, binding of both Rap1 Myb-like domains to DNA allows formation of Rap1-DNA complexes that act through Rif2 in the negative regulation of telomere length and MRX association at DNA ends. On the other hand, Rap1 binding to DNA through a single Myb-like domain allows formation of high stoichiometry Rap1-DNA complexes that act mostly in a Rif2-independent manner. Altogether, these findings indicate that, depending of its DNA binding mode, Rap1 can form complexes with different properties that impact on Rap1 functions *in vivo* and on its ability to interact with Rif2.

Identification of *rif2* alleles that restore DNA damage resistance of *rad50-VM* cells

The lack of Rif2 increases the association of the MRX complex at both DSBs and telomeres, and restores DNA damage resistance and end-tethering of *rad50-VM* cells [Hirano *et al.*, 2009; Martina *et al.*, 2012; Cassani *et al.*, 2016]. To better understand how Rif2 exerts these functions, we searched for *rif2* mutations that, similar to *RIF2* deletion, suppress the hypersensitivity to DNA damaging agents of *rad50-VM* cells. Linear *RIF2* PCR products were obtained by low-fidelity PCR and then transformed into *rad50-VM* cells in order to replace the corresponding *RIF2* wild-type sequence with the mutagenized DNA fragments. As mutations in any MRX subunit (including *rad50-VM*) are particularly sensitive to camptothecin (CPT), which stabilises DNA topoisomerase I cleavage complexes that can lead to replication-dependent DSBs [Deng *et al.*, 2005], transformant clones were screened for increased viability in the presence of CPT compared to *rad50-VM*. This screen yielded 8 *rif2* alleles increasing CPT resistance of *rad50-VM* cells (Figure 9A and B). Suppression was not specific to CPT, as all the *rif2* alleles also suppressed the sensitivity of *rad50-VM* cells to the DNA alkylating agent methyl methanesulphonate (MMS) (Figure 9A and B). Sequence analysis revealed that three alleles contained single missense mutations either in the N-terminus (*rif2-A78D*) or in the C-terminus (*rif2-I295R* and *rif2-L341S*) of the protein (Figure 9C). One other allele had multiple missense mutations (*rif2-S170L, I348F*). The remaining four alleles had a frameshift mutation at codon 193, 294, 360 or 368 (Figure 9C), resulting in truncation of the protein past residue 194, 317, 364 or 387, respectively (with 1, 2, 3, 4 or 19 amino acids added to the end of the protein, respectively, as a result of the frameshift mutation).

Similar to *rif2*Δ, all the *rif2* alleles carrying missense mutations suppressed also the DNA damage hypersensitivity of *rad50-VM tel1*Δ cells (Figure 9D), indicating that Tel1 is not required for the suppression.

Consistently with Rif2 dysfunctions, all the *rif2* mutants displayed overelongated telomeres, although to different extents. In particular, telomere length in *rif2-A78D*, *rif2-I295R*, *rif2-193FS*, *rif2-294FS*, *rif2-360FS*, and *rif2-368FS* cells was similar to that of *rif2*Δ cells (Figure 9E). Tel1 was required for telomere overelongation in both *rif2*Δ and *rif2* mutants, as telomeres in *rif2*Δ, *rif2-A78D*, *rif2-S170L, I348F*, *rif2-I295R*, and *rif2-L341S* cells lacking Tel1 were as short as in *tel1*Δ cells (Figure 9F). The finding that *rif2*Δ, *rif2-A78D*, *rif2-S170L, I348F*, *rif2-I295R*, and *rif2-L341S* alleles restored DNA damage resistance of *rad50-VM* cells even in the absence of Tel1 (Figure 9D) suggests that telomere lengthening is not involved in the suppression mechanism.

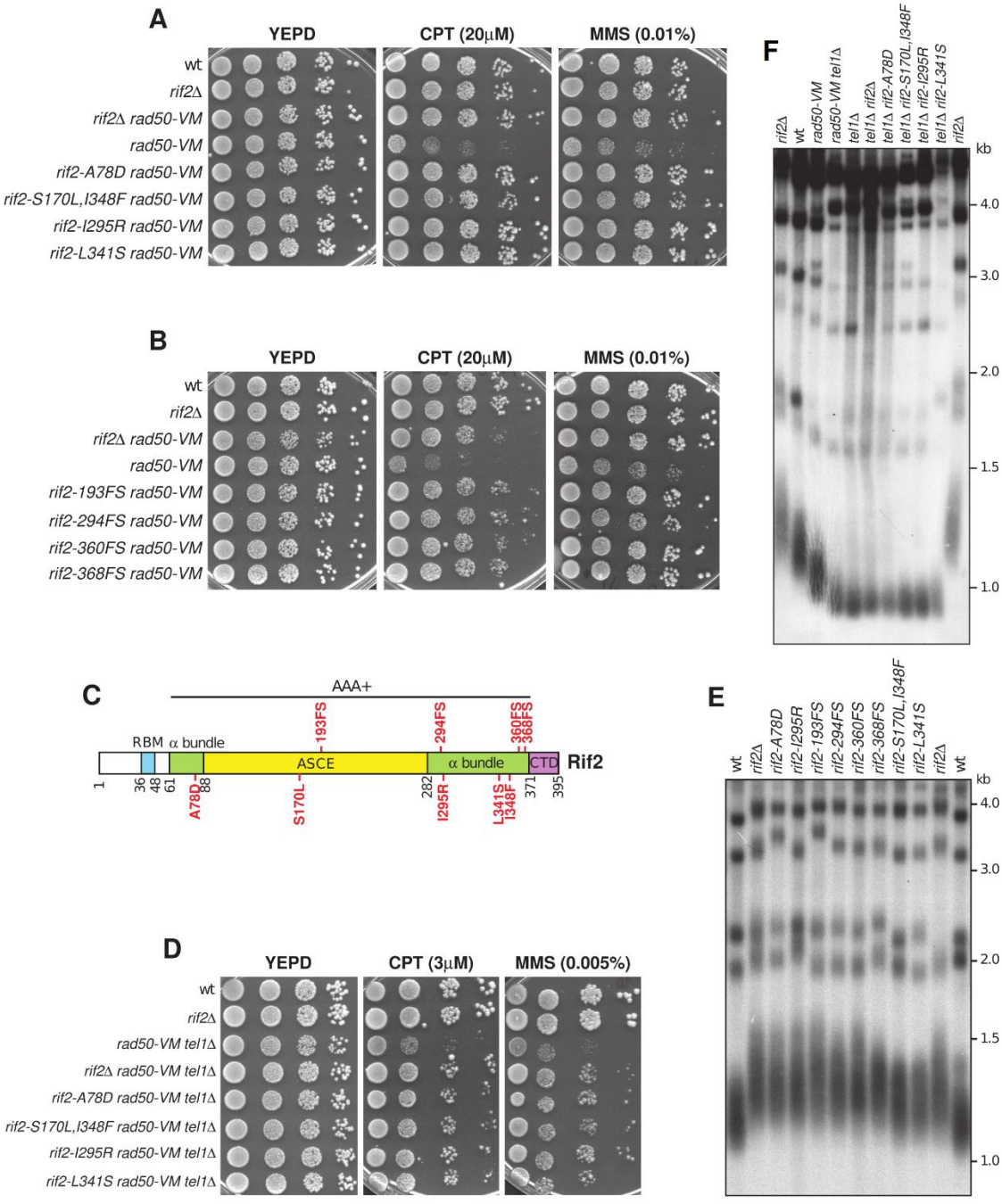
A
YEPD
CPT (20μM)
MMS (0.01%)
wt
rif2Δ
rif2Δ rad50-VM
rad50-VM
rif2-A78D rad50-VM
rif2-S170L,I348F rad50-VM
rif2-I295R rad50-VM
rif2-L341S rad50-VM
B
YEPD
CPT (20μM)
MMS (0.01%)
wt
rif2Δ
rif2Δ rad50-VM
rad50-VM
rif2-193FS rad50-VM
rif2-294FS rad50-VM
rif2-360FS rad50-VM
rif2-368FS rad50-VM
C
AAA+
RBM
α bundle
ASCE
α bundle
CTD
Rif2
193FS
294FS
360FS
368FS
1
36
48
61
88
282
371
395
A78D
S170L
I295R
L341S
I348F
D
YEPD
CPT (3μM)
MMS (0.005%)
wt
rif2Δ
rad50-VM tel1Δ
rif2Δ rad50-VM tel1Δ
rif2-A78D rad50-VM tel1Δ
rif2-S170L,I348F rad50-VM tel1Δ
rif2-I295R rad50-VM tel1Δ
rif2-L341S rad50-VM tel1Δ
E
wt
rif2Δ
rif2-A78D
rif2-I295R
rif2-193FS
rif2-294FS
rif2-360FS
rif2-368FS
rif2-S170L,I348F
rif2-L341S
rif2Δ
wt
kb
4.0
3.0
2.0
1.5
1.0
F
rif2Δ
wt
rad50-VM
rad50-VM tel1Δ
tel1Δ
tel1Δ rif2Δ
tel1Δ rif2-A78D
tel1Δ rif2-S170L,I348F
tel1Δ rif2-I295R
tel1Δ rif2-L341S
rif2Δ
kb
4.0
3.0
2.0
1.5
1.0

Figure 9. Identification of *rif2* alleles that suppress the DNA damage sensitivity of *rad50-VM* cells.
(**A**, **B**) Exponentially growing cells with the indicated genotypes were serially diluted (1:10) and each dilution was spotted out onto YEPD plates with or without CPT or MMS. (**C**) Position of the mutations within the Rif2 sequence. (**D**) Exponentially growing cells were serially diluted (1:10) and each dilution was spotted out onto YEPD plates with or without CPT or MMS. (**E**, **F**) *Xho*I-cut genomic DNA prepared from exponentially growing cells was subjected to Southern blot analysis using a poly(GT) probe.

The lack of Rif2-Rap1 interaction is sufficient to restore DNA damage resistance of *rad50-VM* cells

Rap1 directly binds Rif2 and Rif1 proteins to form a protein complex that negatively controls telomerase-mediated telomere elongation [Wotton and Shore, 1997; Lustig *et al.*, 1990; Marcand *et al.*, 1997]. A so-called 'Velcro-like' macromolecular complex was described [Shi *et al.*, 2013], in which each Rif2 molecule binds two different Rap1 molecules through two independent interfaces: the $Rif2^{AAA+}$ domain, formed by the three-dimensional association of the ASCE motif (residues 88-282) and an α bundle (residues 61-88 together with residues 282-371), and an N-terminal peptide, defined as RBM, comprising residues 36-48. The structure of $Rap1^{RCT}$ domain bound to $Rif2^{AAA+}$ and $Rif2^{RBM}$ domains was resolved [Shi *et al.*, 2013] (PDB code: 4BJ5) (Figure 10A) and revealed that the Rap1 F708 and P705 residues interact hydrophobically with Rif2 residues L79, F342, and V350, while Rap1 R747 forms a salt bridge with Rif2 E347. An additional minor interface is provided by the Rif2 C-terminus comprising residues 371-395 and referred to as CTD.

Although the A78D mutation is located in the Rif2 N-terminal region while I295R and L341S are located in the α helical bundle of the protein, both these two regions compose the AAA+ domain (Figure 10A). These amino acid substitutions did not impair Rif2 protein level, as protein extracts from wild type, *rif2-A78D*, *rif2-I295R*, and *rif2-L341S* cells contained similar amounts of Rif2 protein (Figure 10B). Interestingly, these three mutations affect residues facing a hydrophobic pocket within $Rif2^{AAA+}$ domain (Figure 10A), suggesting that their substitution with polar or charged residues impinges on the stability of the α helical bundle, affecting the interface of the $Rif2^{AAA+}$ domain towards the $Rap1^{RCT}$ domain. Furthermore, apart from the frameshift mutation in position 193 that deletes the majority of the Rif2 polypeptide, truncation of the C-terminus

past residue 364 or 387 by the frameshift mutations at codons 360 and 368, respectively, causes loss of the C-terminal tail, which is involved in the generation of the interface between Rif2 and Rap1. Altogether, these findings raise the possibility that most of the identified *rif2* mutations affect the interaction between Rif2 and Rap1, suggesting that the lack of this interaction is sufficient to restore DNA damage resistance of *rad50-VM* cells.

To investigate whether the missense mutations above could impair Rap1-Rif2 interaction, we focused on Rif2 L341S by exploiting a computational approach based on biased molecular dynamics simulations [Siebenmorgen *et al.*, 2019]. In detail, the simulation protocol was divided into two steps. First, a steered molecular dynamic (SMD) was performed in order to generate a series of configurations along the selected reaction coordinate, that is the separation of Rap1 and Rif2 proteins in the complex. Secondly, an actual umbrella sampling (US) simulation was performed on each single configuration obtained, in order to explore the whole trajectory of the complex dismantling. Finally, the absolute binding free energy can be deduced from the potential of mean force (PMF), which represents the free energy profile G along a given reaction coordinate ξ [Kirkwood, 1935]. In this case, the reaction coordinate is the separation of Rap1 and Rif2 and this allows calculating the difference in free energy within the regions of the phase space corresponding to bound and unbound states, giving an estimate of the free energy of binding (ΔG). As a control, in order to validate the dependability of the computational protocol, we tested the R747L amino acid substitution in Rap1, which is known to specifically affect the interaction between Rap1 and Rif2 [Feeser and Wolberger, 2008]. Consistently with a reduced $Rap1^{R747L}$-Rif2 interaction, the US simulation revealed a significant ΔG increase in the $Rap1^{R747L}$-Rif2 complex (–12.4 kcal/mol) compared to the wild-type Rap1-Rif2 complex (–16.2 kcal/mol) (Figure 10C and Figure 11A and B). Interestingly, a similar ΔG increase can be detected also in the Rap1-

Rif2^{L341S} complex (–13.1 kcal/mol) (Figure 10C and Figure 11A and C), suggesting that the Rif2 L341S mutation reduces the binding affinity between Rif2 and Rap1.

We directly tested this prediction by immunoprecipitating Rap1 from protein extracts from cells expressing either Rif2 or Rif2^{L341S} protein tagged with a Myc epitope. The amount of Rif2^{L341S} was under the detection level in Rap1 immunoprecipitates compared to wild-type Rif2 (Figure 10D), indicating that the Rif2 L341S mutation impairs Rap1-Rif2 interaction.

In addition to R747L, also the H709A amino acid substitution was shown to impair Rap1-Rif2 interaction [Feeser and Wolberger, 2008], whereas the D727A substitution specifically impairs the interaction between Rap1 and Rif1 [Feeser and Wolberger, 2008]. Consistently with the lack of Rap1-Rif2 interaction by the H709A and R747L amino acid substitutions, telomeres in *rap1-H709A* and *rap1-R747L* cells were as long as in *rif2-L341S* cells and the presence of either the *rap1-H709A* or the *rap1-R747L* allele did not further increase the length of telomeres of *rif2-L341S* cells (Figure 10E). To confirm that the lack of Rif2-Rap1 interaction is sufficient to restore DNA damage resistance of *rad50-VM* cells, we investigated the *in vivo* consequences of the *rap1-H709A*, *rap1-R747L*, and *rap1-D727A* alleles. Similar to the *rif2-L341S* allele, both *rap1-H709A* and *rap1-R747L* alleles, which did not cause DNA damage hypersensitivity by themselves (Figure 10F), suppressed the CPT and MMS sensitivity of *rad50-VM* cells, whereas the *rap1-D727A* allele did not (Figure 10G). Altogether, these data indicate that the lack of Rap1-Rif2 interaction is sufficient to restore DNA damage resistance of *rad50-VM* cells.

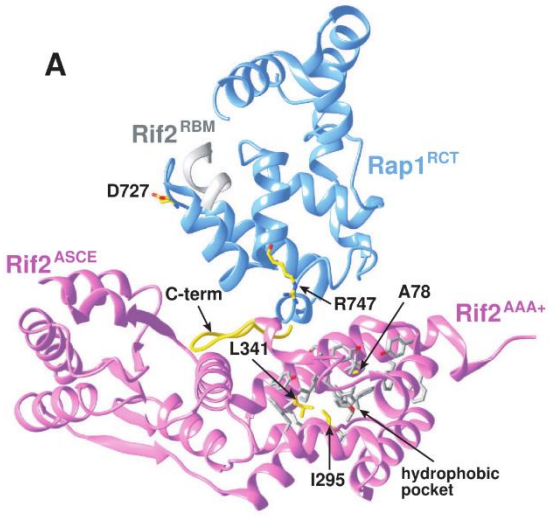
A
Rif2RBM
Rap1RCT
D727
Rif2ASCE
C-term
R747
A78
Rif2AAA+
L341
I295
hydrophobic pocket

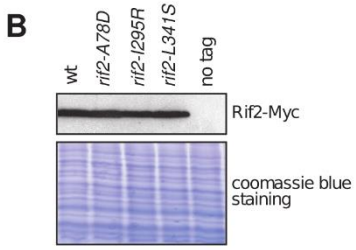
B
wt
rif2-A78D
rif2-I295R
rif2-L341S
no tag
Rif2-Myc
coomassie blue staining

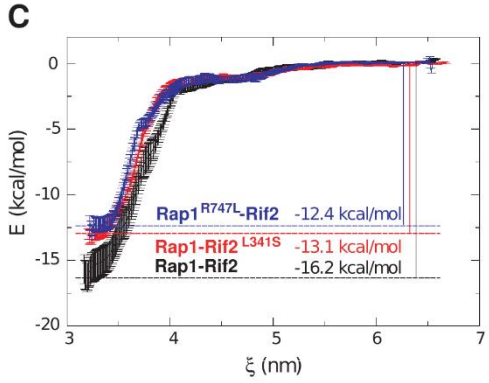
C
E (kcal/mol)
ξ (nm)
Rap1R747L-Rif2 -12.4 kcal/mol
Rap1-Rif2L341S -13.1 kcal/mol
Rap1-Rif2 -16.2 kcal/mol

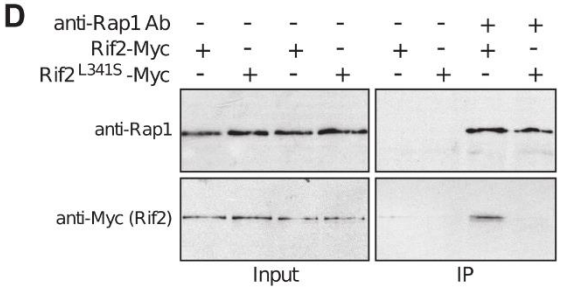
D
anti-Rap1 Ab
Rif2-Myc
Rif2L341S-Myc
anti-Rap1
anti-Myc (Rif2)
Input
IP

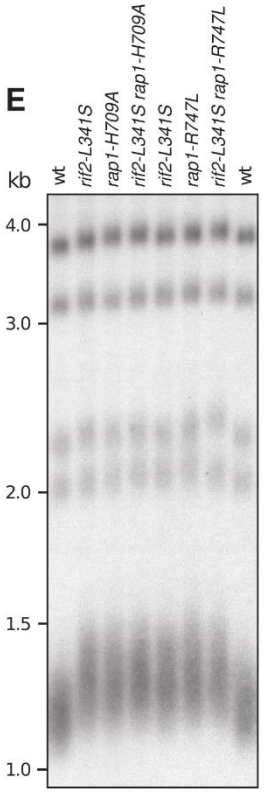
E
kb
wt
rif2-L341S
rap1-H709A
rif2-L341S rap1-H709A
rif2-L341S
rap1-R747L
rif2-L341S rap1-R747L
wt
4.0
3.0
2.0
1.5
1.0

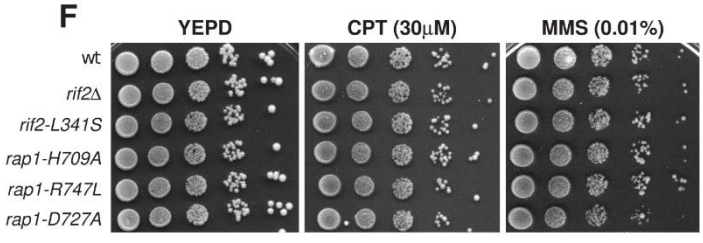
F
YEPD
CPT (30μM)
MMS (0.01%)
wt
rif2Δ
rif2-L341S
rap1-H709A
rap1-R747L
rap1-D727A

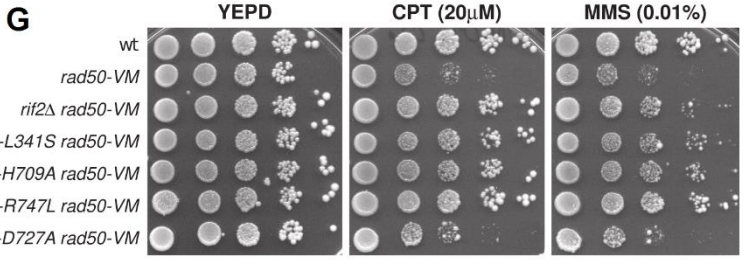
G
YEPD
CPT (20μM)
MMS (0.01%)
wt
rad50-VM
rif2Δ rad50-VM
rif2-L341S rad50-VM
rap1-H709A rad50-VM
rap1-R747L rad50-VM
rap1-D727A rad50-VM

Figure 10. The lack of Rif2-Rap1 interaction restores DNA damage resistance of *rad50-VM* cells.

(**A**) Structure of $Rap1^{RCT}$ (blue) and Rif2 (pink) (PDB code: 4BJ5) complex. The residues affected by the investigated mutations are shown in yellow. (**B**) Western blot analysis with anti-Myc antibodies of protein extracts from the indicated strains. The same amount of extracts was separated on an SDS-PAGE and stained with Coomassie Blue as loading control. (**C**) Average PMF ΔG calculated using Bayesian bootstrapping of umbrella histograms for binding/unbinding of Rap1-Rif2 (in black), Rap1-$Rif2^{L341S}$ (in red) and $Rap1^{R747L}$-Rif2 (in blue) complexes. Standard deviations of ΔG are indicated with vertical error bars. (**D**) Rap1-Rif2 interaction. Protein extracts prepared from exponentially growing cells expressing either Rif2-Myc or $Rif2^{L341S}$-Myc were analysed by western blotting with anti-Rap1 and anti-Myc antibodies either directly (Input) or after immunoprecipitation (IP) with anti-Rap1 antibody. (**E**) *Xho*I-cut genomic DNA prepared from exponentially growing cells was subjected to Southern blot analysis using a poly(GT) probe. (**F**, **G**) Exponentially growing cells were serially diluted (1:10) and each dilution was spotted out onto YEPD plates with or without CPT or MMS.

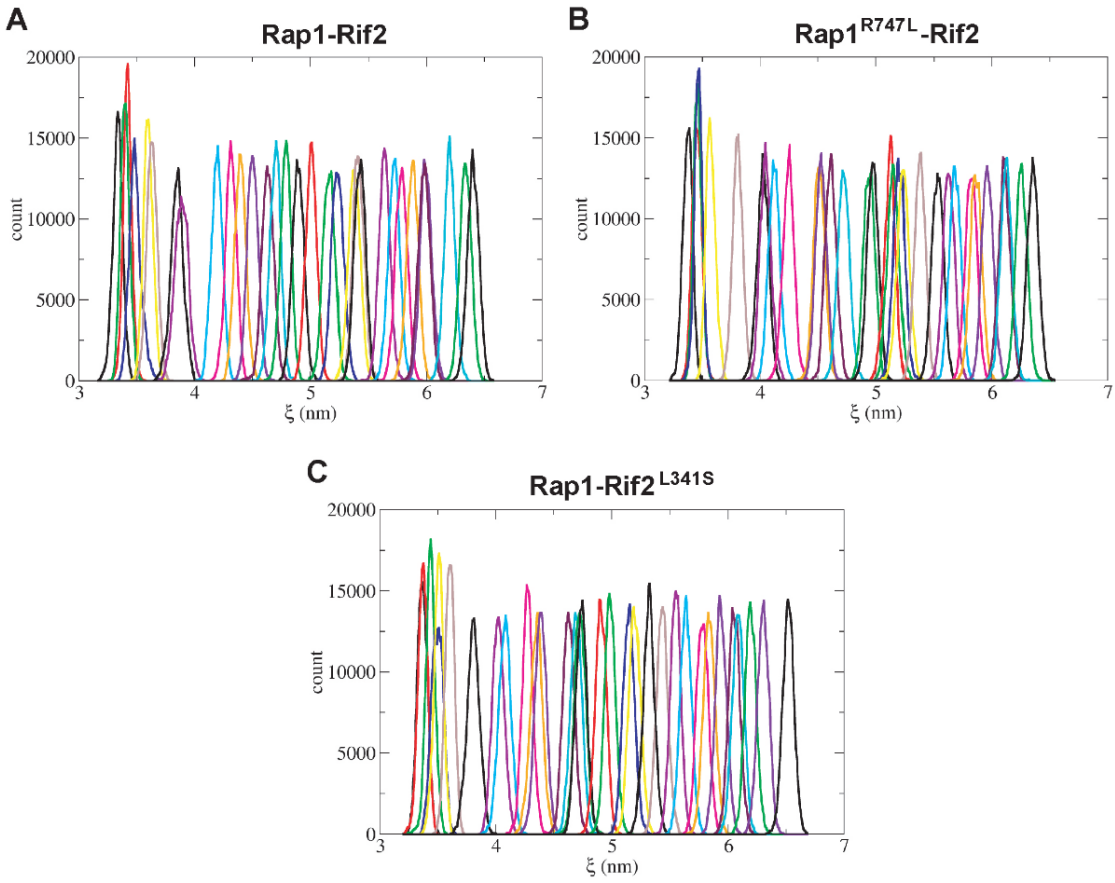

Figure 11. Histogram of umbrella sampling simulations for Rap1-Rif2 (A), Rap1^{R747L}-Rif2 (B), and Rap1-Rif2^{L341S} (C).

The lack of Rif2-Rap1 interaction increases MRX association to DNA ends and restores end-tethering in *rad50-VM* cells

The *rad50-VM* mutation reduces MRX association at broken DNA ends, and *RIF2* deletion suppressed this defect [Cassani *et al.*, 2016]. The finding that Rif2 L341S, Rap1 H709A, and Rap1 R747L amino acid substitutions restored DNA damage resistance of *rad50-VM* cells prompted us to investigate whether they also increased MRX persistence at DSBs. To detect MRX association at the DSB ends, we used JKM139 derivative strains, where a single DSB at the *MAT* locus can be generated by expression of the *HO* endonuclease gene under the control of a galactose-inducible promoter [Lee *et al.*, 1998]. To avoid the influence of DSB repair, this HO-induced DSB cannot be repaired by HR because the homologous donor loci *HML* and *HMR* are deleted. Furthermore, galactose was maintained in the medium to re-cleave the HO sites that were eventually reconstituted by NHEJ. Chromatin immunoprecipitation (ChIP) and quantitative real time PCR (qPCR) showed that, similar to *rif2*Δ cells, *rif2-L341S*, *rap1-H709A*, and *rap1-R747L* cells increased Rad50 association at the HO-induced DSB compared to wild-type cells (Figure 12A). By contrast, Rad50 association to DSBs was not enhanced by the *rap1-D727A* allele (Figure 12A), which did not restore DNA damage resistance of *rad50-VM* cells (Figure 10G). Thus, Rif2 appears to need to interact with Rap1 in order to negatively regulate MRX association to DSBs.

The poor MRX association at DSBs in *rad50-VM* cells does not impair DSB resection [Cassani *et al.*, 2016], while *rad50-VM* cells are defective in keeping the DSB ends tethered to each other [Cassani *et al.*, 2016]. Thus, we asked whether the $Rif2^{L341S}$, $Rap1^{H709A}$, and $Rap1^{R747L}$ variants could restore DNA damage resistance of *rad50-VM* cells by suppressing their end-tethering defect.

To this end, we used a yeast strain harboring a galactose-inducible HO endonuclease and an HO cleavage site at chromosome VII [Kaye *et al.*, 2004]. This strain was deleted for the endogenous HO sites at the *MAT*, *HML*, and *HMR* loci on chromosome III to ensure that the broken chromosomal fragments did not recombine with these loci. The DNA proximal to the HO-induced DSB can be visualized by binding of LacI-GFP fusion protein to multiple repeats of the LacI repressor binding site, *LacO*, that are integrated on both sides of the HO break site [Kaye *et al.*, 2004]. HO was induced by galactose addition to cells that were arrested in G2 with nocodazole and kept blocked in G2 by nocodazole treatment in order to ensure that all cells would arrest in metaphase. The majority of wild-type cells showed a single LacI-GFP focus both before and after HO induction, indicating their ability to keep the broken DNA ends together (Figure 12B). Consistently with previous results [Cassani *et al.*, 2016], *rad50-VM* cells showed an increase of two LacI-GFP spots at 1-2 h after HO induction (Figure 12B), indicating an end-tethering defect. Similar to *rif2*Δ, the presence of the *rif2-L341S*, *rap1-H709A* or *rap1-R747L* allele reduced the number of *rad50-VM* cells showing two LacI-GFP spots after HO induction (Figure 12B), indicating that these *rif2* and *rap1* alleles suppressed the *rad50-VM* end-tethering defect. As the maintenance of the DSB ends in close proximity is important to repair a DSB by both NHEJ and HR [Kaye *et al.*, 2004; Lobachev *et al.*, 2004; Clerici *et al.*, 2005; Nakai *et al.*, 2011], this restored end-tethering could explain the suppression of the DNA damage sensitivity of *rad50-VM* cells by the corresponding $Rif2^{L341S}$, $Rap1^{H709A}$, and $Rap1^{R747L}$ variants.

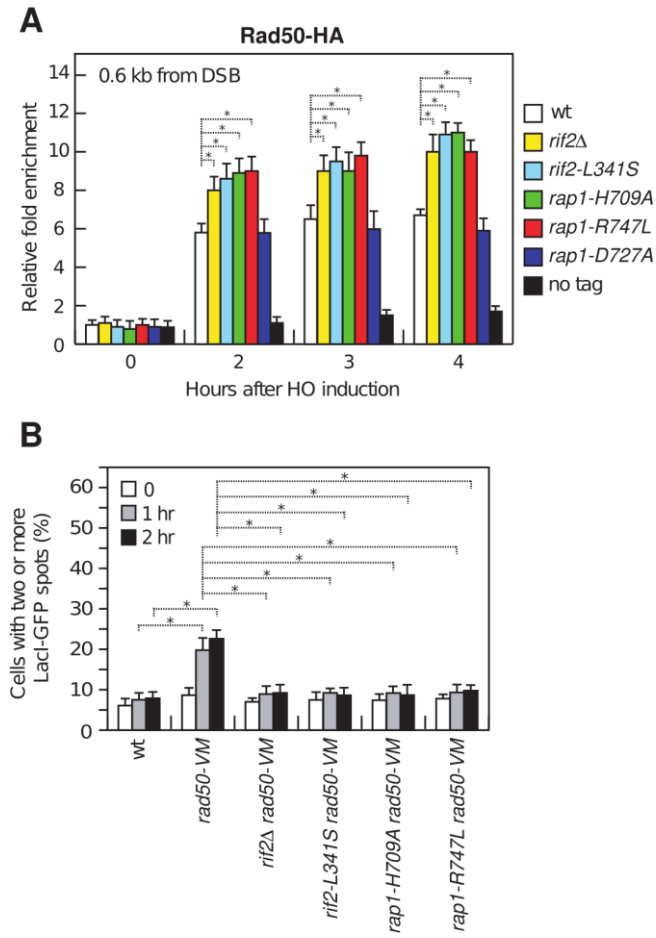

Figure 12. The lack of Rif2-Rap1 interaction increases MRX association to DSBs and restores end-tethering in *rad50-VM* cells.

(**A**) ChIP analysis and qPCR. Exponentially growing YEPR cells were transferred to YEPRG at time zero to induce HO. Relative fold enrichment of Rad50-HA fusion protein at the indicated distances from the HO cleavage site was determined after ChIP with anti-HA antibody and qPCR. (**B**) End-tethering. Exponentially growing YEPR cell cultures were arrested in G2 with nocodazole at time zero and transferred to YEPRG in the presence of nocodazole. 200 cells for each strain were analyzed to determine the percentage of cells showing two or more LacI-GFP foci. In all graphs, mean values are represented with error bars denoting s.d. (n = 3). *P< 0.05 (Student's t-test).

Rap1 binds to DSBs and promotes Rif2 association to them

Rif2 was shown to associate to DSBs, spreading to 2 kb from the HO cleavage site [Cassani *et al.*, 2016]. Because the lack of Rap1-Rif2 interaction is sufficient to increase both DNA damage resistance of *rad50-VM* cells and MRX association to DSBs, we asked whether Rap1 is bound at DSBs and promotes Rif2 association to them. In fact, although Rap1 is known to bind a DNA recognition sequence consisting of two half-sites of 5 bp separated by 1 or 3 bp, it is also capable to bind *in vitro* a single half-site [Del Vescovo *et al.*, 2004] or even a random dsDNA sequence [Feldmann *et al.*, 2014]. Following HO induction by galactose addition, Rap1 was efficiently recruited close to the HO-induced DSB (Figure 13A). Furthermore, the $Rap1^{H709A}$ and $Rap1^{R747L}$ variants reduced Rif2 association at both the HO-induced DSB (Figure 13B) and telomeres (Figure 13C), whereas $Rap1^{D727A}$ did not (Figure 13B and C). This reduced Rif2 association at both DSBs and telomeres is not due to different amount of Rap1 or Rif2 protein, as similar amounts of Rap1 and Rif2 proteins could be detected in protein extracts from wild type, *rap1-H709A*, *rap1-R747L*, and *rap1-D727A* cells (Figure 13D). Finally, the Rif2 L341S amino acid substitution, which impaired Rif2-Rap1 interaction (Figure 10C and D), decreased Rif2 association at both the HO-induced DSB (Figure 13B) and telomeres (Figure 13C). Thus, Rap1 supports Rif2 functions in controlling MRX activity by promoting Rif2 association/persistence at DSBs.

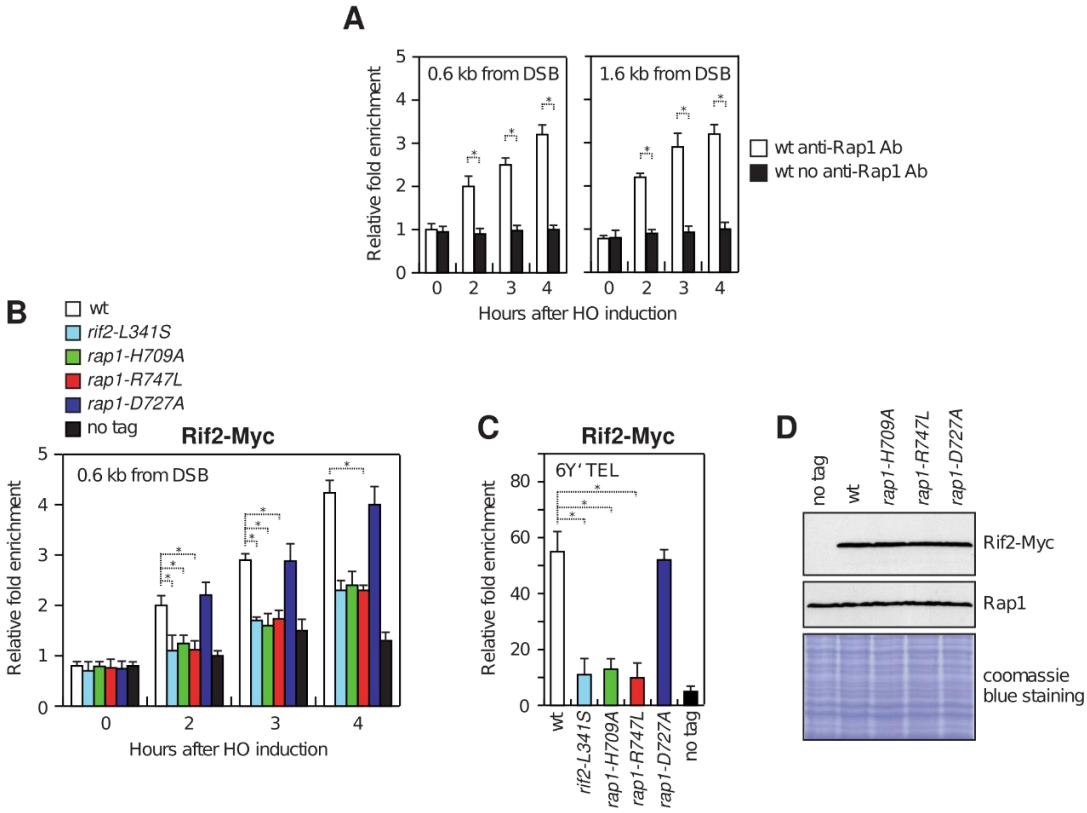

Figure 13. Rap1 is recruited to DSB ends and mediates Rif2 association at both DSBs and telomeres.

(**A**) ChIP analysis and qPCR. Exponentially growing YEPR cell cultures were transferred to YEPRG at time zero to induce HO. Relative fold enrichment of Rap1 at the indicated distances from the HO cleavage site was determined after ChIP with anti-Rap1 antibody and qPCR. (**B**) As in (**A**) but showing Rif2-Myc. (**C**) Relative fold enrichment of Rif2-Myc at six different Y'-containing telomeres (6Y') compared to a non-telomeric locus (*ARO1*) after ChIP with anti-Myc antibody and qPCR. (**D**) Western blot analysis with anti-Myc and anti-Rap1 antibodies of extracts used for the ChIP analysis shown in (**B**) and (**C**). The same amounts of extracts were separated on an SDS-PAGE and stained with Coomassie Blue as loading control. In all graphs, mean values are represented with error bars denoting s.d. ($n = 3$). *$P < 0.05$ (Student's *t*-test).

The Rap1 R381W, P520L and D555N mutations exacerbate the DNA damage sensitivity and the end-tethering defect of *rad50-VM* cells by reducing MRX association to DSBs

As Rap1 is essential for cell viability, to better understand the function of Rap1 at DSBs, we searched for *rap1* mutations that either suppressed or exacerbated the hypersensitivity to DNA damaging agents of *rad50-VM* cells. We used low-fidelity PCR to randomly mutagenize *RAP1* gene and *rad50-VM* cells were transformed with the *RAP1* PCR products in order to substitute the corresponding *RAP1* wild-type sequence with the mutagenized DNA fragments. Transformants clones were then screened for either increased or decreased viability in the presence of CPT compared to *rad50-VM* cells. This screen yielded three *rap1* alleles exacerbating the sensitivity of *rad50-VM* cells not only to CPT but also to MMS (Figure 14A), whereas no *rap1* alleles restoring DNA damage resistance in the same cells were identified. All the identified *rap1* alleles also exacerbated the CPT and MMS hypersensitivity of *rad50-VM tel1*Δ (Figure 14B), indicating that this effect does not require Tel1. Sequence analysis revealed that the three *rap1* alleles contained single missense mutations resulting in the amino acid changes R381W, P520L or D555N, which are all located in the Rap1 DNA binding domain (Figure 14C).

As the R381W, P520L, and D555N amino acid substitutions sensitized *rad50-VM* cells to DNA damaging agents, we investigated whether they decreased MRX association to DSBs. This was indeed the case. In fact, although similar amounts of Rad50 could be detected in protein extracts from wild-type, *rap1-R381W*, *rap1-P520L*, and *rap1-D555N* cells (Figure 14D), the amount of Rad50 bound at the HO-induced DSB was decreased in *rap1-R381W*, *rap1-P520L*, and *rap1-D555N* cells compared to wild-type cells (Figure 14E).

As both Rap1^{R381W} and Rap1^{P520L} exacerbated the DNA damage sensitivity of *rad50-VM* cells (Figure 14A) and decreased MRX association to DSBs (Figure 14E), we asked whether they impair end-tethering and/or exacerbate the end-tethering defect of *rad50-VM* cells. As expected, *rad50-VM* cells showed an increase of two LacI-GFP spots after HO induction compared to wild-type cells (Figure 14F). A similar increase in the frequency of two LacI-GFP foci was observed also in *rap1-R381W* and *rap1-P520L* cells compared to wild type (Figure 14F), indicating an end-tethering defect. This frequency was further increased in *rap1-R381W rad50-VM* and *rap1-P520L rad50-VM* double mutants compared to each single mutant (Figure 14F), suggesting that the increased DNA damage sensitivity of the double mutants compared to each single mutant can be due to a more severe end-tethering defect.

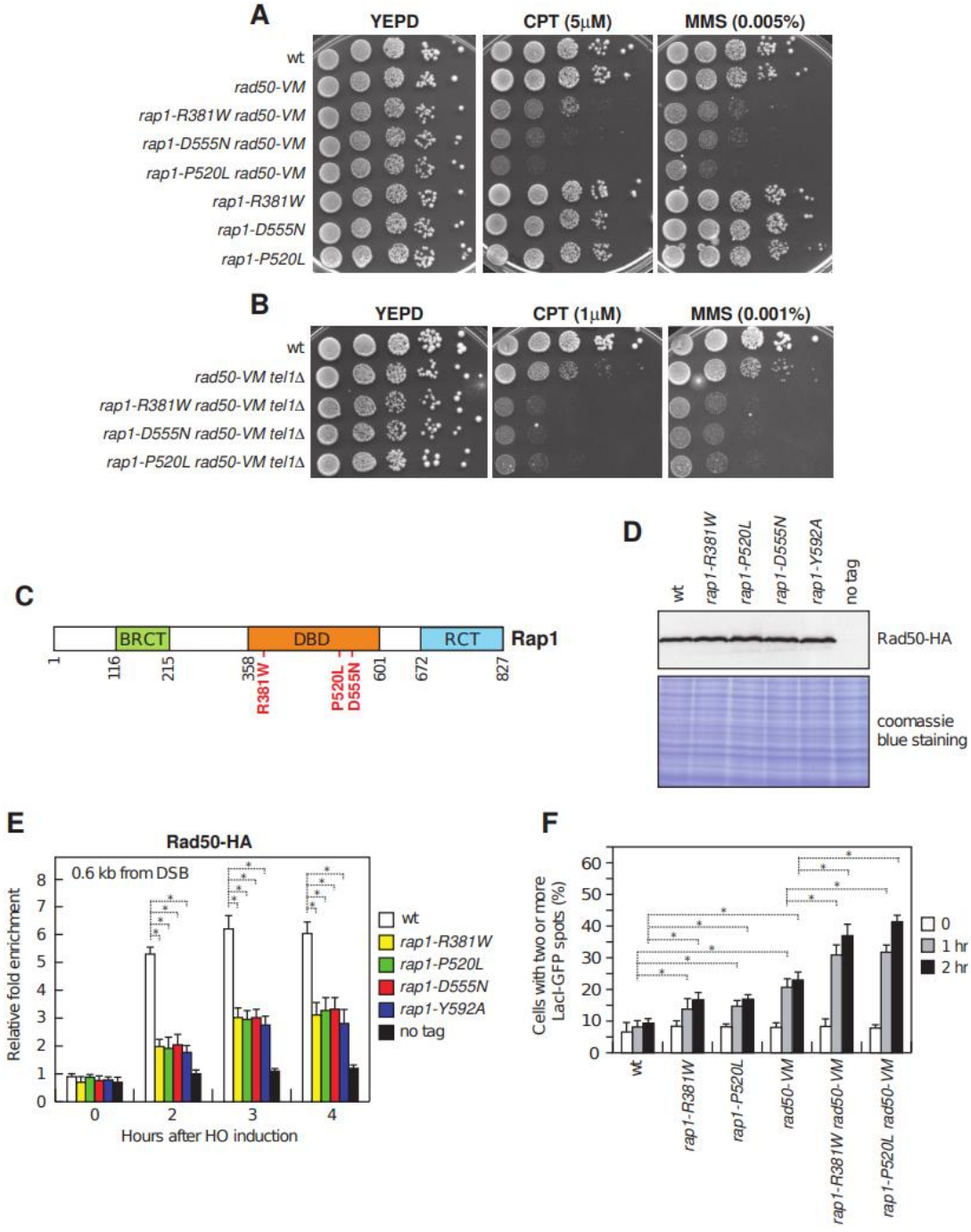
A
YEPD
CPT (5μM)
MMS (0.005%)
wt
rad50-VM
rap1-R381W rad50-VM
rap1-D555N rad50-VM
rap1-P520L rad50-VM
rap1-R381W
rap1-D555N
rap1-P520L
B
YEPD
CPT (1μM)
MMS (0.001%)
wt
rad50-VM tel1Δ
rap1-R381W rad50-VM tel1Δ
rap1-D555N rad50-VM tel1Δ
rap1-P520L rad50-VM tel1Δ
C
BRCT
DBD
RCT
Rap1
1
116
215
358
601
672
827
R381W
P520L
D555N
D
wt
rap1-R381W
rap1-P520L
rap1-D555N
rap1-Y592A
no tag
Rad50-HA
coomassie blue staining
E
Rad50-HA
0.6 kb from DSB
Relative fold enrichment
Hours after HO induction
wt
rap1-R381W
rap1-P520L
rap1-D555N
rap1-Y592A
no tag
F
Cells with two or more Lacl-GFP spots (%)
0
1 hr
2 hr
wt
rap1-R381W
rap1-P520L
rad50-VM
rap1-R381W rad50-VM
rap1-P520L rad50-VM

Figure 14. Identification of *rap1* alleles that exacerbate the DNA damage sensitivity of *rad50-VM* cells by decreasing MRX association to DSBs.
(**A**, **B**) Exponentially growing cells were serially diluted (1:10) and each dilution was spotted out onto YEPD plates with or without CPT or MMS. (**C**) Position of the mutations within the Rap1 sequence. (**D**) Western blot analysis with anti-HA antibodies of extracts used for the ChIP analysis shown in (**E**). The same amounts of extracts were separated on an SDS-PAGE and stained with Coomassie Blue as loading control. (**E**) ChIP analysis and qPCR. Exponentially growing YEPR cell cultures were transferred to YEPRG at time zero to induce HO. Relative fold enrichment of Rad50-HA at the indicated distance from the HO cleavage site was determined after ChIP with anti-HA antibody and qPCR. (**F**) End-tethering. Exponentially growing YEPR cell cultures were arrested in G2 with nocodazole at time zero and transferred to YEPRG in the presence of nocodazole. 200 cells for each strain were analyzed to determine the percentage of cells showing two or more LacI-GFP foci. In all graphs, mean values are represented with error bars denoting s.d. (n = 3). *P< 0.05 (Student's t-test).

The Rap1 R381W and P520L mutations cause hypersilencing and telomere shortening

The finding that *rap1-R381W*, *rap1-P520L*, and *rap1-D555N* mutant cells display phenotypes opposite to *rif2* or *rap1* alleles impairing Rap1 or Rif2 interaction, respectively, suggests that they may encode hypermorphic Rap1 mutant variants. As Rap1 dysfunction can lead to telomere lengthening [Sussel and Shore, 1991; Lustig *et al.*, 1990] and loss of silencing at both *HM* loci and telomeres [Kurtz and Shore, 1991; Sussel and Shore, 1991; Kyrion *et al.*, 1993], we tested the above hypothesis by evaluating these two processes in the mutants. While, as expected [Wotton and Shore, 1997; Kyrion *et al.*, 1993], the lack of $Rap1^{RCT}$ (*rap1-ΔC* in Figure 15A), which mediates Rap1 interaction with Rif1 and Rif2, caused telomere overelongation, telomeres in *rap1-R381W* and *rap1-P520L* cells were shorter than in wild-type cells, whereas the *rap1-D555N* allele did not alter telomere length (Figure 15A).

To examine transcriptional silencing, we inserted the *rap1* alleles in strains carrying the only copy of the *URA3* gene inserted next to the left telomere of chromosome VII or at the *HMLα* locus [Gottschling *et al.*, 1990]. Repression of *URA3* expression can be detected by testing the ability of cells to form colonies on 5-fluoroorotic acid (5-FOA), which kills *URA3* expressing cells. The *rap1-R381W*, *rap1-P520L*, and *rap1-D555N* mutants showed increased *URA3* silencing at both *HMLα* (Figure 15B) and telomeres (Figure 15C) compared to wild type. Hypersilencing in all the above *rap1* mutants was completely dependent on Sir proteins, as the lack of *SIR3* abolished the ability of *rap1-R381W*, *rap1-P520L*, and *rap1-D555N* cells to form colonies on 5-FOA (Figure 15C). Altogether, these findings indicate that the *rap1-R381W*, *rap1-P520L*, and *rap1-D555N* alleles encode hypermorphic Rap1 variants that increase

Rap1 functions in both telomerase repression and transcriptional silencing at *HM* loci and at telomeres.

Next, we measured the association of $Rap1^{R381W}$, $Rap1^{P520L}$, and $Rap1^{D555N}$ to both DSBs and telomeres by ChIP analysis and qPCR. Although the R381W, P520L, and D555N mutations did not alter Rap1 protein level (Figure 15D), the amount of $Rap1^{R381W}$, $Rap1^{P520L}$, and $Rap1^{D555N}$ bound at the HO-induced DSB was higher than that of wild-type Rap1 (Figure 15E). Similarly, the R381W, P520L, and D555N mutations increased Rap1 association at telomeres (Figure 15F). These findings suggest that the increased ability of these Rap1 variants to inhibit telomere elongation and MRX association at both telomeres and DSBs, as well as to repress transcription at least at telomeres could be due to their enhanced persistence to DNA ends.

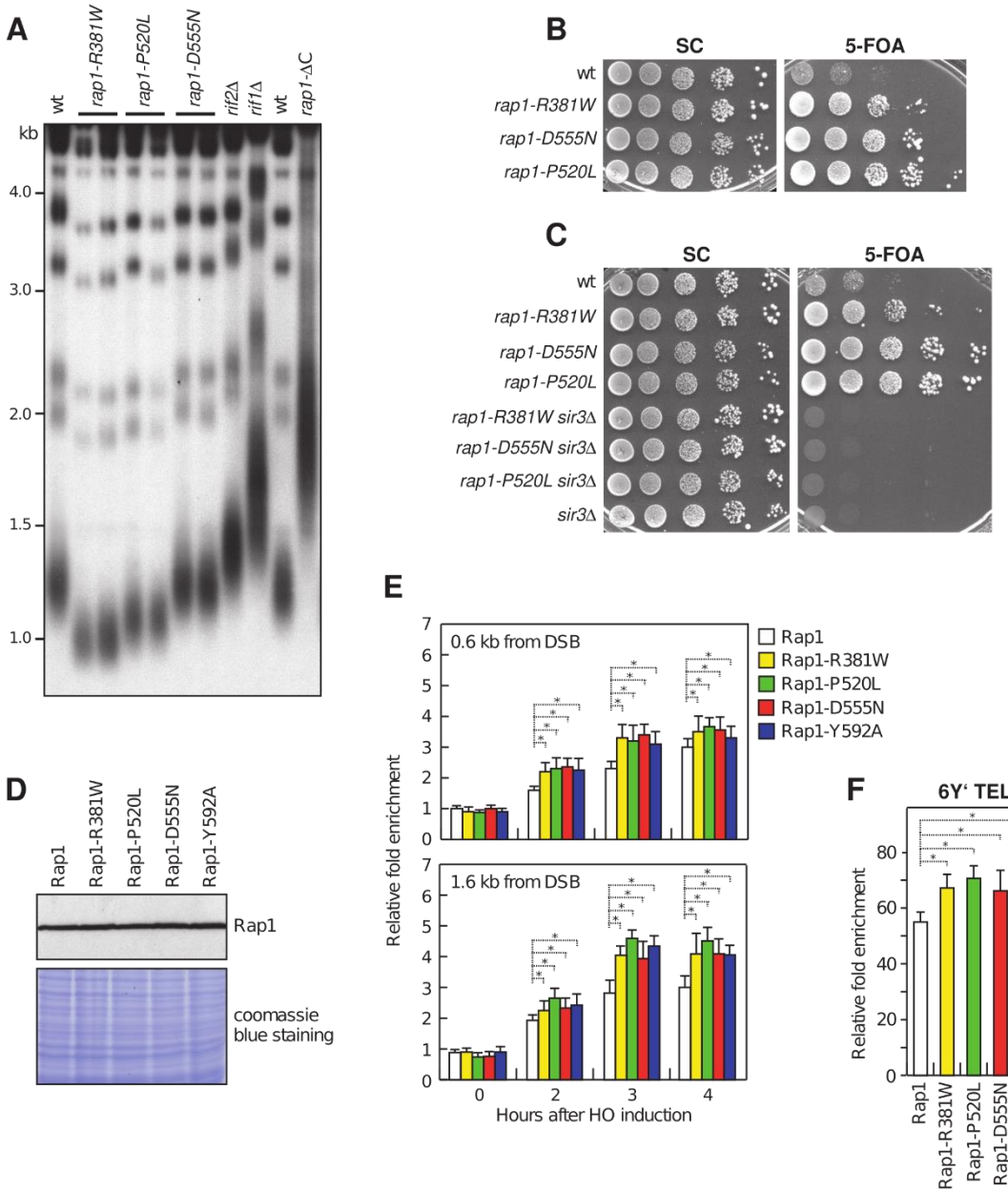
A
wt
rap1-R381W
rap1-P520L
rap1-D555N
rif2Δ
rif1Δ
wt
rap1-ΔC
kb
4.0
3.0
2.0
1.5
1.0
B
SC
5-FOA
wt
rap1-R381W
rap1-D555N
rap1-P520L
C
SC
5-FOA
wt
rap1-R381W
rap1-D555N
rap1-P520L
rap1-R381W sir3Δ
rap1-D555N sir3Δ
rap1-P520L sir3Δ
sir3Δ
D
Rap1
Rap1-R381W
Rap1-P520L
Rap1-D555N
Rap1-Y592A
Rap1
coomassie blue staining
E
0.6 kb from DSB
1.6 kb from DSB
Relative fold enrichment
Hours after HO induction
Rap1
Rap1-R381W
Rap1-P520L
Rap1-D555N
Rap1-Y592A
F
6Y' TEL
Relative fold enrichment
Rap1
Rap1-R381W
Rap1-P520L
Rap1-D555N
Rap1-Y592A

Figure 15. Effects of the *rap1* alleles on telomere length and transcriptional silencing.

(**A**) *Xho*I-cut genomic DNA prepared from exponentially growing cells was subjected to Southern blot analysis using a poly(GT) probe. (**B**, **C**) Exponentially growing cells carrying the *URA3* gene at the *HML*α locus (**B**) or at telomere VII-L (**C**) were serially diluted (1:10) and each dilution was spotted out onto complete synthetic medium (SC) and onto the same medium supplied with 5-FOA (5-FOA) to assay for *URA3* expression. (**D**) Western blot analysis with anti-Rap1 antibodies of extracts used for the ChIP analysis shown in (**E**) and (**F**). (**E**) ChIP analysis and qPCR. Exponentially growing YEPR cell cultures were transferred to YEPRG at time zero to induce HO. Relative fold enrichment of the indicated proteins at the indicated distances from the HO cleavage site was determined after ChIP with anti-Rap1 antibody and qPCR. (**F**) Relative fold enrichment of the indicated protein at six different Y'-containing telomeres (6Y') compared to a non-telomeric locus (*ARO1*) after ChIP with anti-Rap1 antibody and qPCR analysis. In all graphs, plotted values are the mean values with error bars denoting s.d. (n = 3). *P< 0.05 (Student's t-test).

The Rap1 R381W and P520L mutations change the affinity of Myb-like domains for DNA in opposite manners

The Rap1^{DBD} consists of two tandem Myb-like motifs, followed by a C-terminal wrapping loop [Konig *et al.*, 1996; Taylor *et al.*, 2000; Matot *et al.*, 2012]. While R381 resides in the N-terminal Myb-like domain (Myb-N), P520 and D555 are localized in the C-terminal Myb-like domain (Myb-C) (PDB code: 3UKG) (Figure 16A). In particular, R381 forms several hydrogen bonds with surrounding residues, likely conferring stability to the helix-loop-helix folding. By contrast, P520 is localized in a quite rigid loop surrounding the C-terminal Myb-like domain, facing the DNA but with no significant interaction with it. Finally, the D555 residue is situated on the other side of the Myb-C domain, on the side not facing the DNA (Figure 16A), and its role is not trivial to speculate; however, as the Myb-like domains are involved in the binding to telomeric repeat DNA in a sequence-specific manner, the location of D555 aminoacid, that does not directly involve DNA contact, might explain why the corresponding mutation did not affect telomere length.

We focused on R381W and P520L mutations to test their effect on the DNA binding properties of Myb-N and Myb-C domains by biased molecular dynamics simulations. Models representing Myb-N or Myb-C domain bound to DNA were generated starting from the structure of Rap1^{DBD} bound to telomeric DNA (PDB code 3UKG). The R381W mutation was introduced in the Myb-N model, whereas the P520L mutation was introduced in the Myb-C model. PMF was calculated both for DNA-Myb-N^{R381W} (Figure 16B and Figure 17A and B) and DNA-Myb-C^{P520L} (Figure 16C and Figure 17C and D) and these PMFs were compared with those of wild-type DNA-Myb-N and wild-type DNA-Myb-C, respectively.

Consistently with the ChIP results showing increased Rap1^{R381W} binding at both DSBs and telomeres compared to wild-type Rap1 (Figure 15E and F), the R381W mutation increases the binding affinity of Myb-N for dsDNA, reducing the ΔG from −17.1 kcal/mol to −23.3 kcal/mol (Figure 16B).

By contrast, although Rap1^{P520L} showed increased association at both DSBs and telomeres by ChIP (Figure 15E and F), the P520L mutation appears to significantly decrease the stability of the DNA-Myb-C complex by increasing the ΔG from −20.0 kcal/mol to −13.4 kcal/mol (Figure 16C), suggesting that this mutation decreases the binding affinity of the Myb-C domain for dsDNA.

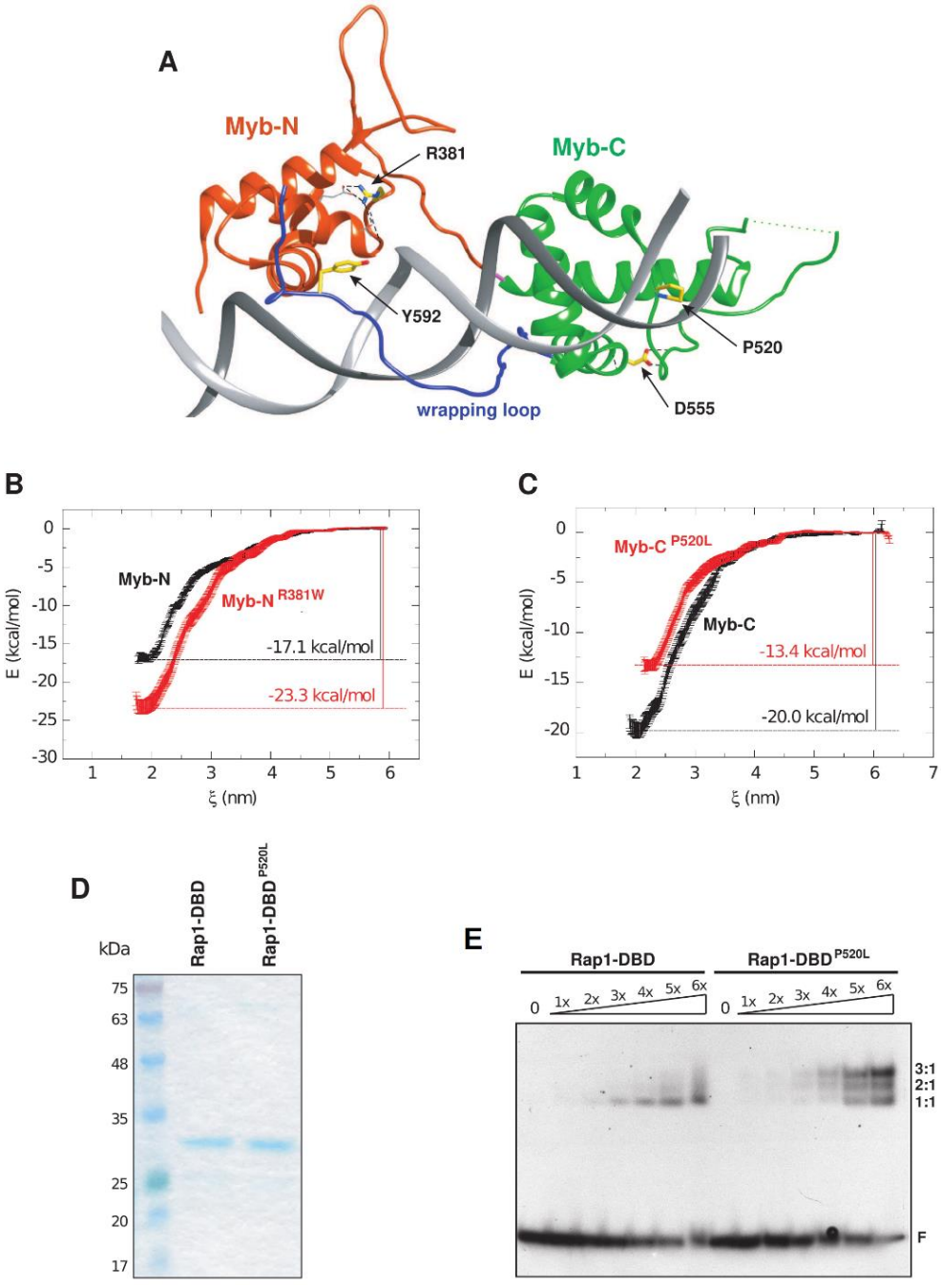
A
Myb-N
R381
Myb-C
Y592
P520
wrapping loop
D555
B
Myb-N
Myb-N R381W
-17.1 kcal/mol
-23.3 kcal/mol
E (kcal/mol)
ξ (nm)
C
Myb-C P520L
Myb-C
-13.4 kcal/mol
-20.0 kcal/mol
E (kcal/mol)
ξ (nm)
D
kDa
Rap1-DBD
Rap1-DBD P520L
75
63
48
35
25
20
17
E
Rap1-DBD
Rap1-DBD P520L
0 1x 2x 3x 4x 5x 6x
0 1x 2x 3x 4x 5x 6x
3:1
2:1
1:1
F

Figure 16. Effect of the Rap1 R381W and P520L mutations on the DNA binding properties of the Myb-like domains.
(**A**) Structure of the high affinity complex between $Rap1^{DBD}$ and telomeric DNA (PDB code: 3UKG). The residues affected by the investigated mutations are shown in yellow. (**B**) Average PMF ΔG calculated using Bayesian bootstrapping of umbrella histograms for binding/unbinding of DNA-Myb-N (black) and DNA-Myb-N^{R381W} (red) complexes. (**C**) Average PMF ΔG calculated using Bayesian bootstrapping of umbrella histograms for binding/unbinding of DNA-Myb-C (black) and DNA-Myb-C^{P520L} (red) complexes. In (**B**) and (**C**), standard deviations of ΔG are indicated with vertical error bars. (**D**) SDS-PAGE for analysis of purified Rap1-DBD and Rap1-DBD^{P520L} and stained with Gel-Code Blue after electrophoresis. (**E**) EMSA with a 21 bp dsDNA and increasing concentrations of Rap1-DBD and Rap1-DBD^{P520L}. Bands corresponding to free DNA (F), and protein-DNA complexes with different stoichiometry (1:1; 2:1; 3:1) are denoted.

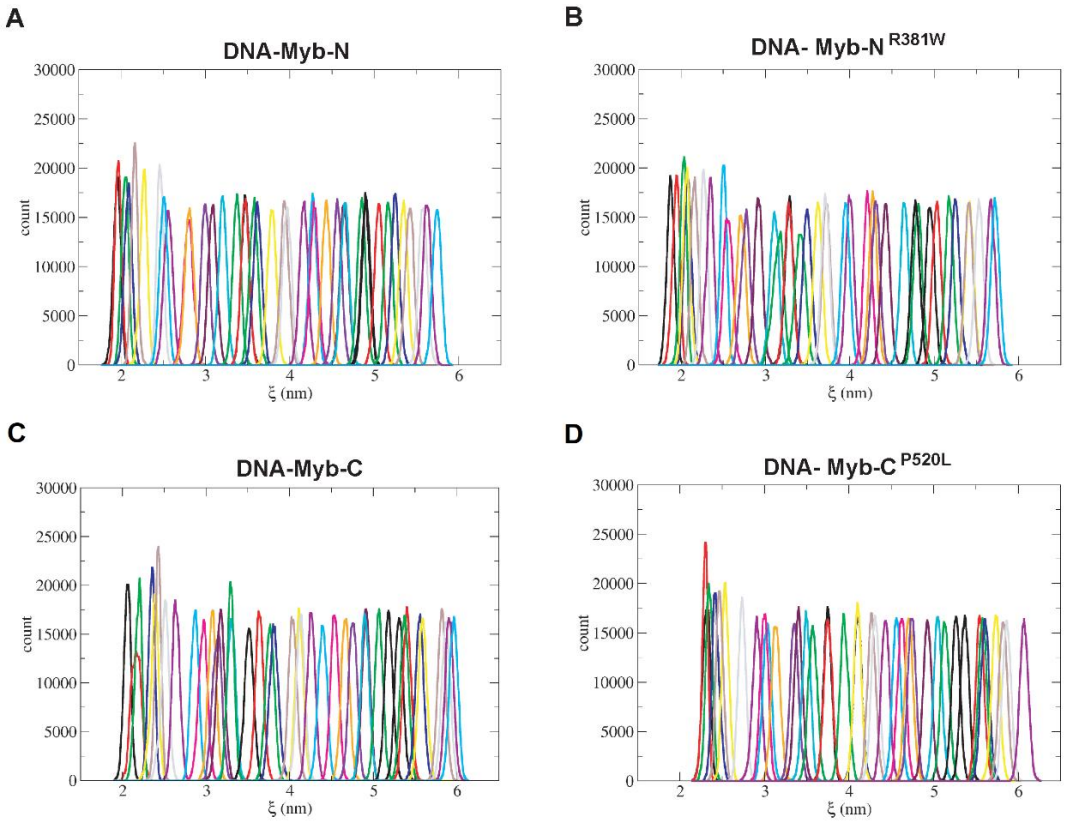

Figure 17. Histogram of umbrella sampling simulations for DNA-Myb-N (A), DNA-Myb-N^{R381W} (B), DNA-Myb-C (C) and DNA-Myb-C^{P520L} (D).

The Rap1 P520L mutation favours formation of high Rap1 stoichiometry complexes on DNA

The Rap1^{DBD} domain binds dsDNA molecules *in vitro* in two different binding modes: a high affinity mode, where the two Myb-like domains both bind dsDNA, and a low affinity mode, where only a single Myb-like domain binds dsDNA [Feldmann and Galletto, 2014; Feldmann *et al.*, 2015]. The presence of a single Myb-like domain on dsDNA has been proposed to allow the binding of multiple Rap1 molecules leading to the formation of Rap1-DNA complexes with high stoichiometry [Feldmann and Galletto, 2014; Feldmann *et al.*, 2015]. As the P520L mutation appears to decrease the affinity of Myb-C for DNA, the increased Rap1^{P520L} association to both DSBs and telomeres detected by ChIP might be due to a destabilization of the clamped structure of Rap1^{DBD}, which would facilitate the binding of multiple Rap1 molecules in a conformation where only Myb-N takes contact to DNA. We therefore analyzed the consequence of P520L amino acid substitution on Rap1^{DBD} ability to bind dsDNA by gel electrophoretic mobility shift assay (EMSA). Both wild-type and mutant Rap1^{DBD} domains, comprising residues 358-601, were expressed and purified from *Escherichia coli* cells as soluble proteins (Figure 16D) and tested for the ability to bind a 21 bp dsDNA substrate carrying the canonical telomeric Rap1 DNA recognition sequence consisting of two hemisites spaced by 3 bp. A fixed amount of DNA binding site was incubated with increasing concentrations of purified Rap1^{DBD} and complex formation was analyzed by EMSA. As previously reported [Taylor *et al.*, 2000; Feldmann and Galletto, 2014; Feldmann *et al.*, 2015], wild-type Rap1^{DBD} was capable to form a 1:1 DBD-DNA complex and increasing Rap1 concentration revealed the appearance of a second faint band (2:1), possibly representing the binding to DNA of more than one DBD molecule (Figure 16E). By contrast, DBD^{P520L} showed a reduction of 1:1 DBD-DNA

complex and the appearance not only of a second (2:1) but also of a third (3:1) band (Figure 16E), suggesting that the P520L amino acid substitution favours transition to higher order DBD^{P520L}-DNA complexes.

Destabilization of the wrapping loop increases Rap1 association to DNA ends and Rap1 activation

As removal of the wrapping loop was shown to favour the transition to a high stoichiometry binding mode [Feldmann *et al.*, 2015], we investigated the consequences of substituting to alanine the Rap1 Y592 residue, which is located on the tip of the loop and contributes to lock the loop around DNA (Figure 16A) [Matot *et al.*, 2012]. The Y592A mutation turned out to increase the DNA damage sensitivity of *rad50-VM* cells (Figure 18A) and to reduce Rad50 association to DSBs (Figure 14E) without altering Rad50 protein level (Figure 14D). Furthermore, although this mutation was shown to decrease Rap1 affinity for dsDNA *in vitro* [Matot *et al.*, 2012], the amount of Rap1^{Y592A} bound at both DSBs and telomeres, as measured by ChIP and qPCR, was higher than that of wild-type Rap1 (Figure 15E and F). This effect was not due to increased level of the mutant protein, as similar amounts of Rap1 were detected in protein extracts from wild-type and *rap1-Y592A* cells (Figure 15D).

As *rap1-Y592A* cells showed reduced cell viability even in the absence of DNA damaging agents (Figure 18A), we could not test their ability to grow on 5-FOA, but we assessed the effect of the Y592A mutation on silencing by evaluating the expression of the *ADE2* reporter gene integrated into a telomeric region using a color-based system [Gottschling *et al.*, 1990]. Expression of *ADE2* results in white colonies, whereas cells that do not express *ADE2* form red-pigmented colonies. When the *ADE2* gene was placed on a telomere such that *ADE2* transcription was directed toward the telomere, cells developed sectored colonies due to transcriptional silencing [Gottschling *et al.*, 1990]. The *rap1-Y592A* allele was introduced in UCC3537 strain, carrying the only copy of the *ADE2* gene inserted into the telomeric region of chromosome V-R. As shown in Figure 18B,

most of wild-type colonies were white or red-sectored indicating that the *ADE2* gene was expressed in most cells. By contrast, most *rap1-Y592A* mutant colonies were completely red, indicating that the telomere-associated *ADE2* gene was transcriptionally silent. The hypersilencing phenotype displayed by *rap1-Y592A* cells was dependent on Sir proteins, as *rap1-Y592A* cells were unable to generate red or sectored colonies in the absence of *SIR3* (Figure 18B).

The Y592A mutation also leads to telomere shortening, as telomeres in *rap1-Y592A* cells were shorter than in wild type and even shorter than in *rap1-R381W* and *rap1-P520L* cells (Figure 18C). Altogether, these data indicate that destabilization of the wrapping domain results in phenotypes similar to those found in the presence of the $Rap1^{P520L}$ variant.

Rap1^{P520L} and Rap1^{Y592A}, but not Rap1^{R381W}, act at both DSBs and telomeres independently of Rif2

Structural studies have shown that the interaction of both Rap1 Myb-like domains with DNA leads to an orientation of the RCT domain almost perpendicular to the DNA axis and this configuration has been proposed to favour RCT interaction with its partners [Matot *et al.*, 2012]. As Rap1 binds Rif2 through the RCT domain, the above hypothesis raises the possibility that both Rap1^{P520L} and Rap1^{Y592A}, which should bind DNA *via* a single Myb-like domain, may be defective in recruiting Rif2 to DNA, whereas Rap1^{R381W}, which should bind DNA with both Myb-like domains, should be able to do it.

We thus investigated whether Rap1^{R381W}, Rap1^{P520L} and/or Rap1^{Y592A} proteins required Rif2 to sensitize *rad50-VM* cells to DNA damaging agents and/or to cause telomere shortening. As expected, *rap1-R381W rad50-VM* cells were more sensitive to DNA damaging agents compared to *rad50-VM* cells (Figure 18D). *RIF2* deletion restored DNA damage resistance not only in *rad50-VM* but also in *rap1-R381W rad50-VM* cells (Figure 18D), indicating that Rap1-R381W needs Rif2 to sensitize *rad50-VM* cells to DNA damaging agents. Furthermore, while *rap1-R381W* cells displayed short telomeres, telomeres in *rif2*Δ *rap1-R381W* cells were as long as in *rif2*Δ cells (Figure 18E). Thus, Rap1^{R381W} appears to act through Rif2 to negatively regulate both MRX function at DSBs and telomere length.

By contrast, *RIF2* deletion was almost unable to restore DNA damage resistance of *rad50-VM* cells carrying the *rap1-Y592A* (Figure 18A) or *rap1-P520L* allele (Figure 18D), indicating that Rap1^{P520L} and Rap1^{Y592A} sensitize *rad50-VM* cells in a Rif2-independent manner. Furthermore, telomeres in *rif2*Δ *rap1-P520L* and *rif2*Δ *rap1-Y592A* cells were shorter than in *rif2*Δ cells, although not as short as in *rap1-P520L* and *rap1-Y592A* cells, respectively, indicating that

Rap1^{P520L} and Rap1^{Y592A} are capable of inhibiting telomerase even in the absence of Rif2 (Figure 18E).

Consistent with the finding that Rap1^{R381W} acts in a Rif2-dependent manner, the amount of Rif2 bound at DSBs was increased in *rap1-R381W* cells (Figure 18F) and this is in agreement with the increased Rap1^{R381W} association to DSBs (Figure 15E). By contrast, both *rap1-P520L* and *rap1-Y592A* cells showed reduced Rif2 accumulation at DSBs (Figure 18F), with *rap1-Y592A* cells showing the major effect, suggesting that the release of the RCT domain from the DBD closure influences the ability of Rap1 to load Rif2 on dsDNA.

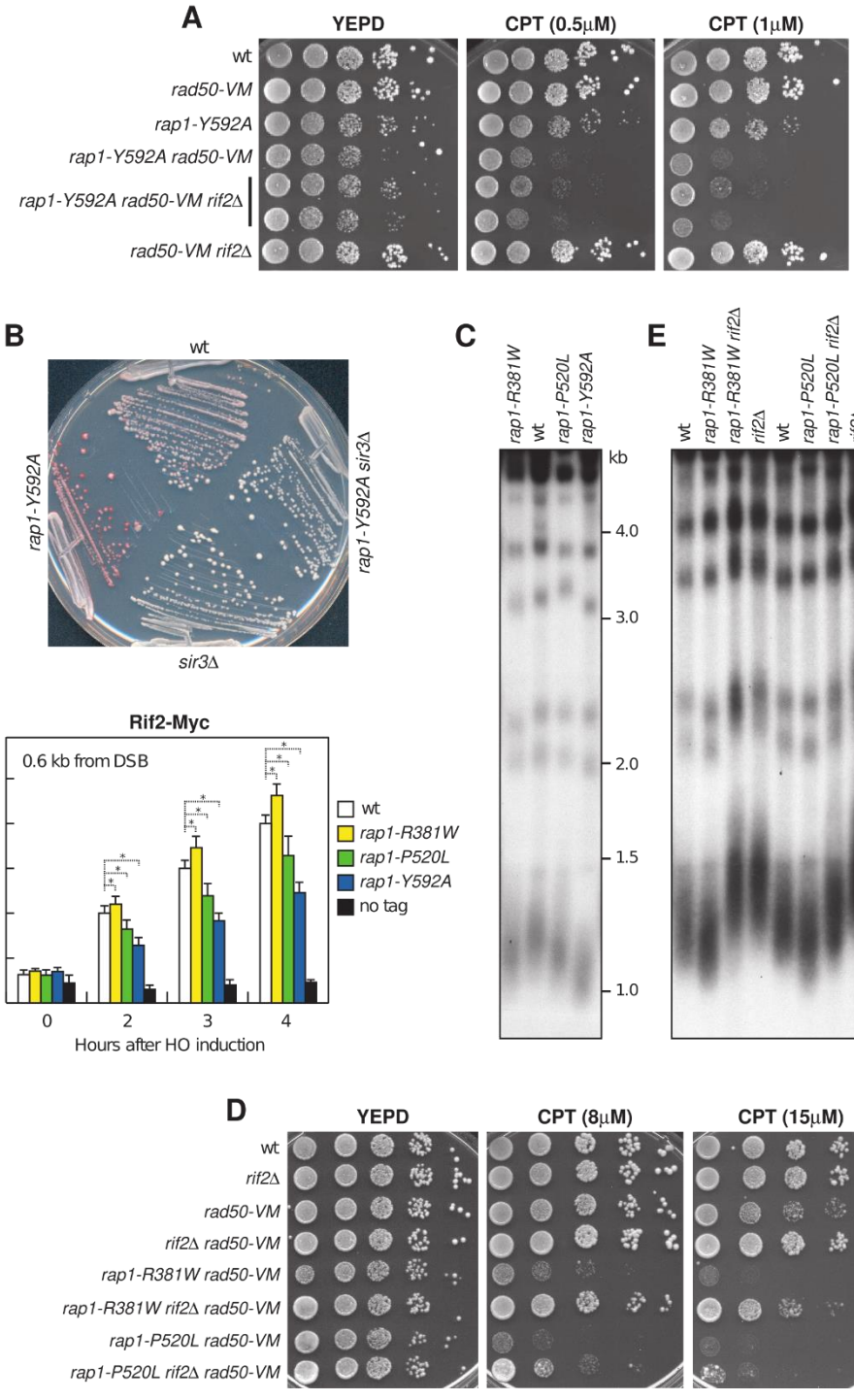
A
YEPD
CPT (0.5μM)
CPT (1μM)
wt
rad50-VM
rap1-Y592A
rap1-Y592A rad50-VM
rap1-Y592A rad50-VM rif2Δ
rad50-VM rif2Δ
B
wt
rap1-Y592A
rap1-Y592A sir3Δ
sir3Δ
C
rap1-R381W
wt
rap1-P520L
rap1-Y592A
kb
4.0
3.0
2.0
1.5
1.0
E
wt
rap1-R381W
rap1-R381W rif2Δ
rif2Δ
wt
rap1-P520L
rap1-P520L rif2Δ
rif2Δ
wt
rap1-Y592A
rap1-Y592A rif2Δ
rif2Δ
kb
4.0
3.0
2.0
1.5
1.0
F
Rif2-Myc
0.6 kb from DSB
Relative fold enrichment
0
1
2
3
4
5
0
2
3
4
Hours after HO induction
wt
rap1-R381W
rap1-P520L
rap1-Y592A
no tag
D
YEPD
CPT (8μM)
CPT (15μM)
wt
rif2Δ
rad50-VM
rif2Δ rad50-VM
rap1-R381W rad50-VM
rap1-R381W rif2Δ rad50-VM
rap1-P520L rad50-VM
rap1-P520L rif2Δ rad50-VM

Figure 18. Effect of the *rap1-Y592A* mutation on *rad50-VM* DNA damage sensitivity, transcriptional silencing, telomere length, and Rif2 association to DSBs. **(A)** Exponentially growing cells were serially diluted (1:10) and each dilution was spotted out onto YEPD plates with or without CPT. (**B**) Cells carrying the *ADE2* gene at telomere V-R were streaked onto SC plates containing a limiting amount of adenine. (**C**) *Xho*I-cut genomic DNA prepared from exponentially growing cells was subjected to Southern blot analysis using a poly(GT) probe. (**D**) Exponentially growing cells were serially diluted (1:10) and each dilution was spotted out onto YEPD plates with or without CPT. (**E**) *Xho*I-cut genomic DNA prepared from exponentially growing cells was subjected to Southern blot analysis using a poly(GT) probe. (**F**) ChIP analysis and qPCR. Exponentially growing YEPR cell cultures were transferred to YEPRG at time zero. Relative fold enrichment of Rif2 at the indicated distances from the HO cleavage site was determined after ChIP with anti-Myc antibody and subsequent qPCR analysis. The mean values are represented with error bars denoting s.d. ($n = 3$). $*P < 0.05$ (Student's *t*-test).

Discussion

In both yeast and mammals, the MRX complex and Tel1 are rapidly recruited to DSBs to initiate repair events and checkpoint signalling [Syed *et al.*, 2018]. Both MRX and Tel1 are also involved in telomere maintenance by allowing access of telomerase to the telomeres [Ritchie *et al.*, 2000]. It has been shown that MRX association at both DSBs and telomeres is negatively regulated by Rif2 [Hirano *et al.*, 2009; Cassani *et al.*, 2016], which is recruited to telomeres by the DNA binding protein Rap1 [Wotton and Shore, 1997].

Rap1 dysfunction has been shown to cause MRX-mediated telomere degradation [Bonetti *et al.*, 2010; Vodenicharov *et al.*, 2010], suggesting that Rap1 can be involved in repressing MRX activity at least at telomeres. Whether Rap1 also acts at DSBs is unknown. Here, we show that Rif2 needs Rap1 to repress MRX association at both DSBs and telomeres. In fact, *rif2* or *rap1* alleles specifically impaired in Rap1 or Rif2 interaction, respectively, behave like *RIF2* deletion in increasing MRX association at DSBs. This enhanced MRX persistence suppresses the DNA damage hypersensitivity and the end-tethering defect caused by the *rad50-VM* mutation, which is known to reduce MRX association to DSBs. Importantly, Rap1 is recruited to DNA DSBs and promotes Rif2 association to them, thus explaining the reason why Rap1 is required to support Rif2 activity at DSBs. The lack of this Rap1/Rif2-mediated inhibition of MRX retention at DSBs not only suppresses the end-tethering defect of *rad50-VM* cells, but it also increases the efficiency of end-tethering and NHEJ in wild-type cells [Cassani *et al.*, 2016]. This finding suggests that inhibition of MRX association at DSBs by Rap1 and Rif2 can be important in the regulation of the choice between DSB repair by HR and NHEJ.

Rif2 has been proposed to inhibit MRX association/persistence to DNA ends by two different mechanisms: (i) it counteracts Tel1-mediated stabilization of MRX

association to DSBs, possibly by competing with Tel1 for MRX binding [Hirano *et al.*, 2009; Martina *et al.*, 2010; Cassani *et al.*, 2016]; (ii) it discharges the ATP-bound form of MRX, which is important to support the DNA binding activity of the complex, by enhancing ATPase activity by Rad50 in a Tel1-independent manner [Cassani *et al.*, 2016; Hailemariam *et al.*, 2019]. The finding that *rif2* and *rap1* alleles specifically impaired in Rap1 or Rif2 interaction, respectively, do not need Tel1 to restore DNA damage resistance of *rad50-VM* cells suggests that their suppression effect could be due at least in part to their failure to enhance ATPase activity by Rad50.

Crystal structures have shown that Rap1 binds telomeric DNA in a high-affinity mode through both tandem Myb-like domains, with the wrapping loop locking Rap1 around DNA by interacting with Myb-N [Konig *et al.*, 1996; Taylor *et al.*, 2000; Matot *et al.*, 2012]. However, the transient opening of the wrapping loop allows Rap1 to bind *in vitro* both telomeric and non-telomeric DNA sequences through only one Myb-like domain leading to formation of Rap1-DNA complexes with high stoichiometry [Del Vescovo *et al.*, 2004; Feldmann and Galletto, 2014; Feldmann *et al.*, 2015]. Whether this alternative binding mode can be adopted *in vivo* and/or it plays any functional role is hitherto unknown.

We provide evidence that Rap1 functions at DNA ends are influenced by its DNA binding mode. In fact, ChIP analyses have shown that the Rap1 R381W and P520L mutations, which cause enhanced Rap1 activity in counteracting telomere elongation and in repressing both MRX association at DNA ends and gene expression, increase the amount of Rap1 bound to DNA ends. However, biased molecular dynamics simulations indicate that, while the R381W mutation enhances Myb-N affinity for DNA, thus straightforwardly explaining the increased $Rap1^{R381W}$ association to DSBs observed by ChIP, the P520L mutation decreases Myb-C affinity for DNA. Importantly, gel electrophoretic mobility shift assays show that Rap1 DBD^{P520L} favours formation of $Rap1^{DBD}$-DNA

complexes with higher stoichiometry. These findings suggest that the increased amount of chromatin bound Rap1^{P520L} detected by ChIP is due to destabilization of the Rap1 clamped structure that results in an easier transition to Rap1-DNA complexes with high stoichiometry, where only Myb-N makes contacts with DNA. Consistently with this hypothesis, opening of the wrapping loop through the Y592A mutation leads to similar phenotypes, i.e. increased Rap1 association to DSBs, decreased MRX association to DSBs, telomere shortening, and hypersilencing. Altogether, these findings indicate that, depending of its DNA binding mode, Rap1 can form protein-DNA complexes with different functional properties. As Rap1 is capable to bind also random dsDNA sequences *in vitro* [Feldmann and Galletto, 2014; Feldmann *et al.*, 2015], its recruitment at DSBs could occur in a sequence-independent manner. In any case, whether other proteins, such as chromatin remodelers or the Ku complex, drive the localization of Rap1 at DSBs remains to be determined.

The interaction of Rap1 with Rif2 occurs exclusively *via* the Rap1^{RCT} domain [Wotton and Shore, 1997; Moretti and Shore, 2001; Liu and Lustig 1996]. Structural analysis has shown that binding of both Myb-like domains around DNA constrains the orientation of the RCT domain in a conformation that may favour its interaction with the functional partners [Matot *et al.*, 2012]. By contrast, in the absence of DNA, the RCT domain can bind to Myb-C *in vitro* possibly limiting RCT interaction ability [Feldmann *et al.*, 2015]. Interestingly, the Rap1^{R381W} mutant variant, which increases the affinity of Myb-N to dsDNA and therefore should bind DNA with both Myb-like domains, exacerbates the DNA damage sensitivity of *rad50-VM* cells and causes telomere shortening mostly in a Rif2-dependent manner. By contrast, both P520L that decreases Myb-C affinity to dsDNA, and Y592A that impairs wrapping loop clamping, hyperactivate Rap1 mostly in a Rif2-independent manner. These findings raise the possibility that the interaction of a single Myb-like domain with DNA limits

Rap1 ability to recruit Rif2 on DNA. In agreement with this hypothesis, although the amount of Rap1^{R381W}, Rap1^{P520L}, and Rap1^{Y592A} bound at DSBs was increased compared to wild-type Rap1, Rap1^{P520L}, and Rap1^{Y592A} decreased Rif2 association to DSBs, whereas Rap1^{R381W} increased it. Altogether, these data indicate that the way Rap1 binds DNA influences its ability to interact with Rif2, with the binding of both Myb-like domains on DNA facilitating Rif2 interaction, possibly by allowing the release of the RCT from the DBD closure of the wrapping loop.

Interestingly, while Rap1^{P520L} and Rap1^{Y592A} act at DSBs and telomeres mostly in a Rif2-independent manner, they increase silencing in a Sir3-dependent manner. This finding suggests that, when Rap1 is in the conformation where only Myb-N binds to DNA, leaving Myb-C free to interact with RCT domain, the RCT domain would be less available for Rif2 binding than for Sir binding. It is worth pointing out that, while Rif2 binds to RCT in two distinct manners, involving either its N-terminal RBM motif or its C-terminal AAA+ domain, Sir3 and Sir4 proteins only bind to Rap1^{RCT} with the RBM motif. Altogether, these considerations suggest a model where RCT binding to Myb-C in Rap1 would reduce the availability of RCT interface to Rif2^{AAA+} domain, without impinging on the availability of RCT pocket for Sir3 and Sir4 and possibly Rif2^{RBM} motifs. We propose that binding of both Rap1 Myb-like domains to DNA allows formation of Rap1-DNA complexes that negatively regulate telomere length and MRX functions to DSBs primarily through Rif2 (Figure 19A). However, the transition to a binding mode where a single Myb-like domain is bound to DNA leads to higher stoichiometry Rap1-DNA complexes that can exert their functions on MRX association to DNA ends and telomere length in a Rif2-independent manner (Figure 19B). Interestingly, while Rap1 should bind its DNA recognition sequence preferentially with both Myb-like domains, the absence of this DNA sequence at DSBs could favour formation of Rap1-DNA complexes with high

stoichiometry, where only one Myb-like domain makes contacts with DNA. The telomeric mammalian proteins TRF1 and TRF2, as well as their fission ortholog Taz1, bind telomeric DNA through Myb-like domains [Chong *et al.*, 1995; Bilaud *et al.*, 1996; Broccoli *et al.*, 1997; Cooper *et al.*, 1997; König and Rhodes, 1997]. Unlike Rap1, TRF1, TRF2, and Taz1 contain a single Myb-like domain, but they bind DNA as homodimer, thus creating an overall architecture that places two Myb-like domains on DNA [Bilaud *et al.*, 1996; Bianchi *et al.*, 1997; Bianchi *et al.*, 1999; Li *et al.*, 2000]. Interestingly, Myb family of proteins appears to be of polyphyletic origin, implying modular evolution [Rosinski and Atchley, 1998]. While having two Myb-like domains in a single protein could ensure stable binding independently of the instantaneous concentration of the protein, the presence of Myb-like domains in two separate proteins could provide higher levels of regulation. In any case, the finding that Rap1 can bind DNA even through a single Myb-like domain highlights the structural plasticity of this protein and suggests that the use of this module for DNA binding has evolved in losing one of them in mammalian proteins rather than in gaining one by yeast Rap1.

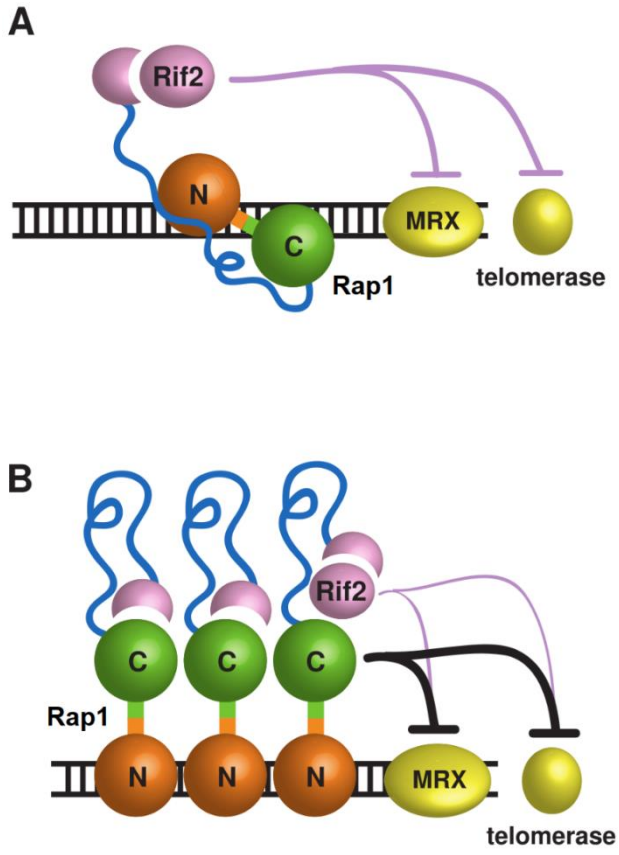

Figure 19. Model for how DNA binding modes can influence Rap1 activity in the regulation of MRX function at DSBs and of telomere length.
(**A**) The binding of both Rap1 Myb-like domains to DNA allows formation of Rap1-DNA complexes that negatively regulate telomere length and MRX functions to DSBs primarily through Rif2. (**B**) By contrast, the transition to a binding mode where a single Myb-like domain is bound to DNA leads to higher stoichiometry Rap1-DNA complexes that can exert their functions on MRX association to DNA ends and telomere length in a Rif2-independent manner. In both figures (**A**) and (**B**), Rap1 N-terminus is shown in orange and Rap1 C-terminus is shown in green.

Nucleic Acids Research

2022 Jul 27; under review

The Ku complex promotes DNA end-bridging and this function is antagonized by Tel1/ATM kinase

Carlo Rinaldi[1], Paolo Pizzul[1], Erika Casari[1],

Renata Tisi[1], Maria Pia Longhese[1*]

[*] Corresponding Author

[1] Dipartimento di Biotecnologie e Bioscienze, Università degli Studi di Milano-Bicocca, Milano, 20126, Italy

DNA double-strand breaks (DSBs) are particularly dangerous forms of damage that must be repaired to maintain genomic integrity. The two main mechanisms devoted to repair DNA DSBs are homologous recombination (HR), which uses intact homologous DNA as a template to restore the genetic information at the break site, and non-homologous end joining (NHEJ), which catalyzes the direct religation of the DSB ends [Mehta and Haber, 2014; Stinson and Loparo, 2021]. Generation of DSBs also triggers activation of a checkpoint response, whose apical proteins include Mec1 (ATR in mammals) and Tel1 (ATM in mammals) kinases that couple DSB repair with cell-cycle progression [Villa *et al.*, 2016].

Ku and MRX/MRN (Mre11-Rad50-Xrs2 in yeast; MRE11-RAD50-NBS1 in mammals) are among the first protein complexes to be recruited at DSBs [Lisby *et al.*, 2004]. In both yeast and mammals, MRX/MRN activates the protein kinase Tel1/ATM that plays an important role in DSB signaling [Nakada *et al.*, 2003; Falck *et al.*, 2005; You *et al.*, 2005]. Furthermore, it initiates DSB resection to generate single-stranded DNA (ssDNA) that is substrate for the recombinase Rad51 to catalyze homologous pairing and strand invasion [Mehta and Haber, 2014]. To initiate DSB resection, the Sae2/CtIP protein stimulates the Mre11 endonuclease activity to catalyze an endonucleolytic cleavage of the 5'-terminated DSB ends [Cannavo and Cejka, 2014]. This step is followed by bidirectional resection, with Mre11 exonuclease resecting towards the end and either Exo1 or Dna2 exonuclease resecting away from the DSB [Mimitou and Symington, 2008; Zhu *et al.*, 2008; Cejka *et al.*, 2010; Niu *et al.*, 2010; Garcia *et al.*, 2011; Nimonkar *et al.*, 2011; Shibata *et al.*, 2014; Reginato *et al.*, 2017; Wang *et al.*, 2017].

The Ku complex, which comprises the two Ku70 and Ku80 subunits, recognizes with avid affinity and no sequence specificity a large variety of DNA ends, including blunt ends, hairpin DNA, and ends with protruding single-stranded overhangs [Mimori and Hardin, 1986; Griffith *et al.*, 1992; Blier *et al.*, 1993]. Ku

orthologs are found in organisms ranging from bacteria to humans [Aravind and Koonin, 2001; Downs and Jackso, 2004]. In eukaryotes, the two Ku subunits share three structural domains, consisting of an N-terminal von Willebrand A (vWA)-like domain, a central β-barrel domain, and an α-helical C-terminal arm. Structural analyses have revealed that Ku70 and Ku80 subunits form an heterodimer that adopts a quasi-symmetric structure with a ring that encircles the duplex DNA [Yaneva *et al.*, 1997; Walker *et al.*, 2001]. Furthermore, Ku binds DNA ends asymmetrically, with the Ku70 vWA-like domain facing outwards in close proximity to the DNA end and the Ku80 vWA-like domain facing inwards [Walker *et al.*, 2001; Rivera-Calzada *et al.*, 2007; Ribes-Zamora *et al.*, 2007].

The Ku complex plays two important functions in DSB repair: it acts as a hub to directly or indirectly recruit downstream NHEJ components [Zahid *et al.*, 2021] and it protects the DSB ends from degradation [Clerici *et al.*, 2008; Zierhut and Diffley, 2008]. Consequently, deletion of either *KU70* or *KU80* gene partially suppresses both the DNA damage sensitivity and the resection defect of cells lacking Sae2 in an Exo1-dependent manner, indicating that Ku prevents access of Exo1 to the DSB ends [Mimitou and Symington, 2010; Shim *et al.*, 2010; Foster *et al.*, 2011; Langerak *et al.*, 2011]. Canonical proteins involved in NHEJ in mammals include the DNA-dependent protein kinase catalytic subunit (DNA-PKcs), XRCC4 (Lif1 in yeast), XLF (Nej1 in yeast), and PAXX [Chaplin and Blundell, 2020]. The final NHEJ step relies on DNA ligase IV (Dnl4 in yeast), which forms a constitutive complex with XRCC4/Lif1 to ligate the broken DNA ends. In mammals, formation of high-order structural assemblies by the above proteins has been proposed to occur in a two-step mechanism, in which the DNA ends are initially held together in a long-range synaptic complex formed by Ku, DNA-PKcs, DNA Ligase IV, XRCC4, and XLF. Upon dissociation of DNA-PKcs, this complex is converted into a short-range synaptic assembly, in which

the Ku bound DNA ends are aligned for processing and ligation [Graham *et al.*, 2016; Chaplin *et al.*, 2021; Chen *et al.*, 2021].

One of the most important questions in NHEJ concerns how the two DNA ends resulting from a DSB are held in close physical proximity for repair, a function that in *S. cerevisiae* involves the MRX complex and Sae2 [Kaye *et al.*, 2004; Lobachev *et al.*, 2004; Lee *et al.*, 2008; Clerici *et al.*, 2005; Nakai *et al.*, 2011]. Biochemical and electron microscopy approaches showed that in mammals the DNA-PKcs alone is responsible for bridging the DNA ends together [DeFazio *et al.*, 2002], whereas other studies have attributed to the DNA-PK holoenzyme, composed of Ku and DNA-PKcs, the main bridging activity [Weterings *et al.*, 2003; Spagnolo *et al.*, 2006; Wang *et al.*, 2018]. However, in other studies DNA PKcs was not found to be necessary for DSB tethering, which required Ku plus XRCC4-DNA ligase IV [Reid *et al.*, 2015; Chang *et al.*, 2016; Zhao *et al.*, 2019]. Furthermore, a single molecule study of bacterial NHEJ, a mechanism relying on a homodimeric Ku and Ligase D, revealed that the Ku dimer alone is sufficient to form DNA bridges that are stabilized upon addition of Ligase D [Öz *et al.*, 2021]. This situation is similar to the NHEJ mechanism found in yeast cells, which do not possess DNA-PKcs. These observations leave open the possibility that Ku may be the central component in the formation of a molecular DSB bridge. Consistent with this hypothesis, early atomic force and electron microscopy experiments showed that recombinant Ku was capable to mediate DNA looping and to coprecipitate two labelled DNA molecules [Cary *et al.*, 1997; Ramsden and Gallert, 1998]. The involvement of the Ku complex in end-to-end association of linear DNA molecules and formation of DNA loops has been supported by scanning force microscopy experiments [Yaneva *et al.*, 1997; Pang *et al.*, 1997]. In addition, the mammalian Ku heterodimer can heterotetramerize independently of DNA-PKcs and the α5 helix of the Ku70

vWA like domain is crucial for Ku-Ku self-interaction and, in yeast, for DSB repair by NHEJ [Ribes-Zamora *et al.*, 2007; Ribes-Zamora *et al.*, 2013].

Despite these observations, whether the Ku complex is important to support end-tethering *in vivo* remains to be elucidated. Here, we report the identification and characterization of the *S. cerevisiae ku70-C85Y* allele that, like *KU70* deletion, restores DNA damage resistance of *sae2*Δ cells. However, unlike *KU70* deletion that suppresses the resection defect of *sae2*Δ cells by relieving inhibition of Exo1 resection activity [Mimitou and Symington, 2010; Shim *et al.*, 2010; Foster *et al.*, 2011; Langerak *et al.*, 2011], the *ku70-C85Y* allele suppresses the end-tethering defect of *sae2*Δ cells, whereas the lack of Ku70 exacerbates it. The C85Y mutation, which targets the β-hairpin structure that is localized near the α5 helix previously identified as involved in Ku70-Ku80 heterotetramer formation in humans [Ribes-Zamora *et al.*, 2007; Ribes-Zamora *et al.*, 2013], increases Ku persistence closeness to the DSB end and decreases it at more distant sites. Suppression of *sae2*Δ end-tethering defect and increased Ku persistence very closed to the DSB ends can be observed also when histone removal around a DSB is defective either by eliminating Tel1 kinase activity or nucleosome remodelers. Altogether, these findings lead to a model whereby Ku contributes to keeping the DNA ends tethered to each other, whereas Tel1 kinase antagonizes this Ku function by promoting histone removal around DSBs and Ku sliding inwards.

Identification of *ku70* alleles that suppress the DNA damage sensitivity of *sae2*Δ cells

Deletion of *KU70* suppressed the sensitivity to camptothecin (CPT) and methyl methanesulfonate (MMS) of *sae2*Δ cells, whereas it conferred no rescue of sensitivity to phleomycin (Figure 20A) [Mimitou and Symington, 2010; Foster *et al.*, 2011], suggesting that the basis of the phleomycin sensitivity of *sae2*Δ mutants differs from that of CPT and MMS. To understand if diverse Ku functions contribute to DNA damage resistance, we searched for *ku70* mutants that restored resistance of *sae2*Δ cells to phleomycin. *KU70* gene was amplified by low-fidelity PCR together with *URA3* gene located 500 bp upstream of the *KU70* ATG start codon, followed by transformation with the linear PCR products into *sae2*Δ cells in order to replace the corresponding *KU70* wild-type sequence with the mutagenized DNA fragments. Transformants were then screened for increased viability in the presence of phleomycin compared to *sae2*Δ cells, followed by genetic tests in order to confirm that suppression cosegregated with the *URA3* marker. This analysis allowed us to identify the *ku70-G79S*, *ku70-C85Y*, *ku70-A90T*, *ku70-N104Y*, and *ku70-D173G* alleles. These five mutations restored DNA damage resistance of *sae2*Δ cells not only to phleomycin, but also to CPT and MMS, whereas, as expected, *ku70*Δ was effective only in the suppression of *sae2*Δ CPT and MMS sensitivity (Figure 20A).

The Ku subunits, Ku70 and Ku80, share a similar topology. Their structure is composed of three different domains: an N-terminal α/β domain similar to a vWA domain, a β-barrel with the function of enclosing the nucleic acid, and a helical C-terminal arm that leans towards the vWA-like domain of the other subunit [Walker *et al.*, 2001] (Figure 20B). The identified Ku70 mutations are all localized in the conserved N-terminal vWA-like domain. In detail, both C85Y and A90T mutations target the β-hairpin structure, which is localized in the same region of the conserved α5 helix that was shown to be involved in tetramer

formation in humans [Ribes-Zamora *et al.*, 2013] (Figure 20B and C). The N104Y mutation resides in a loop immediately adjacent to the same β-hairpin, whereas G79S and D173G affect residues localized in the embedded β-sheet within the vWA-like domain, with G79S being nearby the 84-93 amino acid turn (Figure 20B and C).

The lack of Ku affects the length of telomeres by destabilizing the interaction between the telomerase subunit Est1 and the telomeric DNA [Williams *et al.*, 2014; Lemon *et al.*, 2019; Bertuch and Lundblad, 2003]. We found that the *ku70-G79S*, *ku70-A90T*, and *ku70-N104Y* alleles shortened telomeres although not severely as *ku70*Δ, whereas both *ku70-C85Y* and *ku70-D173G* did not (Figure 20D). As the C85Y mutation does not affect telomere length and targets the β-hairpin localized in the same region of the conserved α5 helix, we focused the analysis on this mutation.

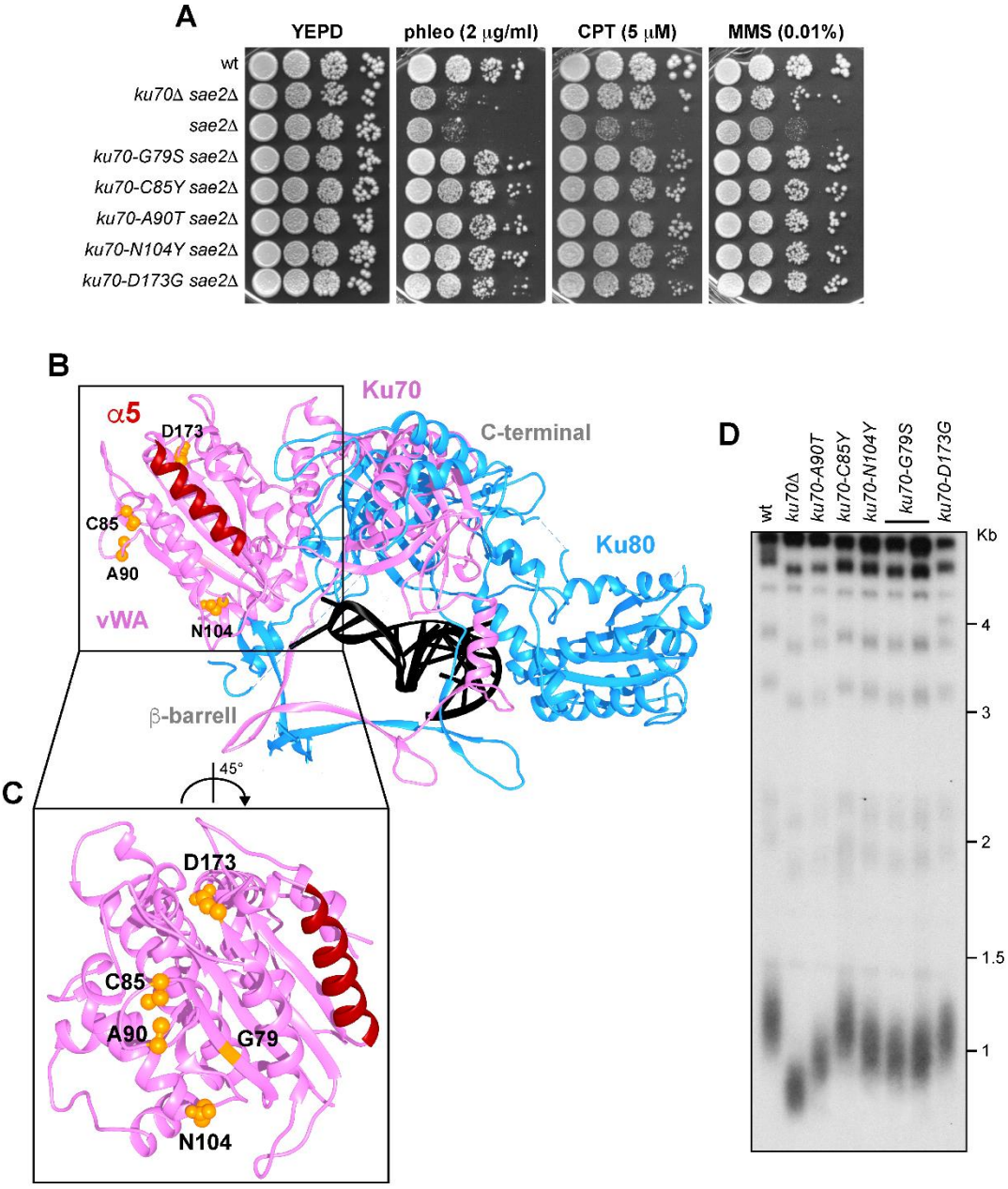
A
YEPD
phleo (2 μg/ml)
CPT (5 μM)
MMS (0.01%)
wt
ku70Δ sae2Δ
sae2Δ
ku70-G79S sae2Δ
ku70-C85Y sae2Δ
ku70-A90T sae2Δ
ku70-N104Y sae2Δ
ku70-D173G sae2Δ
B
α5
D173
C85
A90
vWA
N104
Ku70
C-terminal
Ku80
β-barrell
45°
C
D173
C85
A90
G79
N104
D
wt
ku70Δ
ku70-A90T
ku70-C85Y
ku70-N104Y
ku70-G79S
ku70-D173G
Kb
4
3
2
1.5
1

Figure 20. Identification of *ku70* alleles that suppress the sensitivity to phleomycin of *sae2*Δ cells.

(**A**) Exponentially growing cultures were serially diluted (1:10) and each dilution was spotted out onto YEPD plates with or without phleomycin (phleo), camptothecin (CPT) or methyl methanesulfonate (MMS). (**B**) The structure of yeast Ku70-Ku80 heterodimer (PDB ID: 5Y58) is shown as a cartoon. Ku70 is in pink (with α5 helix in red), Ku80 in blue, and the nucleic acid in black. The residues affected by the mutations are shown as orange balls. (**C**) The structure of Ku70 vWA-like domain is shown in detail with α5 helix in red. The residues affected by the mutations are shown in orange balls. (**D**) Telomere length. *Xho*I-cut genomic DNA from exponentially growing cells was subjected to Southern blot analysis using a radiolabeled poly(GT) telomere-specific probe.

The *ku70-C85Y* allele suppresses the DNA damage sensitivity of *sae2*Δ cells in an Exo1-independent manner

The Ku complex protects the DNA ends from degradation by Exo1. As a consequence, the lack of Ku70 partially suppresses both the hypersensitivity to DNA damaging agents and the resection defect of cells lacking Sae2 or expressing the nuclease defective *mre11-H125N* allele by relieving inhibition of Exo1 nuclease [Mimitou and Symington, 2010; Shim *et al.*, 2010; Foster *et al.*, 2011; Langerak *et al.*, 2011]. Thus, we asked whether the *ku70-C85Y* allele behaves like *ku70*Δ and therefore restores DNA damage resistance of *sae2*Δ cells by allowing Exo1 access to DNA. Consistent with the requirement of Exo1 in the suppression of *sae2*Δ DNA damage sensitivity by *KU70* deletion, *ku70*Δ failed to suppress the sensitivity to CPT and MMS of *sae2*Δ *exo1*Δ cells (Figure 21A). By contrast, although the *exo1*Δ mutation increased the DNA damage sensitivity of *sae2*Δ cells, *ku70-C85Y sae2*Δ *exo1*Δ cells were more resistant to CPT and MMS than *sae2*Δ *exo1*Δ cells (Figure 21A), indicating that Exo1 is dispensable for this suppression. Similar results have been obtained also with the other *G79S*, *A90T*, *N104Y*, and *D173G* mutations (Figure 21B).

Consistent with different suppression mechanisms by the *ku70*Δ and *ku70-C85Y* alleles, deletion of *KU70* suppressed the hypersensitivity to CPT and MMS of *mre11-H125N* cells, whereas *ku70-C85Y* did not (Figure 21C), suggesting that the C85Y mutation bypasses a Sae2 function that does not involve DSB resection. As the lack of Ku70 suppresses the resection defect of *sae2*Δ cells because Exo1 inhibition is relieved [Mimitou and Symington, 2010; Shim *et al.*, 2010], we investigated the effect of the *ku70-C85Y* allele on DSB resection by using a strain background carrying a galactose-inducible HO endonuclease that, upon galactose addition, generates a single DSB at the *MAT* locus [Lee *et al.*, 1998]. To minimize the effect of DSB repair, the *MAT* homologous regions *HML* and *HMR* were

deleted, leading to a DSB that cannot be repaired by HR. Because ssDNA cannot be cleaved by restriction enzymes, its generation was assessed by testing resistance to cleavage as resection proceeds beyond the *Ssp*I restriction site located at different distances from the HO-cut site at the *MAT* locus. *Ssp*I-resistant ssDNA can be detected as appearance of slower migrating bands (r1-r6) after denaturing gel electrophoresis of *Ssp*I-digested genomic DNA and hybridization with a probe that anneals to the unresected strand at one side of the DSB. As expected, *sae2*Δ cells showed a resection defect of the HO-induced DSB that was similar to that of *ku70-C85Y sae2*Δ cells (Figure 21D and E), indicating that *ku70-C85Y* did not suppress the DNA damage sensitivity of *sae2*Δ cells by restoring DSB resection.

Interestingly, while *KU70* deletion did not affect DSB resection [Clerici *et al.*, 2008], *ku70-C85Y* cells showed a resection defect compared to wild-type cells (Figure 21D and E). As Ku limits DSB resection by inhibiting recruitment of Exo1 to DSBs [Shim *et al.*, 2010], we analyzed the effect of the *ku70-C85Y* mutation on Exo1 association with DSBs. To minimize the effect of DSB resection on protein binding to DSBs, HO was induced in G1-arrested cells that were kept arrested in G1 with α-factor throughout the experiment. In fact, the low Cdk1 activity in G1 cells prevents resection of the HO-induced DSB [Aylon *et al.*, 2004; Ira *et al.*, 2004]. Consistent with previous observations [Shim *et al.*, 2010], chromatin immunoprecipitation (ChIP) and quantitative PCR (qPCR) showed that the lack of Ku70 increased Exo1 association with the HO-induced DSB (Figure 21F). By contrast, although protein extract from wild-type and *ku70-C85Y* cells contained similar amount of Exo1 (Figure 21G), *ku70-C85Y* cells showed a decreased Exo1 association with the HO-induced DSB compared to wild-type cells (Figure 21F). This finding indicates that the *ku70-C85Y* allele encodes an hypermorphic Ku70 variant that limits Exo1 association with the DSB ends more efficiently than wild-type Ku70.

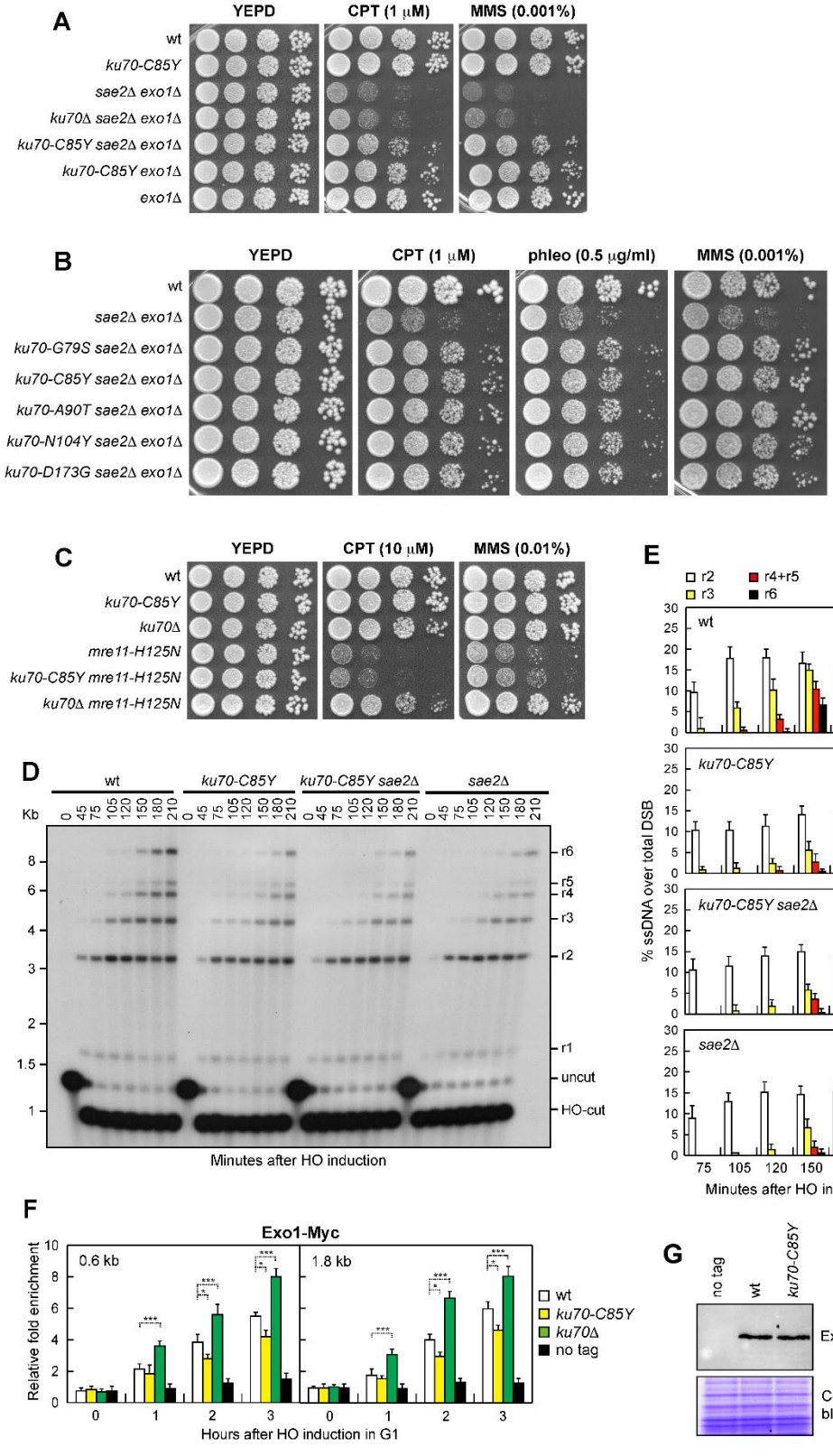
A
YEPD
CPT (1 μM)
MMS (0.001%)
wt
ku70-C85Y
sae2Δ exo1Δ
ku70Δ sae2Δ exo1Δ
ku70-C85Y sae2Δ exo1Δ
ku70-C85Y exo1Δ
exo1Δ
B
YEPD
CPT (1 μM)
phleo (0.5 μg/ml)
MMS (0.001%)
wt
sae2Δ exo1Δ
ku70-G79S sae2Δ exo1Δ
ku70-C85Y sae2Δ exo1Δ
ku70-A90T sae2Δ exo1Δ
ku70-N104Y sae2Δ exo1Δ
ku70-D173G sae2Δ exo1Δ
C
YEPD
CPT (10 μM)
MMS (0.01%)
wt
ku70-C85Y
ku70Δ
mre11-H125N
ku70-C85Y mre11-H125N
ku70Δ mre11-H125N
D
wt
ku70-C85Y
ku70-C85Y sae2Δ
sae2Δ
Kb
0 45 75 105 120 150 180 210
8
6
4
3
2
1.5
1
r6
r5
r4
r3
r2
r1
uncut
HO-cut
Minutes after HO induction
E
r2
r3
r4+r5
r6
wt
ku70-C85Y
ku70-C85Y sae2Δ
sae2Δ
% ssDNA over total DSB
0 5 10 15 20 25 30
75 105 120 150 180 210
Minutes after HO induction
F
Exo1-Myc
0.6 kb
1.8 kb
Relative fold enrichment
0 2 4 6 8 10
0 1 2 3
Hours after HO induction in G1
wt
ku70-C85Y
ku70Δ
no tag
G
no tag
wt
ku70-C85Y
Exo1-Myc
Coomassie blue

Figure 21. Suppression of *sae2*Δ DNA damage sensitivity by *ku70-C85Y* does not involve DSB resection and Exo1.

(**A**, **B**, **C**) Exponentially growing cultures were serially diluted (1:10) and each dilution was spotted out onto YEPD plates with or without phleomycin, CPT or MMS. (**D**) DSB resection. YEPR exponentially growing cell cultures of JKM139 derivative strains, carrying the HO cut site at the *MAT* locus, were transferred to YEPRG at time zero. *Ssp*I digested genomic DNA was hybridized with a single-stranded *MAT* probe that anneals with the unresected strand. 5'-3' resection produces *Ssp*I fragments (r1 through r6) detected by the probe. (**E**) Densitometric analysis of the resection products. The mean values of three independent experiments as in (**D**) are represented with error bars denoting standard deviation (s.d.). (**F**) ChIP analysis and qPCR. Exponentially growing YEPR cell cultures of JKM139 derivative strains were arrested in G1 with α-factor and transferred to YEPRG to induce HO in the presence of α-factor. Relative fold enrichment of Exo1-Myc at the indicated distances from the HO cleavage site was determined after ChIP with anti-Myc antibody and qPCR. The mean values of three independent experiments are represented with error bars denoting s.d. ***p<0.005; *p<0.05 (unpaired two-tailed Student's t-test). (**G**) Western blot with anti-Myc antibodies of extracts used for the ChIP analysis shown in (**F**). The same amounts of extracts were separated on an SDS-PAGE and stained with Coomassie Blue as loading control.

The *ku70-C85Y* allele suppresses the end-tethering defect of *sae2*Δ cells

To assess the mechanism underlying *sae2*Δ suppression by the Ku70^{C85Y} variant, we investigated whether DSB repair by NHEJ is required to support *ku70-C85Y sae2*Δ DNA damage resistance. We found that the *ku70-C85Y* allele still suppressed the DNA damage sensitivity of *sae2*Δ cells lacking the NHEJ component Nej1 (Figure 22A), whose loss leads to end-joining defects [Frank-Vaillant *et al.*, 2001; Kegel *et al.*, 2001; Valencia *et al.*, 2001], indicating that DSB repair by NHEJ is not required for this suppression.

We also investigated the effect of *ku70-C85Y* on the DNA damage sensitivity of cells lacking Mre11 or expressing the *rad50-VM* allele, which encodes a Rad50 mutant variant that specifically impairs tethering of the DSB ends [Cassani *et al.*, 2016]. The *ku70-C85Y* allele failed to suppress the severe DNA damage sensitivity of *mre11*Δ cells (Figure 22B), whereas it was capable to partially restore DNA damage resistance of *rad50-VM* cells (Figure 22C). This result, together with the observation that Sae2 is involved in keeping the DSB ends tethered to each other [Lee *et al.*, 2008; Clerici *et al.*, 2005], raises the possibility that the Ku70^{C85Y} variant suppresses the DNA damage sensitivity of *sae2*Δ cells by restoring DSB end-tethering.

To visualize DNA regions flanking to an HO-induced DSB break, we used a strain background where multiple repeats of the LacI repressor binding site were integrated 50 kb upstream and downstream of an irreparable HO break site located on chromosome VII in cells constitutively expressing a LacI-GFP fusion protein [Kaye *et al.*, 2004]. The level of end-tethering upon DSB formation was determined by measuring generation of one or two LacI-GFP spots. HO expression was induced by galactose addition to cell cultures that were arrested in G2 with nocodazole and kept blocked in G2 by nocodazole in order to ensure

that all cells would arrest in metaphase. Consistent with previous results [Clerici *et al.*, 2005], ~90% of wild-type cells showed a single LacI-GFP focus 1-2 hr after HO induction, whereas an increase of two LacI-GFP spots compared to the uninduced condition could be detected in *sae2*Δ cells (Figure 22D). Strikingly, *sae2*Δ cells harboring the *ku70-C85Y* allele showed a decrease in the percentage of untethered ends (Figure 22D), indicating that this mutation suppresses the end-tethering defect caused by the lack of Sae2. A slight but significant decrease of two LacI-GFP spots compared to wild-type cells can be detected also in *ku70-C85Y* cells (Figure 22D), suggesting that this mutant variant possesses by itself an increased end-tethering activity. Consistent with a role of the Ku complex in DSB end-tethering, the lack of Ku70 increased the percentage of untethered ends after HO induction and this percentage was further increased in *ku70*Δ *sae2*Δ cells compared to each single mutant (Figure 22D).

The effect of *ku70*Δ and *ku70-C85Y* alleles on the frequency of LacI-GFP foci after HO induction was primarily due to end-tethering and not to cohesion defects. In fact, similar results have been obtained when HO was induced in α-factor-arrested cells that were kept arrested in G1 by α-factor in the presence of galactose (Figure 22E).

The function of Ku in DSB end-tethering appears to be independent of MRX, as the *ku70-C85Y* mutation decreased the amount of two LacI-GFP spots of both *rad50-VM* and *mre11*Δ cells (Figure 22D and E). While the severe DNA damage hypersensitivity of *mre11*Δ cells, which was not suppressed by the *ku70-C85Y* allele (Figure 22B), is due to the lack of MRX functions in several aspects of the DNA damage response, *rad50-VM* cells are specifically defective in DSB tethering [Cassani *et al.*, 2016]. Therefore, the increased DNA damage resistance of *ku70-C85Y rad50-VM* cells compared to *rad50-VM* cells (Figure 22C) can be due to the suppression of the end-tethering defect.

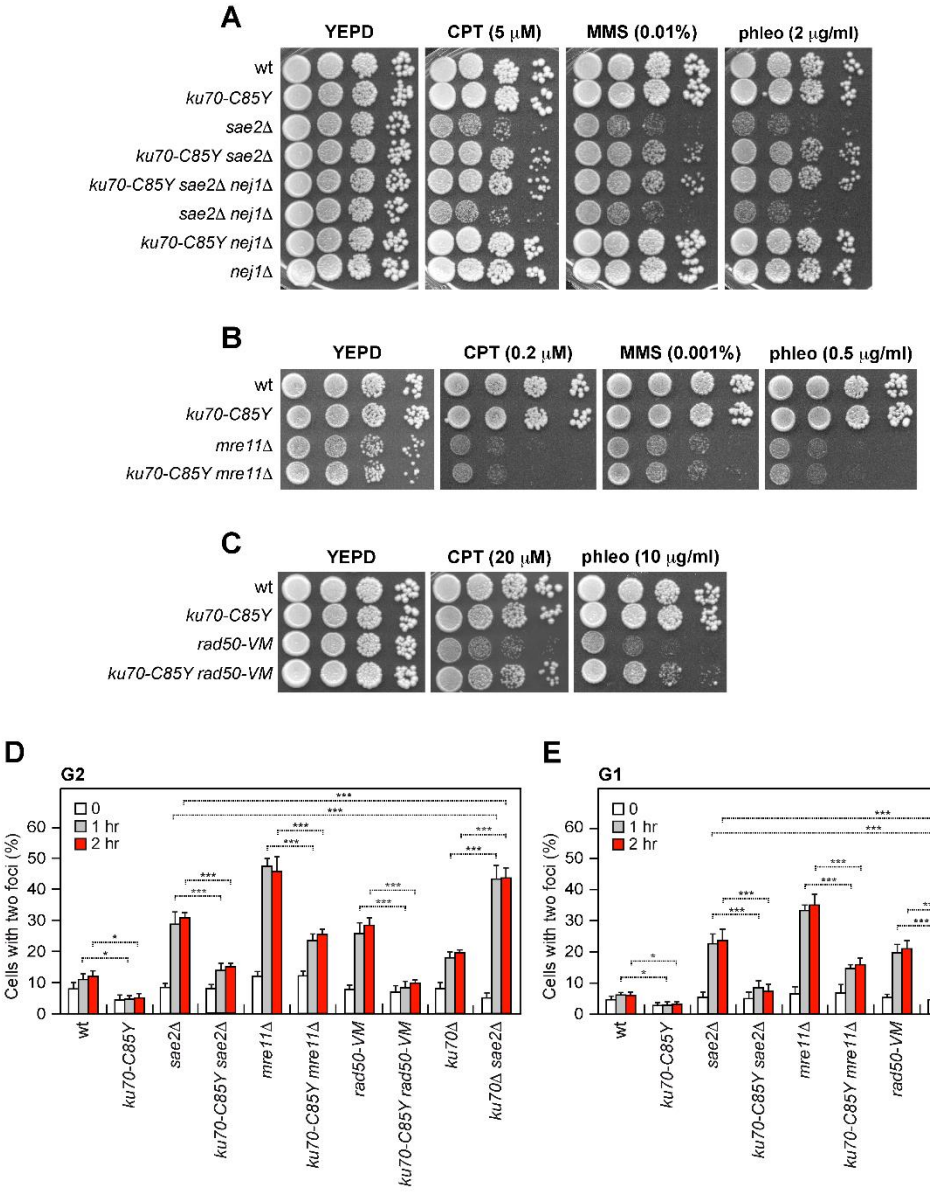
A
YEPD
CPT (5 μM)
MMS (0.01%)
phleo (2 μg/ml)
wt
ku70-C85Y
sae2Δ
ku70-C85Y sae2Δ
ku70-C85Y sae2Δ nej1Δ
sae2Δ nej1Δ
ku70-C85Y nej1Δ
nej1Δ
B
YEPD
CPT (0.2 μM)
MMS (0.001%)
phleo (0.5 μg/ml)
wt
ku70-C85Y
mre11Δ
ku70-C85Y mre11Δ
C
YEPD
CPT (20 μM)
phleo (10 μg/ml)
wt
ku70-C85Y
rad50-VM
ku70-C85Y rad50-VM
D
G2
0
1 hr
2 hr
Cells with two foci (%)
wt
ku70-C85Y
sae2Δ
ku70-C85Y sae2Δ
mre11Δ
ku70-C85Y mre11Δ
rad50-VM
ku70-C85Y rad50-VM
ku70Δ
ku70Δ sae2Δ
E
G1
0
1 hr
2 hr
Cells with two foci (%)
wt
ku70-C85Y
sae2Δ
ku70-C85Y sae2Δ
mre11Δ
ku70-C85Y mre11Δ
rad50-VM
ku70-C85Y rad50-VM
ku70Δ
ku70Δ sae2Δ

Figure 22. The *ku70-C85Y* allele suppresses the end-tethering defect of *sae2*Δ cells. (**A**, **B**, **C**) Exponentially growing cultures were serially diluted (1:10) and each dilution was spotted out onto YEPD plates with or without CPT, MMS or phleomycin. (**D**, **E**) DSB end-tethering. Exponentially growing YEPR cell cultures were arrested in G2 with nocodazole (**D**) or in G1 with α-factor (**E**) at time zero and transferred to YEPRG in the presence of nocodazole or α-factor, respectively. 200 cells for each strain were analyzed to determine the percentage of cells showing two LacI-GFP foci. The mean values of three independent experiments are represented with error bars denoting s.d. ***$p<0.005$; *$p<0.05$ (unpaired two-tailed Student's *t*-test).

The Ku heterodimer can self-associate and the C85Y mutation increases Ku70 persistence close to the DSB ends

A role for Ku in DSB end-bridging predicts that two Ku70-Ku80 heterodimers can heterotetramerize. Consistent with this hypothesis, atomic force microscopy showed that DNA-bound Ku can self-associate [Cary *et al.*, 1997] and an interaction between two Ku heterodimers has been observed by coimmunoprecipitation in human cells [Ribes-Zamora *et al.*, 2013]. Furthermore, Ku heterotramerization was shown to require Ku70 α5 helix that is located in the vWA-like domain and whose D195A mutation in *S. cerevisiae* impairs DSB repair by NHEJ [Ribes-Zamora *et al.*, 2007; Ribes-Zamora *et al.*, 2013]. To assess the existence of Ku70-Ku80 heterotetramer in yeast as well, we performed coimmunoprecipitation using protein extracts prepared from cells carrying differentially tagged versions of Ku70. We detected Ku70-Flag in Ku70-HA immunoprecipitates (Figure 23A). As neither Ku70 nor Ku80 homodimerizes and they are both unstable when not heterodimerized [Griffith *et al.*, 1992; Ono *et al.*, 1994; Errami *et al.*, 1998], these results are consistent with differentially tagged Ku heterodimers forming multimers. Because $Ku70^{C85Y}$ possesses an increased tethering efficiency (Figure 22D and E), we performed ChIP analysis to investigate the effect of the C85Y mutation on Ku70 association with DSBs. Although the mutation did not alter Ku70 protein level (Figure 23B), the amount of $Ku70^{C85Y}$ bound very closed to the HO-induced DSB (0.2 kb) was increased compared to wild-type Ku70 (Figure 23C), suggesting that this higher persistence might account for both the enhanced Exo1 inhibition and end-tethering activity displayed by the $Ku70^{C85Y}$ mutant variant. Interestingly, the amount of $Ku70^{C85Y}$

bound to the HO-induced DSB was much lower than wild-type Ku70 as the distance from the DSB increased (0.6 and 1.8 kb) (Figure 23C). As Ku was known to slide along DNA in an ATP-independent manner [de Vries *et al.*, 1989], the different amount of DSB bound-Ku70^{C85Y} depending on the distance from the DSB end is consistent with a defect of the Ku70^{C85Y}-Ku80 mutant dimer to slide over the broken DNA end. The C85Y mutation might stabilize Ku70 association with the DSB end either because it leads to conformational changes that impair the passive Ku diffusion on DNA or because it increases Ku-Ku self-interaction. As we failed to detect an increase in Ku70-Ku70 interaction by coimmunoprecipitation, we conducted an *in silico* analysis of protein-protein docking with several available suites. In particular, we analyzed the compatibility of two Ku70 vWA-like domains as interacting surfaces, by imposing the condition of the involvement of the α5 helices in the interaction.

The resulting structures were filtered according to the constraint that the Ku70 vWA-like domains from two Ku dimers bind each other in an orientation that allow accession to Lig4 to both of the DNA ends in the region between the interacting dimers (Figure 23D), according to the mechanism proposed for bacterial and yeast DNA end repair [Öz *et al.*, 2021]. In this conformation, most of the interactions occur between the α5 helices in the wild-type cluster (Figure 23E), but the residues affected by the mutations that we identified could impinge on the flexibility of the vWA-like domain, allowing the formation of additive interactions between the two facing Ku70 subunits. It is noteworthy that this conformation is the top scoring complex for the mutant Ku70^{C85Y} protein, while it has similar score to several different conformations for the wild-type protein, suggesting that it is stabilized by the presence of the C85Y mutation.

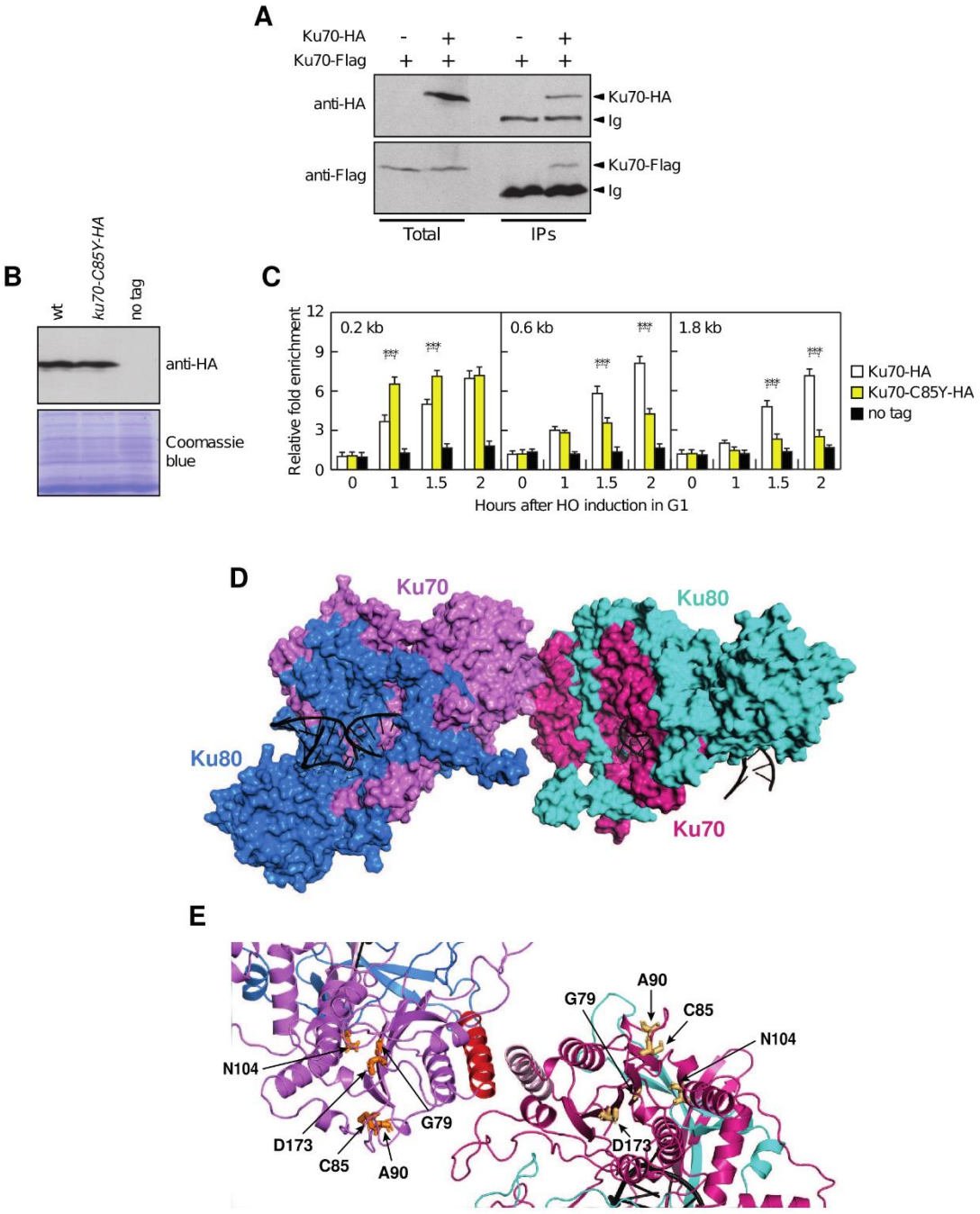
A
Ku70-HA
Ku70-Flag
anti-HA
anti-Flag
Ku70-HA
Ig
Ku70-Flag
Ig
Total
IPs
B
wt
Ku70-C85Y-HA
no tag
anti-HA
Coomassie blue
C
Relative fold enrichment
0.2 kb
0.6 kb
1.8 kb
Ku70-HA
Ku70-C85Y-HA
no tag
Hours after HO induction in G1
D
Ku70
Ku80
Ku80
Ku70
E
N104
G79
D173
C85
A90
A90
G79
C85
N104
D173

Figure 23. Ku-Ku self-interaction and Ku70 association with DSBs.
(**A**) Coimmunoprecipitation. Protein extracts were analyzed by western blotting with anti-HA and anti-Flag antibodies either directly (Total) or after immunoprecipitation (IPs) with anti-HA antibody. (**B**) Western blot with anti-HA antibody of extracts used for the ChIP analysis shown in (**C**). The same amount of protein extracts was separated on an SDS-PAGE and stained with Coomassie Blue as loading control. (**C**) ChIP analysis and qPCR. Exponentially growing YEPR cell cultures were arrested in G1 with α-factor and transferred to YEPRG to induce HO in the presence of α-factor. Relative fold enrichment of Ku70-HA and $Ku70^{C85Y}$-HA at the indicated distances from the HO cleavage site was determined after ChIP with anti HA antibody and qPCR. The mean values of three independent experiments are represented with error bars denoting s.d. ***$p<0.005$ (unpaired two-tailed Student's *t* test). (**D**) Structure of a possible conformation of Ku heterotetramer, built by protein-protein docking simulations as described in the materials and methods section, where the interface spans two vWA-like domains of the Ku70 subunits. (**E**) Detail of the interface between two opposing Ku70 vWA-like domains. The residues affected by the identified mutations are indicated as orange or beige sticks.

Tel1 kinase antagonizes Ku function in DSB end-tethering

The lack of Tel1 increases Ku persistence very close to the DSB ends [Iwasaki *et al.*, 2016]. Furthermore, mammalian ATM antagonizes end-tethering at single-ended DSBs [Britton *et al.*, 2020], raising the possibility that Tel1/ATM can modulate DSB end-tethering by regulating Ku association with DNA. However, the possible role of Tel1 in regulating Ku-mediated DSB end-tethering can be masked by the fact that Tel1 has a structural role in promoting MRX persistence at DSBs and therefore the lack of Tel1 impairs end-tethering by decreasing the amount of MRX bound at DSBs [Lee *et al.*, 2008; Cassani *et al.*, 2016; Oh *et al.*, 2018]. As Tel1 increases MRX retention at DSBs independently of its kinase activity [Cassani *et al.*, 2016], we analyzed DSB tethering and Ku association with DSBs in cells expressing a Tel1 kinase defective (*tel1-kd*) allele [Mallory and Petes, 2000], which has been already reported to suppress the DNA damage sensitivity of *sae2*Δ cells [Gobbini *et al.*, 2015]. We detected a significant decrease in percentage of two LacI-GFP spots in *tel1-kd sae2*Δ cells compared to *sae2*Δ cells (Figure 24A and B), indicating that Tel1 antagonizes DNA bridging. Furthermore, similar to $Ku70^{C85Y}$, the lack of Tel1 kinase activity increased the amount of Ku70 bound in close proximity to the HO-induced DSB ends and this effect was more pronounced in the presence of the $Ku70^{C85Y}$ mutant variant (Figure 24C). The amount of Ku70 bound at more distant sites (0.6 and 1.8 kb) from the HO-induced DSB was much lower in *tel1-kd* cells compared to wild type (Figure 24C), indicating that Tel1 controls Ku persistence at the DSB ends.

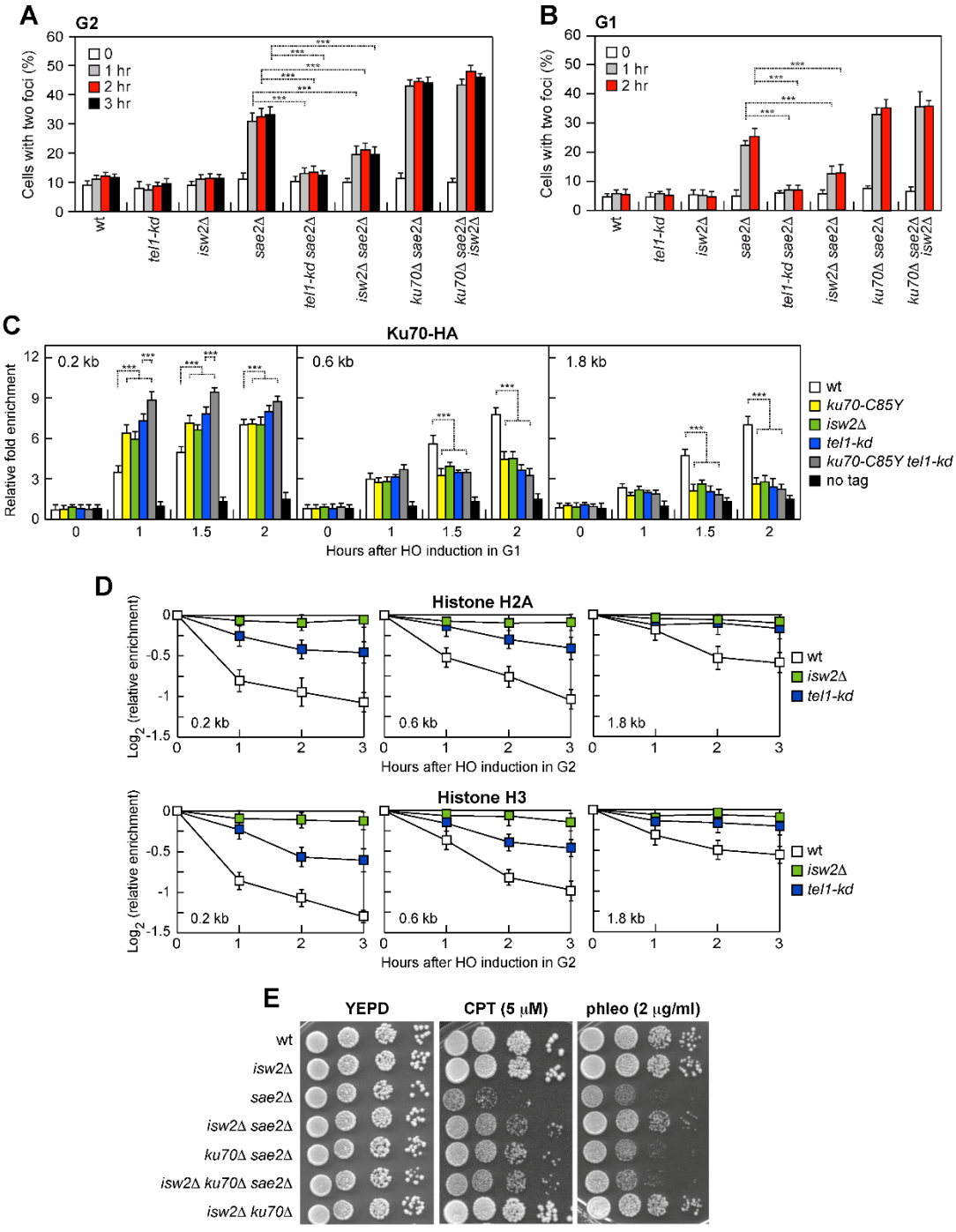
A
G2
Cells with two foci (%)
0
1 hr
2 hr
3 hr
wt
tel1-kd
isw2Δ
sae2Δ
tel1-kd sae2Δ
isw2Δ sae2Δ
ku70Δ sae2Δ
ku70Δ sae2Δ isw2Δ
B
G1
C
Ku70-HA
Relative fold enrichment
0.2 kb
0.6 kb
1.8 kb
Hours after HO induction in G1
ku70-C85Y
isw2Δ
tel1-kd
ku70-C85Y tel1-kd
no tag
D
Histone H2A
Histone H3
Log2 (relative enrichment)
Hours after HO induction in G2
E
YEPD
CPT (5 μM)
phleo (2 μg/ml)
isw2Δ ku70Δ sae2Δ
isw2Δ ku70Δ

Figure 24. The lack of Tel1 kinase or of Isw2 suppresses the DSB end-tethering defect of *sae2*Δ cells and increases Ku persistence close to the DSB ends.
(**A**, **B**) DSB end-tethering. Exponentially growing YEPR cell cultures were arrested in G2 with nocodazole (**A**) or in G1 with α-factor (**B**) at time zero and transferred to YEPRG in the presence of nocodazole or α-factor, respectively. 200 cells for each strain were analyzed to determine the percentage of cells showing two LacI-GFP foci. The mean values of three independent experiments are represented with error bars denoting s.d. ***$p<0.005$ (unpaired two-tailed Student's *t*-test). (**C**) ChIP analysis and qPCR. Exponentially growing YEPR cell cultures of JKM139 derivative strains were arrested in G1 with α-factor and transferred to YEPRG to induce HO in the presence of α-factor. Relative fold enrichment of Ku70-HA at the HO-induced DSB was evaluated after ChIP with anti-HA antibody and qPCR. The mean values of three independent experiments are represented with error bars denoting s.d. ***$p<0.005$ (unpaired two-tailed Student's *t*-test). (**D**) ChIP analysis and qPCR. HO expression was induced at time zero by galactose addition to G2-arrested cells that were kept arrested in G2 by nocodazole throughout the experiment. Relative fold enrichment of H2A or H3 at the HO-induced DSB was evaluated after ChIP with anti-H2A or anti-H3 antibody and qPCR analysis. The mean values of three independent experiments are represented with error bars denoting s.d. (**E**) Serial dilutions of exponentially growing cultures onto YEPD plates with or without CPT or phleomycin.

Nucleosome removal from DSBs antagonizes Ku function in DSB end-tethering

Previous work has shown that Ku sliding is inefficient on nucleosome-associated DNA ends [Roberts and Ramsden, 2007]. Furthermore, Ku and phosphorylated histone H2AX (γH2AX) foci are mutually exclusive [Britton *et al.*, 2013], suggesting that Ku localizes to DNA ends that are locally depleted of nucleosomes. Chromatin immunoprecipitation experiments support nucleosome disassembly near DSBs [Tsukuda *et al.*, 2005], with histone loss promoted by mammalian ATM [Berkovich *et al.*, 2007; Li and Tyler, 2016]. These findings lead to the hypothesis that Tel1 can control Ku spreading by promoting histone disassembly around a DSB. Thus, we evaluated the effect of the lack of Tel1 kinase activity on histone H2A and H3 occupancy centromere-proximal to the irreparable HO-induced DSB at the *MAT* locus. HO expression was induced by galactose addition to G2-arrested cells that were kept arrested in G2 with nocodazole to exclude possible effects of DNA replication on histone association with DNA. As expected, H2A and H3 signals near the HO-induced DSB decreased in wild-type cells, while they remained high in *tel1-kd* cells (Figure 24D), indicating that Tel1 kinase promotes nucleosome loss from DSBs.

If Tel1 antagonizes Ku bridging activity by promoting histone removal from DSBs and Ku sliding inwards, failure to remove histones should mimic the effect caused by the lack of Tel1 kinase activity on DSB tethering and Ku association with DSBs. The density of nucleosome packaging is regulated by ATP-dependent chromatin remodelers, which use the energy derived from ATP hydrolysis to evict, assemble, reposition or exchange histones throughout the genome.

We have previously shown that the lack of the chromatin remodeler Isw2 dramatically impairs nucleosome disassembly at DSBs [Casari *et al.*, 2021], prompting us to test the effect of its deletion on *sae2*Δ suppression, Ku association with DSBs, and DSB tethering.

The lack of Isw2, which impaired H2A and H3 removal from the HO-induced DSB (Figure 24D), partially suppressed both the DNA damage sensitivity (Figure 24E) and the end-tethering defect of *sae2*Δ cells (Figure 24A and B). Furthermore, similar to both *ku70-C85Y* and *tel1-kd*, it increased Ku70 association very close to the HO-induced DSB end, whereas it decreased it at more distant sites (Figure 24C). Suppression of both the DNA damage sensitivity and the end-tethering defect of *sae2*Δ cells by *ISW2* deletion requires Ku70. In fact, *isw2*Δ failed to suppress the phleomycin sensitivity of *sae2*Δ *ku70*Δ cells and did not further increase resistance to CPT of *sae2*Δ *ku70*Δ cells (Figure 24E). Furthermore, *isw2*Δ did not restore end-tethering of *ku70*Δ *sae2*Δ cells (Figure 24A and B). Unfortunately, the effect of the *tel1-kd* mutation on *ku70*Δ *sae2*Δ cells cannot be tested due the senescence phenotype of *ku70*Δ *tel1-kd* cells [Porter *et al.*, 1996]. Altogether, these data indicate that histone removal from DSBs antagonizes Ku mediated DSB bridging.

Discussion

By preventing the damaged chromatid from physically separating from the rest of the chromosome, the maintenance of the DSB ends tethered to each other facilitates their correct repair by NHEJ and the homology search during HR. This function, called end-tethering, involves both the MRX complex and Sae2 protein in *S. cerevisia*e. However, whether the Ku heterodimer has a role in bridging the DSB ends together has remained unclear. Thus, to better understand the effects of Ku complex the DNA damage response, we investigated the role of Ku to maintain the broken ends close to each other.

By characterizing a *ku70* mutation that increases DNA damage resistance of *sae2Δ* cells in a Exo1-independent manner, we provide evidence that the Ku complex has a role in maintaining an intrachromosomal association between the ends of broken chromosomes. In fact, the *ku70-C85Y* allele increases DSB end-tethering and suppresses the end-tethering defect of *sae2*Δ cells. This Ku bridging function occurs independently of MRX, as the *ku70-C85Y* allele also partially suppresses the bridging defects of *mre11*Δ and *rad50-VM* cells. Consistent with a role of Ku in DSB end-tethering, the lack of Ku70 exacerbates the end-tethering defect of *sae2*Δ cells. Interestingly, while suppression of *sae2*Δ resection defect by *KU70* deletion results in an increased CPT and MMS resistance [Mimitou and Symington, 2010; Shim *et al.*, 2010; Foster *et al.*, 2011], suppression of *sae2*Δ end-bridging defect by the *ku70-C85Y* allele also restores resistance to phleomycin. This finding indicates that end-tethering is more important than end-resection to repair phleomycin-induced DNA lesions. Consistent with this hypothesis, *mre11* mutations that increase resistance of *sae2*Δ cells to phleomycin by suppressing their end-tethering but not their resection defect, have been previously identified in Longhese's lab [Cassani *et al.*, 2018].

This finding also implies that phleomycin induced DNA lesions possess enough ssDNA to induce DSB repair by HR. As the end-tethering function of MRX was shown to be important to repair a DSB by synthesis dependent strand annealing (SDSA) possibly because it facilitates the annealing of the displaced strand to the other end of the DSB [Cassani *et al.*, 2016], the increased DNA damage resistance of *sae2*Δ cells conferred by the *ku70-C85Y* mutation might be due to a more efficient DSB repair by SDSA.

How does Ku70^{C85Y} enhance DSB end-tethering? The C85Y mutation increases the amount of Ku70 bound at the end of a DSB, arguing that this increased persistence can account for its better tethering activity and decreased Exo1 association to DSBs. The Ku heterodimer, once bound to a DSB, is known to slide along DNA with an energy-free mechanism [de Vries *et al.*, 1989]. The finding that the amount of DSB-bound Ku70^{C85Y} is higher than wild-type Ku70 very close to the DSB end, whereas it decreases with increasing distance from the DSB end, is consistent with a sliding defect that retains Ku at the DNA end.

How Ku slides on DNA in an energy-free manner is poorly understood. In the Ku-DNA complex structure, the Ku channel fits sterically with the minor and major DNA grooves so that it is too tight to allow a linear diffusion of the DNA [Walker *et al.*, 2001]. This finding suggests that Ku translocation requires either conformational changes of the ring or Ku moving in a helical manner through the DNA helix. Thus, one possibility is that the mutant Ku70^{C85Y}-Ku80 heterodimer adopts a conformation that is different from the physiological one and incompatible with the sliding. Alternatively, the limited Ku70^{C85Y} diffusion might be due to a more persistent heterotetramerization of the Ku70^{C85Y}-K80 heterodimers that helps the retainment of Ku on DNA ends. The C85Y mutation, as well as all the amino acid substitutions that suppress the DNA damage sensitivity of *sae2*Δ cells in an Exo1-independent manner, is located in the conserved N-terminal vWA-like Ku70 domain in the same region of the α5 helix

that was previously identified as required for NHEJ in yeast [Ribes-Zamora *et al.*, 2007] and involved in tetramer formation in humans [Ribes-Zamora *et al.*, 2013]. Interestingly, the analysis of the Ku70-Ku80 heterotetramer structure that we obtained by protein docking simulations raises the possibility that the C85Y residue substitution could stabilize the association of the Ku heterodimers in a conformation that can be adopted by the wild-type heterotetramer as well. Thus, although we failed to detect an increase in Ku-Ku association by coimmunoprecipitation, we favour the hypothesis that the C85Y mutation increases the ability of Ku to self-associate, thus imposing a higher energetic barrier to inward movement of Ku on DNA and thereby helping the retainment of Ku at the DNA ends.

High-resolution microscopy experiments have shown that Ku translocation on DNA appears to be more limited in a cellular context [Britton *et al.*, 2013], suggesting the existence of mechanisms that suppress Ku diffusion. We found that the lack of Tel1 kinase activity suppresses the end-tethering defect of *sae2*Δ cells. Furthermore, it increases the amount of Ku70 bound very close to the DSB end and decreases it at more distant sites, suggesting that Tel1 kinase antagonizes the ability of Ku to maintain DSB end-tethering by limiting Ku persistence at the DSB end. Several studies conducted in mammals and yeast support nucleosome eviction in the immediate vicinity of DSB sites with phosphorylated H2AX (γH2AX) being generated in the adjacent chromatin [Tsukuda *et al.*, 2005; Berkovich *et al.*, 2007; Shroff *et al.*, 2004; Kim *et al.*, 2007]. Interestingly, Ku was shown to be less able to load and translocate internally on nucleosome-associated DNA ends [Walker *et al.*, 2001; Roberts and Ramsden, 2007]. Furthermore, in mammals Ku and γH2AX foci are mutually exclusive, with Ku foci being flanked by γH2AX [Britton *et al.*, 2013], suggesting that Ku localizes to DNA ends that are locally depleted of nucleosomes. We found that Tel1 promotes histone disassembly from DSBs. Furthermore, the lack of Isw2

chromatin remodeler, which increases histone persistence at the DSB end, mimics the effect caused by the lack of Tel1 kinase on Ku-mediated DSB end-tethering and Ku persistence at DSBs, suggesting that the presence of nucleosomes helps to retain Ku at the DNA end and therefore to promote its end-bridging function. In any case, although *ISW2* deletion impairs nucleosome removal from DSBs more severely than the lack of Tel1 kinase activity, the *tel1-kd* allele suppresses the end-tethering defect of *sae2*Δ cells more efficiently than *isw2*Δ, suggesting that Tel1, besides removing histones, could act directly on Ku to regulate its DSB association.

In summary, we propose that Ku heterodimers are loaded on each side of a DSB to form a heterotetrameric complex that contributes to hold the DNA ends together. This function occurs independently of MRX and Sae2 that also posses and end-tethering function. Tel1 kinase counteracts this Ku function by promoting nucleosome removal from DSBs and Ku sliding inwards (Figure 25). As the presence of Ku at the DSB ends prevents the access of resection nucleases, this Tel1-mediated regulation of Ku association with the DSB ends provides an important layer of control in the choice between NHEJ and HR.

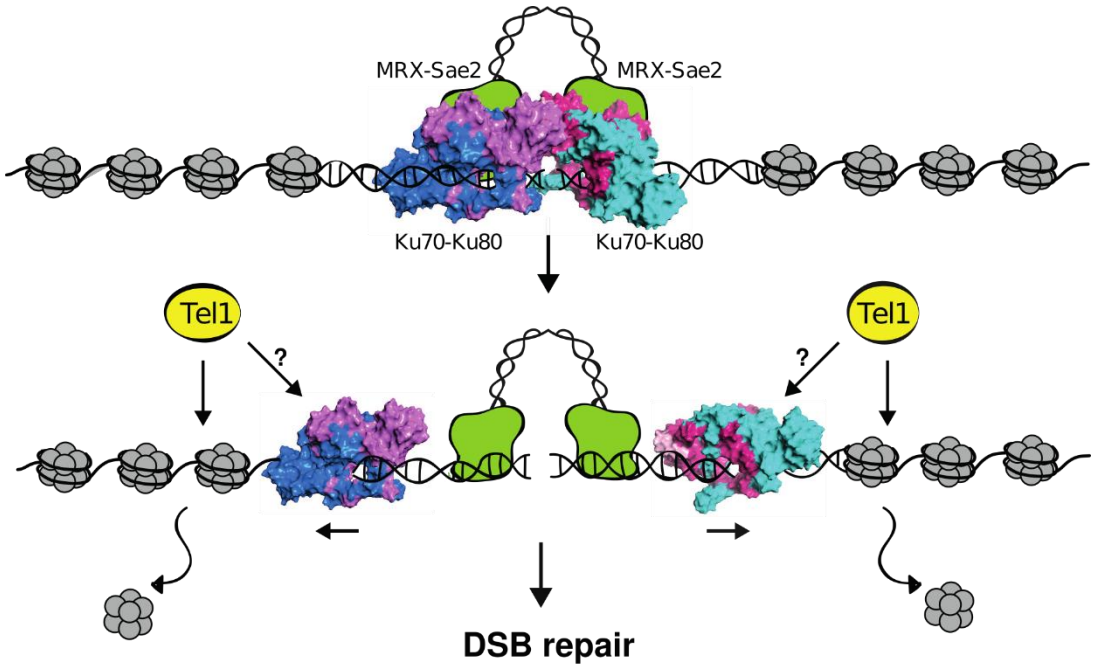

Figure 25. Model for Ku function at DSBs.
After DSB formation, two Ku heterodimers are loaded onto both sides of the DSB and contribute to maintain them in close proximity by interacting to each other. This function occurs independently of the MRX complex and Sae2, which also possess an end-tethering function. Tel1 counteracts Ku persistence at the DSB ends by promoting histone removal from DSBs and Ku sliding over the broken DNA end (black arrows). We cannot exclude the possibility that Tel1 can also act directly on Ku to control its association with the DSB ends. Ku sliding inwards can allow the loading of nucleases that initiate DSB resection and channel DSB repair into HR.

METHODS

Yeast strains and growth conditions

Saccharomyces cerevisiae is the experimental model used in this study. The strains are derivatives of W303 (*MATa/α ade2-1 can1-100 his3-11,15 leu2-3,112 trp1-1 ura3-1 rad5-535*), JKM139 (*MATa ho hmlΔ::ADE1 hmrΔ::ADE1 ade1-100 leu2-3,112 lys5 trp1::hisG ura3-52 ade3::GAL-HO*), YJK 40.6 (*MATΔ hmlΔ hmrΔ can1 lys5 ade2 leu2 trp1 ura3 his3 ade3:: GAL-HO VII::TRP1-HO LacI-GFP::URA3 LacO::LYS5 LacO::KanR*), UCC3537 (*MAT*a *ade2-101 ura3-52 lys2-801 trp1-Δ63 his3-Δ200 leu2-Δ1 URA3-TEL-VII-L ADE2-TEL-V-R*), and UCC3515 (*MATα ade2-101 his3-Δ200 leu2-Δ1 lys2-801 trp1Δ63 ura3-52 hml::URA3*). Strain genotypes are listed in Table 1. Strain JKM139, used to detect DSB resection, HO checkpoint, and to perform ChIP analysis, was kindly provided by J. Haber (Brandeis University, Waltham, USA). Strains YJK40.6, used to detect end-tethering, was kindly provided by D. P. Toczyski (University of California, San Francisco, USA). UCC3537 and UCC3515 strains, used to detect transcriptional silencing, were kindly provided by D. Gottschling (Fred Hutchinson Cancer Research Center, Seattle, USA). Plasmids containing the *rap1-H709A* and *rap1-D727A* alleles were a gift from C. Wolberger (Johns Hopkins University, Baltimore, USA), while plasmids containing the *rap1-R747L* and *rap1-Y592A* alleles were generated by site-directed mutagenesis. To integrate these alleles into the genome, *RAP1* ORFs were amplified and fused by PCR to a *LEU2* marker. The resulting PCR amplification products, containing the *RAP1* coding sequence and the *LEU2* marker gene, were used to transform cells in order to replace the *RAP1* wild-type sequence with the mutagenized DNA fragments.

Gene disruptions and tag fusions were generated by one-step PCR homology cassette amplification and standard yeast transformation procedure.

Strain	Relative genotype	Source
W303	*MAT*a *ade2-1 can1-100 his3-11,15 leu2-3,112 trp1-1 ura3-1 rad5-535*	Bonetti *et al.*, 2009
YLL1134	W303 *rif2Δ::KANMX*	Anbalagan *et al.*, 2011
YLL1223	W303 *rif1Δ::HIS3*	Anbalagan *et al.*, 2011
YLL2946	W303 *rap1ΔC::KANMX*	This study
YLL4120	W303 *rap1-R381W::LEU2 rad50-V1269M::KANMX tel1Δ::HIS3*	This study
YLL4211	W303 *rap1-D555N::LEU2 rad50-V1269M::KANMX tel1Δ::HIS3*	This study
YLL4212	W303 *rap1-P520L::LEU2 rad50-V1269M::KANMX tel1Δ::HIS3*	This study
YLL4220	W303 *RIF2-18MYC::HIS3*	This study
YLL4243	W303 *rif2-A78D::LEU2 rad50-V1269M::KANMX tel1Δ::HIS3*	This study
YLL4244	W303 *rif2-L341S::LEU2 rad50-V1269M::KANMX tel1Δ::HIS3*	This study
YLL4245	W303 *rif2-I295R::LEU2 rad50-V1269M::KANMX tel1Δ::HIS3*	This study
YLL4246	W303 *rif2-S170L,I348F::LEU2 rad50-V1269M::KANMX tel1Δ::HIS3*	This study
YLL4247	W303 *rif2-193FS::LEU2*	This study
YLL4248	W303 *rif2-294FS::LEU2*	This study
YLL4249	W303 *rif2-360FS::LEU2*	This study
YLL4250	W303 *rif2-368FS::LEU2*	This study
YLL4289	W303 *rif2-L341S-18MYC::HIS3*	This study
DMP5781/1B	W303 *rad50-V1269M::KANMX*	Cassani *et al.*, 2016
DMP5928/2C	W303 *rad50-V1269M::KANMX tel1Δ::HIS3*	Cassani *et al.*, 2016
DMP6121/2D	W303 *rif2Δ::KANMX rad50-V1269M::KANMX*	Cassani *et al.*, 2016
DMP6121/5D	W303 *rif2Δ::KANMX rad50-V1269M::KANMX tel1Δ::HIS3*	Cassani *et al.*, 2016
DMP6970/1B	W303 *rap1-R747L::LEU2*	This study
DMP6970/1D	W303 *rap1-R747L::LEU2 rif2-L341S::LEU2*	This study
DMP7010/1D	W303 *rap1-H709A::LEU2*	This study
DMP7010/2D	W303 *rap1-H709A::LEU2 rif2-L341S::LEU2*	This study
DMP7010/3D	W303 *rap1-H709A::LEU2 rad50-V1269M::KANMX*	This study
DMP7011	W303 *rap1-D727A::LEU2 rad50-V1269M::KANMX*	This study
DMP7013	W303 *rap1-R747L::LEU2 rad50-V1269M::KANMX*	This study

DMP7012/3D	W303 *rap1-D555N::LEU2 rad50-V1269M::KANMX*	This study
DMP7012/6C	W303 *rap1-D555N::LEU2*	This study
DMP7016/5C	W303 *rap1-R381W::LEU2 rad50-V1269M::KANMX*	This study
DMP7016/1C	W303 *rap1-R381W::LEU2*	This study
DMP7016/2C	W303 *rap1-R381W::LEU2 rif2Δ::HIS3*	This study
DMP7016/3D	W303 *rap1-R381W::LEU2 rad50-V1269M::KANMX rif2Δ::HIS3*	This study
DMP7017/1C	W303 *rap1-P520L::LEU2 rad50-V1269M::KANMX*	This study
DMP7017/3D	W303 *rap1-P520L::LEU2*	This study
DMP7017/1D	W303 *rap1-P520L::LEU2 rad50-V1269M::KANMX rif2Δ::HIS3*	This study
DMP7019/2D	W303 *rif2-A78D::LEU2*	This study
DMP7019/5C	W303 *rif2-A78D::LEU2 rad50-V1269M::KANMX*	This study
DMP7020/3B	W303 *rif2-L341S::LEU2 rad50-V1269M::KANMX*	This study
DMP7020/3C	W303 *rif2-L341S::LEU2*	This study
DMP7021/1B	W303 *rif2-I295R::LEU2 rad50-V1269M::KANMX*	This study
DMP7021/1D	W303 *rif2-I295R::LEU2*	This study
DMP7051/1A	W303 *rap1-Y592A::LEU2*	This study
DMP7051/1D	W303 *rap1-Y592A::LEU2 rad50-V1269M::KANMX*	This study
DMP7065	W303 *rap1-P520L::LEU2 rif2Δ::HIS3*	This study
DMP7066/2C	W303 *rap1-Y592A::LEU2 rif2Δ::HIS3*	This study
DMP7083/5C	W303 *rap1-Y592A::LEU2 rad50-V1269M::KANMX rif2Δ::HIS3*	This study
DMP7085	W303 *rif2-193FS::LEU2 rad50-V1269M::KANMX*	This study
DMP7086	W303 *rif2-294FS::LEU2 rad50-V1269M::KANMX*	This study
DMP7087	W303 *rif2-360FS::LEU2 rad50-V1269M::KANMX*	This study
DMP7088	W303 *rif2-368FS::LEU2 rad50-V1269M::KANMX*	This study
DMP7089/1A	W303 *rif2-S170L,I348F::LEU2*	This study
DMP7089/1C	W303 *rif2-S170L,I348F::LEU2 rad50-V1269M::KANMX*	This study
YLL1069.3	W303 *MATa sae2Δ::KANMX*	Gobbini *et al.*, 2015
YLL4537.3	W303 *MATa ku70-C85Y::URA3 sae2Δ::KANMX*	This study
YLL4610.8	W303 *MATa ku70-A90T::URA3 sae2Δ::KANMX*	This study
YLL4611.7	W303 *MATa ku70-N104Y::URA3 sae2Δ::KANMX*	This study
YLL4612.20	W303 *MATa ku70-G79S::URA3 sae2Δ::KANMX*	This study
YLL4551.2	W303 *MATa ku70-D173G::URA3 sae2Δ::KANMX*	This study
DMP7521/1A	W303 *MATα ku70-C85Y::URA3 sae2Δ::KANMX*	This study
DMP7523/2A	W303 *MATα ku70-C85Y::URA3*	This study
YLL4609.4	W303 *MATa ku70-G79S::URA3*	This study

YLL4535.2	W303 *MATa ku70-A90T::URA3*	This study
YLL4608.2	W303 *MATa ku70-N104Y::URA3*	This study
DMP7586/10B	W303 *MATa ku70-D173G::URA3*	This study
YLL941.1	W303 *MATa ku70Δ::HIS3*	Marsella *et al.*, 2021
DMP7541/7B	W303 *MATα ku70Δ::HIS3 sae2Δ::KANMX*	This study
DMP7560/4C	W303 *MATα ku70Δ::HIS3 sae2Δ::KANMX*	This study
DMP7609.1	W303 *MATa/α KU70-3HA::URA3/KU70-FLAG::KANMX*	This study
DMP5781/1B	W303 *MATa rad50-V1269M:: KANMX*	Cassani *et al.*, 2016
DMP7615/1B	W303 *MATa ku70-C85Y::URA3 rad50-V1269M:: KANMX*	This study
DMP7648/6D	W303 *MATa exo1Δ::HIS3*	This study
DMP7648/3C	W303 *MATa ku70-C85Y::URA3 exo1Δ::HIS3*	This study
DMP7648/4D	W303 *MATa ku70-C85Y::URA3 sae2Δ::KANMX exo1Δ::HIS3*	This study
DMP7647/6D	W303 *MATa ku70-A90T::URA3 sae2Δ::KANMX exo1Δ::HIS3*	This study
DMP7649/2A	W303 *MATα ku70-N104Y::URA3 sae2Δ::KANMX exo1Δ::HIS3*	This study
DMP7650/1A	W303 *MATα ku70-D173G::URA3 sae2Δ::KANMX exo1Δ::HIS3*	This study
DMP7651/4C	W303 *MATa ku70-G79S::URA3 sae2Δ::KANMX exo1Δ::HIS3*	This study
DMP7652/22B	W303 *MATα sae2Δ::KANMX exo1Δ::HIS3*	This study
DMP7657/4A	W303 *MATα ku70Δ::HIS3 sae2Δ::KANMX exo1Δ::HIS3*	This study
DMP7653/3B	W303 *MATα mre11-H125N*	This study
DMP7641/7C	W303 *MATa ku70Δ::HIS3*	This study
DMP7653/9A	W303 *MATα ku70-C85Y::URA3 mre11-H125N*	This study
DMP7654/7B	W303 *MATα ku70Δ::HIS3 mre11-H125N*	This study
DMP7660/11A	W303 *MATa ku70-C85Y::URA3 mre11Δ::HIS3*	This study
DMP7660/9B	W303 *MATa mre11Δ::HIS3*	This study
DMP7613/10C	W303 *MATa ku70-C85Y::URA3 sae2Δ::KANMX nej1Δ::HIS3*	This study
DMP7614/10D	W303 *MATa sae2Δ::KANMX nej1Δ::HIS3*	This study
DMP7612/5A	W303 *MATa ku70-C85Y::URA3 nej1Δ::HIS3*	This study
DMP7612/1A	W303 *MATa nej1Δ::HIS3*	This study
YLL4189.3	W303 *MATa isw2Δ::HIS3*	Casari *et al.*, 2021
DMP7636/5D	W303 *MATa ku70Δ::HIS3 sae2Δ::KANMX isw2Δ::HIS3*	This study
DMP7636/5D	W303 *MATa isw2Δ::HIS3 sae2Δ::KANMX*	This study

DMP7642/8D	W303 *MATα sae2Δ::KANMX*	This study
DMP7643/8B	W303 *MATa isw2Δ::HIS3 ku70Δ::HIS3*	This study
JKM139	*MATa hmlΔ::ADE1 hmrΔ::ADE1 ade1-100 lys5 leu2-3, 112 trp::hisG ura3-52 ho ade3::GAL-HO site*	Lee *et al.*, 1998
YLL3501	JKM139 *RAD50-3HA::URA3*	Cassani *et al.*, 2016
YLL3611	JKM139 *RIF2-18MYC::TRP1*	This study
YLL3612	JKM139 *RIF2-18MYC::URA3*	This study
YLL4120	JKM139 *RIF2-18MYC::TRP1 rap1-R747L::LEU2*	This study
YLL4222	JKM139 *rap1-R381W::LEU2*	This study
YLL4223	JKM139 *RIF2-18MYC::URA3 rap1-R381W::LEU2*	This study
YLL4552	JKM139 *RAD50-3HA::URA3 rap1-R381W::LEU2*	This study
YLL4224	JKM139 *rap1-P520L::LEU2*	This study
YLL4200	JKM139 *RIF2-18MYC::URA3 rap1-P520L::LEU2*	This study
YLL4171	JKM139 *RAD50-3HA::URA3 rap1-P520L::LEU2*	This study
YLL4225	JKM139 *rap1-D555N::LEU2*	This study
YLL4551	JKM139 *RAD50-3HA::URA3 rap1-D555N::LEU2*	This study
YLL4227	JKM139 *rap1-Y592A::LEU2*	This study
YLL4221	JKM139 *RIF2-18MYC::URA3 rap1-Y592A::LEU2*	This study
YLL4242	JKM139 *RAD50-3HA::URA3 rif2-L341S::LEU2*	This study
DMP6157	JKM139 *RAD50-3HA::URA3 rif2Δ::HIS3*	This study
DMP7034	JKM139 *RAD50-3HA::URA3 rap1-R747L::LEU2*	This study
DMP7044/1D	JKM139 *RAD50-3HA::URA3 rap1-Y592A::LEU2*	This study
DMP7090	JKM139 *RIF2-18MYC::URA3 rap1-H709A::LEU2*	This study
DMP7091	JKM139 *RIF2-18MYC::URA3 rap1-D727A::LEU2*	This study
DMP7096	JKM139 *RAD50-3HA::URA3 rif2-L341S::LEU2*	This study
DMP7126	JKM139 *RAD50-3HA::URA3 rap1-D727A::LEU2*	This study
DMP7127	JKM139 *RAD50-3HA::URA3 rap1-H709A::LEU2*	This study
YLL1523.3	JKM139 *MATa sae2Δ::KANMX*	Gobbini *et al.*, 2015
DMP7529/2D	JKM139 *MATa ku70-C85Y::URA3*	This study
YLL4548.6	JKM139 *MATa ku70-C85Y::URA3 sae2Δ::KANMX*	This study
DMP6433/6C	JKM139 *MATa KU70-3HA::URA3 bar1Δ::TRP1*	Gobbini *et al.*, 2018
DMP7562/2B	JKM139 *MATa ku70-C85Y-3HA::TRP1 bar1Δ::TRP1*	This study
DMP7621/12A	JKM139 *MATa KU70-3HA::URA3 tel1-kd::LEU2 bar1Δ::TRP1*	This study
DMP7622/24A	JKM139 *MATa ku70-C85Y-3HA::URA3 tel1-kd::LEU2 bar1Δ::TRP1*	This study
DMP7638/19D	JKM139 *MATa KU70-3HA::URA3 isw2Δ::HPHMX*	This study

	bar1Δ::TRP1	
DMP6758/8B	JKM139 *MATa EXO1-MYC bar1Δ::HPHMX*	Gobbini *et al.*, 2018
DMP7655/1A	JKM139 *MATa EXO1-18MYC::TRP1 ku70Δ::URA3 bar1Δ::HPHMX*	This study
DMP7625/4C	JKM139 *MATa EXO1-MYC ku70-C85Y::URA3 bar1Δ::HPHMX*	This study
DMP6187/3B	JKM139 *MATa tel1-kd::LEU2*	Gobbini *et al.*, 2015
YLL4264.1	JKM139 *MATa isw2Δ::HPHMX*	Casari *et al.*, 2021
YJK40.6	*MATΔ hmlΔ hmrΔ can1 lys5 ade2 leu2 trp1 ura3 his3 ade3:: GAL-HO VII::TRP1-HO LacI-GFP::URA3 LacO::LYS5 LacO::KanR*	Kaye *et al.*, 2004
YLL3641.6	YJK40.6 *rad50-V1269M::HPHMX*	Cassani *et al.*, 2016
YLL3642.1	YJK40.6 *rad50-V1269M::HPHMX rif2Δ::LEU2*	Cassani *et al.*, 2016
YLL4280	YJK40.6 *rad50-V1269M::HPHMX rap1-R381W::LEU2*	This study
YLL4281	YJK40.6 *rad50-V1269M::HPHMX rap1-P520L::LEU2*	This study
YLL4283	YJK40.6 *rap1-R381W::LEU2*	This study
YLL4284	YJK40.6 *rap1-P520L::LEU2*	This study
YLL4286	YJK40.6 *rad50-V1269M::HPHMX rap1-R747L::LEU2*	This study
YLL4287	YJK40.6 *rad50-V1269M::HPHMX rap1-H709A::LEU2*	This study
YLL4288	YJK40.6 *rad50-V1269M::HPHMX rif2-L341S::LEU2*	This study
YLL4538.11	YJK40.6 *ku70-C85Y::LEU2*	This study
YLL1709.11	YJK40.6 *sae2Δ::NATMX*	Clerici *et al.*, 2015
YLL4540.2	YJK40.6 *ku70-C85Y::LEU2 sae2Δ::NATMX*	This study
YLL4555.4	YJK40.6 *ku70Δ::LEU2*	This study
YLL4558.1	YJK40.6 *ku70Δ::LEU2 sae2Δ::NATMX*	This study
YLL1731.29	YJK40.6 *mre11Δ::NATMX*	Clerici *et al.*, 2015
YLL4574.1	YJK40.6 *ku70-C85Y::LEU2 mre11Δ::NATMX*	This study
YLL3641.6	YJK40.6 *rad50-V1269M::HPHMX*	Cassani *et al.*, 2016
YLL4570.1	YJK40.6 *ku70-C85Y::LEU2 rad50-V1269M::HPHMX*	This study
YLL4589.4	YJK40.6 *tel1-kd::LEU2*	This study
YLL4587.2	YJK40.6 *tel1-kd::LEU2 sae2Δ::NATMX*	This study
YLL4591.2	YJK40.6 *isw2Δ::LEU2*	This study
YLL4592.11	YJK40.6 *isw2Δ::LEU2 sae2Δ::NATMX*	This study
YLL4608.3	YJK40.6 *isw2Δ::HPHMX ku70Δ::LEU2 sae2Δ::NATMX*	This study

UCC3537	*MAT*a *ade2-101 ura3-52 lys2-801 trp1-Δ63 his3-Δ200 leu2-Δ1 URA3-TEL-VII-L ADE2-TEL-V-R*	Huang *et al.*, 1997
YLL405	UCC3537 *sir3Δ::KANMX4*	Longhese *et al.*, 2000
YLL4208	UCC3537 *rap1-Y592A::LEU2*	This study
YLL4213	UCC3537 *rap1-R381W::LEU2*	This study
YLL4214	UCC3537 *rap1-D555N::LEU2*	This study
YLL4215	UCC3537 *rap1-P520L::LEU2*	This study
YLL4238	UCC3537 *rap1-P520L::LEU2 sir3Δ::KANMX4*	This study
YLL4239	UCC3537 *rap1-D555N::LEU2 sir3Δ::KANMX4*	This study
YLL4240	UCC3537 *rap1-R381W::LEU2 sir3Δ::KANMX4*	This study
YLL4241	UCC3537 *rap1-Y592A::LEU2 sir3Δ::KANMX4*	This study
UCC3515	*MATα ade2-101 his3-Δ200 leu2-Δ1 lys2-801 trp1Δ63 ura3-52 hml::URA3*	Singer *et al.*, 1998
YLL4209	UCC3515 *rap1-Y592A::LEU2*	This study
YLL4216	UCC3515 *rap1-R381W::LEU2*	This study
YLL4217	UCC3515 *rap1-D555N::LEU2*	This study
YLL4218	UCC3515 *rap1-P520L::LEU2*	This study

Table 1. *Saccharomyces cerevisiae* strains used in these studies.

Yeast growth media

YEP (Yeast-Extract Peptone) is the standard rich medium for *S. cerevisiae* and contains 10 g/L yeast extract, 20 g/L peptone, and 50 mg/L adenine. YEP must be supplemented with 2% glucose (YEPD), 2% raffinose (YEPR) or 2% raffinose and 3% galactose (YEPRG) as carbon source. YEP-based selective media are obtained including 400 μg/mL G418, 300 μg/mL hygromicin-B (HPH) or 100 μg/ml nourseothricin (NAT). Solid media are obtained including 2% agar. Stock solutions are 50% glucose, 30% raffinose, 30% galactose, 80 mg/mL G418, 50 mg/mL hygromicin-B, 50 mg/mL nourseothricin. YEP and glucose stock solution are autoclave-sterilized and stored at RT. Sugars and antibiotics stock solutions are sterilized by microfiltration and stored at 30°C/37°C and -20°C, respectively. S.C. (Synthetic Complete) is the minimal growth medium for *S.*

cerevisiae and contains 1.7 g/L YNB (Yeast Nitrogen Base) without amino acids, 5 g/L ammonium sulphate, 200 μM inositol, 25 mg/L uracil, 25 mg/L adenine, 25 mg/L hystidine, 25 mg/L leucine, 25 mg/L tryptophan. S.C. can be supplemented with drop-out solution (20 mg/L arginine, 60 mg/L isoleucine, 40 mg/L lysine, 10 mg/L methionine, 60 mg/L phenylalanine, 50 mg/L tyrosine), based on yeast strains requirements. One or more amino acid/base can be omitted to have S.C selective media (e.g. S.C. -ura is S.C. lacking uracil). Solid media are obtained by including 2% agar. S.C. medium and S.C. medium with 5-fluoroorotic acid (5-FOA) (1%) were used to assay *URA3* gene silencing. S.C. medium containing a limiting concentration of adenine (2 mg/l) was used for the colony color assay based on the *ADE2* reporter gene. Stock solutions are 17 g/L YNB + 50 g/L ammonium sulphate (or 10 g/L monosodic glutamic acid), 5 g/L uracil, 5 g/L adenine, 5 g/L hystidine, 5 g/L leucine, 5 g/L tryptophan, 100X drop out solution (2 g/L arginine, 6 g/L isoleucine, 4 g/L lysine, 1 g/L methionine, 6 g/L phenylalanine, 5 g/L tyrosine), 20 mM inositol. All these solutions are sterilized by micro-filtration and stored at 4°C. VB sporulation medium contains 13.6 g/L sodium acetate, 1.9 g/L KCl, 0.35 g/L $MgSO_4$, 1.2 g/L NaCl and pH is adjusted to 7.0. To obtain solid medium include 2% agar. Media are autoclave-sterilized.

Synchronization of yeast cells with α-factor

By using α-factor, it is possible to synchronize a population of yeast cells in G1 phase of the cell cycle. This pheromone activates a signal transduction cascade that arrests the cell cycle in G1 phase. Only *MAT*a cells are responsive to α-factor. To synchronize a population of exponentially growing yeast cells in YEPD, 2 μg/mL α-factor are added to cell cultures at the concentration of $8x10^6$ cells/mL.

If the percentage of budded cells falls below 5%, cells are considered G1-arrested. To detect end-tethering, cells are then washed and resuspended in fresh medium with 5 μg/mL α-factor to maintain G1-arrest cells.

Synchronization of yeast cells with nocodazole

By using nocodazole, it is possible to synchronize a population of yeast cells in G2 phase of the cell cycle. This drug causes the depolymerization of microtubules, thus activating the mitotic checkpoint which arrests cell cycle at the metaphase to anaphase transition. To synchronize a population of exponentially growing yeast cells in YEPD, 5 μg/mL nocodazole, together with DMSO at a final concentration of 1% (use a stock solution of nocodazole 0,5 mg/mL in 100% DMSO), are added to cell cultures at the concentration of $8x10^6$ cells/mL. If the percentage of dumbbell cells reaches 95%, cells are considered G2-arrested. To detect end-tethering, cells are then washed and resuspended in fresh medium with 15 μg/mL nocodazole to maintain G2-arrest cells.

Transformation of *S. cerevisiae* cells

Transformation of *S. cerevisiae* cells YEPD exponentially growing yeast cells are harvested by centrifugation and washed with 1 mL 1 M lithium acetate (LiAc) pH 7.5. Cells are then resuspended in 1 M LiAc pH 7.5 to obtain a cells/LiAc 1:1 solution. 24 μL cells/LiAc are incubated 1 hour at RT with 90 μL 50% PEG (PolyEthylene Glycol) 4000, 8 μL carrier DNA (salmon sperm DNA) and 4-10 μL PCR DNA of interest (divide these quantities for transformation with plasmids). After the addition of 12 μL 60% glycerol, cells are incubated at RT for 1 hour, heat-shocked at 42°C for 10-20 minutes, and plated on appropriate selective medium.

Search for *rif2* mutations that suppress the DNA damage sensitivity of *rad50-VM* cells

To search for *rif2* alleles that suppress the *rad50-VM* sensitivity to camptothecin (CPT), genomic DNA from a strain carrying the *LEU2* gene located 245 bp downstream of the *RIF2* stop codon was used as template to amplify by low-fidelity PCR a *RIF2* region spanning from position −550 bp to +410 bp from the *RIF2* coding sequence. 30 independent PCR reaction mixtures were prepared, each containing 5U GoTaq® G2 Flexi DNA polymerase (Promega), 10 ng genomic DNA, 500 ng each primer, 0.5 mM each dNTP (dATP, dTTP, dCTP), 0.1 mM dGTP, 0.5 mM $MnCl_2$, 10 mM Tris-HCl pH 8.3, 50 mM KCl, and 3 mM $MgCl_2$. The resulting PCR amplification products, containing the *RIF2* coding sequence and the *LEU2* marker gene, were used to transform a *rad50-VM* mutant strain (DMP5781/1B) in order to replace the *RIF2* wild-type sequence with the mutagenized DNA fragments. Transformant clones were selected on synthetic medium without leucine and then assayed by drop test for increased viability in the presence of CPT compared to *rad50-VM* cells.

Search for *rap1* mutations that suppress or exacerbate the DNA damage sensitivity of *rad50-VM* cells

To search for *rap1* alleles that suppress or exacerbate the *rad50-VM* sensitivity to CPT, genomic DNA from a strain carrying the *LEU2* gene located 350 bp upstream of the *RAP1* ATG start codon was used as template to amplify by low-fidelity PCR a *RAP1* region spanning from position −500 bp to +220 bp from the *RAP1* coding sequence. 30 independent PCR reaction mixtures were prepared, each containing 5U GoTaq® G2 Flexi DNA polymerase (Promega), 10 ng genomic DNA, 500 ng each primer, 0.5 mM each dNTP (dATP, dTTP, dCTP),

0.1 mM dGTP, 0.5 mM $MnCl_2$, 10 mM Tris-HCl pH 8.3, 50 mM KCl, and 3 mM $MgCl_2$. The resulting PCR amplification products, containing the *RAP1* coding sequence and the *LEU2* marker gene, were used to transform a *rad50-VM* mutant strain (DMP5781/1B) in order to replace the *RAP1* wild-type sequence with the mutagenized DNA fragments. Transformant clones were selected on synthetic medium without leucine and then assayed by drop test for increased or decreased viability in the presence of CPT compared to *rad50-VM* cells.

Search for *ku70* mutations that suppress the DNA damage sensitivity of *sae2*Δ cells

To search for *ku70* alleles that suppress the *sae2*Δ sensitivity to different genotoxic agents, genomic DNA from strains carrying the *URA3* gene located 500 bp upstream of the *KU70* ORF was used as template to amplify by low-fidelity PCR the *KU70* coding region, respectively. Thirty independent PCR reaction mixtures were prepared, each containing 5U EuroTaq DNA polymerase (Euroclone), 10 ng genomic DNA, 500 ng each primer, 0.5 mM each dNTP (dATP, dTTP, dCTP), 0.1 mM dGTP, 0.5 mM $MnCl_2$, 10 Mm Tris-HCl pH 8.3, 50 mM KCl, and 1.5 mM $MgCl_2$. The resulting PCR amplification products, containing the *KU70* coding sequence and the *URA3* marker gene, were used to transform a *sae2*Δ strain (YLL1069.3). 3000 transformants were selected on synthetic medium without uracil and then assayed by drop tests for decreased sensitivity to phleomycin compared to *sae2*Δ cells.

Extraction of yeast genomic DNA (Teeny yeast DNA preps)

About $5x10^8$ yeast cells from overnight exponentially growing cultures (or cultures treated to induce damage) are harvested by centrifugation and washed

with 1 mL of a 0.9 M sorbitol, 0.1 M EDTA pH 7.5 solution. Dried pellet can eventually be stored -20°C or it can be resuspended in 400 µL of the previous solution supplemented with 14 mM β-mercaptoethanol. Yeast cells wall is digested by 1-hour incubation at 37°C with 0.4 mg/mL 20T zymolyase. Spheroplasts are harvested by 1-minute centrifugation and resuspended in 400 µL 1X TE (10 mM Tris-HCl pH 7.5, 1 mM EDTA pH 7.5). After addition of 90 µL of a solution containing 278 mM EDTA pH 8.5, 445 mM Tris-base and 2.2% SDS, spheroplasts are incubated 30 minutes at 65°C. Following the addition of 80 µL 5M potassium acetate, samples are kept on ice for 1 hour. Cell residues are eliminated by 30 minutes centrifugation at 4°C. DNA is then precipitated with chilled 100% ethanol, resuspended in 500 µL 1X TE and incubated 1 hour with 2,5 µL 1 mg/mL RNase to eliminate RNA. DNA is then precipitated with 500 µL isopropanol and resuspended in the appropriate volume of 1X TE solution.

Polymerase Chain Reaction (PCR)

By using PCR, it is possible to obtain a high copy number of a specific DNA fragment starting from a very low quantity of DNA. The reaction is directed to the DNA fragment of interest, by using a couple of oligonucleotides flanking the specific DNA sequence. These oligonucleotides work as primers for the DNA polymerase. The reaction consists of several polymerization cycles, based on 3 main temperature-dependent steps: denaturation of DNA (which occurs over 90°C), primer annealing to the DNA (it typically takes place at 45-55°C depending on primers features), synthesis of the sequence of interest by a thermophilic DNA polymerase (which usually works at 72°C). Different polymerases with different properties (processivity, fidelity, working temperature) are commercially available and suitable for different purposes. Taq polymerase is generally used for analytical or mutagenic PCR. High-fidelity polymerases, like Phusion and VENT polymerases, are generally employed when

100% accuracy is required. The typical 50 µL PCR mixture contains 1µL template DNA, 0.5 µM each primer, 200 µM dNTPs, 5 µL 10X Reaction Buffer, 1 mM $MgCl_2$, 1-2 U DNA polymerase and water to 50 µL. The typical cycle-program for a reaction is as follows: step 1, 2 minutes denaturation at 94-95°C; step 2, 30 seconds denaturation at 94-95°C; step 3, 1 minute annealing at primers Tm (melting temperature); step 4, 1 minute synthesis per kb at 72°C; step 5, return to step 2 and repeat 30 times; step 6, 10 minutes at 72°C. The choice of primers sequences determines the working Tm, which depends on the length (L) and GC% content of the oligonucleotides and can be calculated as follows: $Tm = 59.9 + 0.41(GC\%) – 675/L$.

Agarose gel electrophoresis

Agarose gel electrophoresis is the easiest and most common way to separate and analyze DNA molecules. This technique allows the separation of DNA fragments based on their different molecular weight (or length in kb). The purpose of this technique might be to visualize the DNA, to quantify it or to isolate a particular DNA fragment. The DNA is visualized by the addition in the gel of Ethidium Bromide (EtBr), a fluorescent dye that intercalates between the bases of nucleic acids. Ethidium Bromide absorbs UV light and emits the energy as visible orange light, revealing the DNA molecules to which it is bound. To pour a gel, agarose powder is mixed with 1X TAE (0.04 M Tris-Acetate, 0.001 M EDTA) to the desired concentration, and the solution is heated until it is completely melted.

Most gels are between 0.8% and 2% agarose. A 0.8% gel displays good resolution of large DNA fragments (5-10 kb), while a 2% gel shows good resolution of small fragments (0.2-1 kb). Ethidium Bromide is added to the gel at a final concentration of 1 µg/mL to facilitate visualization of the DNA after electrophoresis. After cooling the gel solution to about 60°C, it is poured into

a casting tray containing a samplecomb and it is placed at RT or at 4°C to solidify. Then, the gel is placed into an electrophoresis chamber, it is covered with 1X TAE buffer, and the comb is removed. Samples containing DNA mixed with loading buffer are pipetted into the sample wells. The loading buffer contains 0.05% bromophenol blue and 5% glycerol, which give color and density to the sample. A marker containing DNA fragments of known length and concentration is loaded in parallel to determine the size and the quantity of DNA fragments in the samples. Current is applied and DNA migrates toward the positive electrode. When adequate migration has occurred, DNA fragments are visualized by placing the gel under an UV transilluminator.

Spot assays

Cells grown overnight were diluted to $1x10^7$ cells/ml. 10-fold serial dilutions were spotted on YEPD with or without indicated concentrations of DNA damaging drugs. Plates were incubated for three days at 25°C or 30°C.

DSB resection at *MAT* locus (Southern blot method)

YEPR exponentially growing cell cultures of JKM139 derivative strains, carrying the HO cut site at the *MAT* locus, were transferred to YEPRG at time zero. Genomic DNA was extracted at different time points following the induction of the HO endonuclease. The *Ssp*I-digested genomic DNA was precipitated by adding 0.3 M NaAc pH 5.2, 5 mM EDTA pH 8, and two volumes EtOH 100%. After chilling overnight, samples are centrifuged 30 minutes at 4°C and pellet is resuspended in alkaline gel loading buffer (50 mM NaOH, 1 mM EDTA pH 8, 2.5% Ficoll (type 400), and 0.025% bromophenol blue). Denatured DNA is loaded onto a 0.8% agarose gel, previously equilibrated in alkaline

electrophoresis buffer (50 mM NaOH, 1 mM EDTA pH 8), and a glass plate is placed on the gel to prevent the dye diffusing from the agarose during the run. Denaturing gel is run slowly at low voltages (e.g. 30V overnight). After the DNA has migrated about 14 cm, the gel can be stained with 0.5 μg/mL Ethidium Bromide in 1X TAE buffer for 1 hour and DNA is visualized by placing the gel under an UV transilluminator. Gel is then soaked in 0.25 N HCl for 7 minutes with gentle agitation, rinsed with water for 10 minutes, soaked in 0.5 NaOH, 1.5 M NaCl for 30 minutes and rinsed again with water for 10 minutes. DNA is blotted overnight by capillary transfer onto neutral nylon membrane using 10X SSC. Membrane is then neutralized in 0.5M Tris-HCl pH 7.5, 1 M NaCl, air dried and UV-crosslinked. Hybridization is carried out by incubating the membrane for 5 hours at 42°C with pre-hybridization buffer (5X SSPE, 50% formamide, 4X denhardt's solution +BSA, 6% destran sulphate, 100 μg/mL salmon sperm DNA, 200 μg/mL tRNA carrier), followed by overnight incubation at 42°C with the pre-hybridization buffer supplemented with the single-stranded RNA (ssRNA) probe, that anneals with the unresected strand at one side of the HO-induced DSB [Casari *et al.,* 2021]. This probe was obtained by *in vitro* transcription using Promega Riboprobe System-T7 and plasmid pML514 as a template. Plasmid pML514 was constructed by inserting in the pGEM7Zf *Eco*RI site a 900-bp fragment containing part of the *MAT* locus (coordinates 200870 to 201587 on chromosome III) and labelling it with [α-32P]-UTP. Following hybridization, membrane is washed twice with 5X SSPE (20X SSPE: 3 M NaCl, 200 mM NaH_2PO_4, 20mM EDTA, pH 7.4) at 42°C for 15 minutes; 30 minutes with 1X SSPE 0.1%, SDS at 42°C; 30 minutes with 0.1X SSPE, 0.1% SDS at 42°C; twice with 0.2X SSPE 0.1%, SDS at 68°C for 15 minutes; and 5 minutes with 0.2X SSPE at RT. Finally, membrane is air dried and exposed to an autoradiography film.

Quantitative analysis of DSB resection was performed by calculating the ratio of

band intensities for ssDNA and total amount of DSB products. The resection efficiency was normalized with respect to the HO cleavage efficiency for each time point. The amount of ssDNA was normalized to cut efficiency by subtracting the value of the uncut band from the total amount of DSB products for each time point. Densitometric analysis of band intensities was performed using Scion Image Beta 4.0.2 software.

Southern blot analysis of telomere length

To determine the length of native telomeres, genomic DNA was extracted from YEPR exponentially growing cell cultures of W303 derivative strains. The *Xho*I-digested genomic DNA was precipitated by adding 0.3 M NaAc pH 5.2, 5 mM EDTA pH 8.0, and two volumes EtOH 100%. After chilling overnight, samples are centrifuged 30 minutes at 4°C and pellet is resuspended in a gel-loading buffer with 0.025% bromophenol blue. *Xho*I-digested genomic DNA was subjected to 0.8% agarose gel electrophoresis at low voltages (e.g. 60V overnight). After the DNA has migrated about 20 cm, the gel can be stained with 0.5 μg/mL Ethidium Bromide in 1X TAE buffer for 1 hour and DNA is visualized by placing the gel under an UV transilluminator. Gel is then soaked with gentle agitation in 0.2 M NaOH, 0.6 M NaCl solution for 45 minutes, rinsed with water for 10 minutes, soaked in 1.5 M NaCl, 1 M Tris pH 7.4 solution for 45 minutes and rinsed again with water for 10 minutes. DNA is blotted overnight by capillary transfer onto neutral nylon membrane using 10X SSC. Membrane is then air dried and UV-crosslinked. Hybridization is carried out by incubating the membrane for 5 hours at 55°C with pre-hybridization buffer (0.5 M $NaPO_4$ pH 7.2, 1 mM EDTA pH 7.5, SDS 7%, BSA 1%), followed by overnight incubation at 55°C with the pre-hybridization buffer supplemented with a 32^P-labeled poly(GT) probe. This probe anneals with telomeric DNA, and it was obtained by *in vitro* transcription using DECAprime II kit (Thermo Fisher Scientific) and labelling it with [α-32^P]-

ATP. Following hybridization, membrane is washed twice with 0.2 M $NaPO_4$ pH 7.2, SDS 1% solution at 55°C for two hours. Finally, membrane is air dried and exposed to an autoradiography film.

Western blotting

Protein extracts for western blot analysis were prepared by trichloroacetic acid (TCA) precipitation. Total protein extracts are prepared from $1x10^8$ cells, collected from exponentially growing yeast cultures (or cultures treated to induce damage). Cells are harvested by centrifugation, washed with 1 mL 20% trichloracetic acid (TCA) to prevent proteolysis, and then resuspended in 100 or 200 µL 20% TCA. After the addition of acid-washed glass beads, the samples were vortexed for 10 min. The beads were washed with 200 µL of 5% TCA twice and the extract was collected in a new tube. The crude extract was precipitated by centrifugation at 850 xg for 10 min. TCA was discarded and samples were resuspended in 70 µL 6X Laemmli buffer (60 mM Tris, pH 6.8, 2% SDS, 10% glycerol, 100mM DTT, 0.2% bromophenol blue) and 30 µL 1M Tris pH 8.0. Prior to loading, samples were boiled at 100°C for 2 minutes and centrifuged at 850 xg for 10 min. Supernatant containing the solubilized proteins were separated on 10% polyacrylamide gels. (10% Running gel: 375 mM Tris-HCl pH 8.8, 0,1% SDS, 10% Acrylamide, 0,13% Bisacrylamide, 0,1% APS, 0.001% Temed – Stacking gel: 125 mM Tris-HCl pH 6.8, 0,1% SDS, 5% Acrylamide, 0,14% Bisacrylamide, 0,1% APS, 0.001% Temed). Proteins are separated based on their molecular weight by polyacrylamide gel electrophoresis in the presence of sodium dodecyl sulphate (SDS-PAGE). When adequate migration has occurred, proteins are blotted onto nitrocellulose membrane. Membrane is usually saturated by 1-hour incubation in 1X TBS (150 mM NaCl, 50 mM Tris-HCl pH 8) supplemented with 4% milk and 0.2% triton X-100. Membranes are then incubated for 2 hours with primary antibodies (in 1X TBS + 4% milk + 0.2%

triton) and washed three times for 10 minutes with 1X TBS. Subsequently membranes are incubated for 1 hour with secondary antibodies (in 1X TBS + 4% milk + 0,2% triton) and again washed three times with 1X TBS. Detection is performed with ECL (Enhanced ChemiLuminescence - Genespin) and autoradiography films according to the manufacturer. HA- or Myc- or Flag-tagged proteins were detected by using anti-HA (12CA5) (1:2000) or anti-Myc (9E10) (1:1000) or anti-Flag (F1804 by Sigma) (1:500) antibodies, respectively.

Coimmunoprecipitation (CoIP)

Total protein extracts were prepared by breaking cells in 300 µl of buffer containing 50 mM HEPES pH 7.5, 250 mM NaCl, 20% glycerol, 1 mM sodium orthovanadate, 60 mM β-glycerophosphate, 1 mM PMSF and protease inhibitor cocktail (Roche Diagnostics). An equal volume of phosphate buffer containing 250 mM NaCl was added to clarified protein extracts and tubes were incubated for 2 hours at 4°C with 50 µl of a 50% (v/v) Protein A-Sepharose together with anti-Rap1 polyclonal antibodies (gift from D. Shore, University of Geneva, Switzerland) or with 50 µL of Protein G Dynabeads and 5 µg anti-HA (12CA5) antibodies. The resins were then washed twice with 1 ml of phosphate buffer containing 250 mM NaCl. Bound proteins were visualized by western blotting with anti-Rap1 or anti-Myc (9E10) or anti-HA (12CA5) (1:2000) or anti-Flag (F1804 by Sigma) (1:500) antibodies after electrophoresis on a 10% SDS-polyacrylamide gel.

Chromatin immunoprecipitation (ChIP) and qPCR

YEPR exponentially growing cell cultures (50 mL at concentration of $8x10^6$ cells/mL) of JKM139 derivative strains, carrying the HO cut site at the *MAT*

locus, were transferred to YEPRG at time zero. Crosslinking was done with 1% formaldehyde for 10 min (Rad50, Exo1) or 15 min (Rif2, Rif2-L341S, Rap1, Rap1-R381W, Rap1-P520L, Rap1-D555N, Rap1-Y592A, Ku70, Ku70-C85Y, H2A histone, and H3 histone). The reaction was stopped by adding 0.125 M Glycine for 5 min. Treated cells are kept on ice until centrifugation at 3000 rpm for 5 minutes at 4°C.

Cell pellet is washed with 30 mL HBS buffer (50 mM HEPES pH 7.5, 140 mM NaCl) and then with 25 mL ChIP lysis buffer (50 mM HEPES pH 7.5, 140 mM NaCl, 1 mM EDTA pH 8, 1% IGEPAL CA-630, 0.1% Sodium deoxycholate). After centrifugation at 3000 rpm for 5 minutes, the supernatant is carefully and completely removed. Then 0.4 mL of ChIP lysis buffer, supplemented with complete anti-proteolitic tablets (Roche) and 1 mM phenylmethylsulfonyl fluoride (PMSF), is added and samples are resuspended and stored at -80°C. The following day, cells are broken at 4°C with glass beads by mechanical disruption. After breaking cells, the glass beads are eliminated. This passage is followed by centrifugation at 4°C at 14000 rpm for 30 minutes. Pellet is resuspended in 0.5 mL ChIP lysis buffer, supplemented with antiproteolitics and PMSF, and then sonicated (5 cycles of 25 seconds at 40% power output), to share DNA in fragments of 500-1000 bp. After centrifugation at 4°C at 10000 rcf for 5 minutes, 460 µL supernatant are retained and further clarified by centrifugation at 4°C at 10000 rcf for 15 minutes. 400 µL of clarified supernatant are immunoprecipitated with Dynabeads coated with specific antibodies, while 5 µL supernatant are kept as "*input DNA*". Immunoprecipitation was performed by incubating samples with Dynabeads Protein G (Thermo Fisher Scientific) for 3 hours at 4°C in the presence of 5 µg anti-Rap1 or anti-HA (12CA5) or anti-Myc (9E10) antibodies. H2A and H3 histones were immunoprecipitated by using 5 µg anti-H2A (39945, Active Motif) and 4 µg anti-H3 (ab1791, Abcam) antibodies, respectively. After 3 hours incubation with the desired antibodies, dynabeads are

washed at RT as follow: twice with SDS buffer (50 mM HEPES pH 7.5, 1 mM EDTA pH 8, 140 mM NaCl, 0.025% SDS), once with High-Salt buffer (50 mM HEPES pH 7.5, 1 mM EDTA pH 8, 1 M NaCl), once with T/L buffer (20 mM Tris-HCl pH 7.5, 250 mM LiCl, 1 mM EDTA pH 8, 0.05% sodium deoxycholate, 0.5% IGEPAL CA630), and finally twice with T/E buffer (20 mM Tris-HCl pH 7.5, 0.1 mM EDTA pH 8). All the washes are done by pulling down Dynabeads and then nutating them for 5 minutes with the specific washing buffer. After the last wash, Dynabeads are resuspended in 145 µL 1X TE + 1% SDS, shaked on a vortex for 2 minutes, kept at 65°C for 10 minutes, shaked on vortex again and then pulled down. Then, 120 µL of the supernatant are put at 65°C overnight for reverse cross-linking. Also the previously taken input DNA samples must be put at 65°C overnight after the addition of 115 µL of 1X TE + 1% SDS buffer. The next day, DNA is purified by using QIAGEN QIAquick PCR purification kit. 600 µL PB buffer are added to each sample and, after vortexing, the sample is loaded onto spin columns, followed by centrifugation at 5000 rpm for 1 minute. 400 µL PE buffer are added to the columns, followed by centrifugation at 14000 rpm for 1 minute, then 300 µL PE buffer are added to the columns again and, after 5 minutes waiting, columns are centrifuged at 14000 rpm for 2 minutes. Finally, 25 µL EB buffer are added in the columns and, after 1 minute of incubation, DNA is eluted by centrifuging at 14000 rpm for 1 minute. Elution is repeated a second time in the same way, then input DNA is diluted 1:50 in EB buffer. Quantification of immunoprecipitated DNA was achieved by qPCR on a Bio- Rad CFX Connect™ Real-Time System apparatus or on a Bio-Rad MiniOpticon apparatus, and by using Bio-Rad CFX Maestro 1.1 software. Triplicate samples in 20 µl reaction mixture containing 10 ng of template DNA, 300 nM for each primer (located at different distances from the HO-induced DSB and at the *ARO1* locus of chromosome IV), 2× SsoFast™ EvaGreen® supermix (Bio-Rad #1725201) (2X reaction buffer with dNTPs, Sso7d-fusion polymerase,

$MgCl_2$, EvaGreen dye and stabilizers) were run in white 96-well PCR plates Multiplate (Bio-Rad #MLL9651) or 48-well PCR plates Multiplate (BioRad #MLL4851). The qPCR program was as follows: step 1, 98°C for 2 min; step 2, 90°C for 5 s; step 3, 60°C for 15 s; step 4, return repeat 40 times from step 2. At the end of the cycling program, a melting program (from 65°C to 95°C with a 0.5°C increment every 5 s) was run to test the specificity of each qPCR.

Data are expressed as fold enrichment at the HO-induced DSB over that at the non-cleaved *ARO1* locus, after normalization of the ChIP signals to the corresponding input for each time point. Fold enrichment was then normalized to the efficiency of DSB induction (cut efficiency). Rif2 and Rap1 binding was also detected at six different Y'- containing telomeres (6Y') [Iglesias *et al.*, 2011]. Data are expressed as fold enrichment at 6Y' over that at the non-telomeric *ARO1* locus, after normalization of each ChIP signal to the corresponding input. For histone loss, the fold enrichment from each sample after HO induction was divided by the foldenrichment from uninduced cells, and $\log_2$ of the resulting values was calculated.

DBD expression and purification

The coding region of Rap1 or Rap1^{P520L} DNA binding domain (residues 358-601) was cloned into the bacterial expression vector pET21a at *Eco*RI and *Xho*I restriction sites. Recombinant proteins were produced in Lennox medium (LM) (10 g/l tryptone, 5 g/l yeast extract, 5 g/l NaCl) with addition of 100 mg/l ampicillin. Cultures were grown in LM at 37°C until OD_{600} ~0.6-0.8, and induced with 10 mM isopropylthiogalactoside at 20°C for 18 hours. Proteins were extracted and purified from the soluble fractions by immobilized-metal affinity chromatography on nickel-nitrilotriacetic acid agarose (Jena Bioscience, Jena, Germany) as previously described [Mangiagalli *et al.*, 2018]. Elution fractions containing highest protein concentrations were buffer exchanged by gel

filtration chromatography on PD10 (GE Healthcare, Little Chalfont, UK) against 10 mM sodium phosphate buffer pH 7.0. Protein concentration was determined by Bradford protein assay (Bio-Rad), using bovine serum albumin as standard. SDS-PAGE was performed on 14% SDS polyacrylamide gel and stained with Gel-Code Blue (Pierce, Rockford, USA) after electrophoresis.

Electrophoretic mobility shift assay (EMSA)

EMSA was performed by incubating 20 nM of 21 bp 32^{P}-labeled dsDNA (5′-CCGCACACCCACACACCAGTG-3′) with purified $Rap1^{DBD}$ (from 20 nM to 120 nM) at room temperature for 15 minutes in binding buffer (20 mM HEPES-KOH pH 7.6, 10% v/v glycerol, 100 mM KCl, 0.1 mM EDTA, 1 mM DTT, 25 µg/ml BSA) to a final volume of 20 µl. Reactions were loaded on a 6% acrylamide/bisacrylamide 0.5× TBE gel and separated by running for 2 hours at 150 V. Gels were soaked for 15 min in 10% methanol, 10% acetic acid solution, vacuum-dried, and exposed to an autoradiography film.

Model construction

For the Rap1-Rif2 models, crystal structure of Rap1, spanning from 675 to 825 amino acids, in complex with Rif2, spanning from 64 to 388 amino acids, was retrieved from protein data bank (PDB code: 4BJ5). The loops not resolved in the PDB structure were modelled with Prime (Schrödinger Release 2019-2: Prime, Schrödinger, LLC, New York, NY, 2019). This structure was mutated *in silico* by using the PyMOL mutagenesis tool (The PyMOL Molecular Graphics System, Version 2.0 Schrödinger, LLC) to generate Rap1-$Rif2^{L341S}$ and $Rap1^{R747L}$-Rif2. For the Myb-DNA models, crystal structure of Rap1 spanning from 358 to 602 amino acids in complex with telomeric dsDNA is present in protein data bank (PDB code: 3UKG) with a level of resolution of 2.95 Å. Such X ray crystal

structure was cut into two submodels: the first one includes Myb-N domain (from 358 to 446 residues) and DNA, while the second one includes Myb-C domain (from 447 to 586 residues) and DNA. These submodels were used to generate the mutant variants by performing *in silico* substitution using PyMOL. Four models were generated: DNA-Myb-N, DNA-Myb-N^{R381W}, DNA-Myb-C, and DNA-Myb-C^{P520L}.

Refine of models

All models were relaxed with unbiased molecular dynamics simulation using GROMACS [Abraham *et al.*, 2015].

For each system, five replicas were performed at 300 K and 1 atm for 150 ns with an integration step of 2 fs for a total of 750 ns of simulation time. All structures were placed in a cubic box with minimum distance between atoms of the solute and box edges being 1.0 nm. Boxes were filled with CHARMM-appropriate TIP3P water molecules and electrically neutralized by adding an appropriate number of K^+ and Cl^- ions. Proper protonation state of residues was calculated at 7.0 pH. Such simulations were carried out using CHARMM36 [Huang and MacKerell, 2013] as force field that well reproduces protein and nucleic acids behavior. The concatenated trajectories were analyzed using cluster analysis in order to select the most representative conformation for each system that were used as starting point for subsequent umbrella sampling simulations.

Umbrella sampling

Umbrella sampling (US) represents one of the most powerful conformational sampling techniques and it is used to estimate the relative free energy of different states along reaction coordinates [Zheng *et al.*, 2019]. In this computational method, a bias potential is applied along a reaction coordinate and this bias

potential drives the system from one thermodynamic state to another [Vermaaas *et al.*, 2016]. The potential bias is defined as an additional energy term that is applied to a system in order to overcome free energy barriers in free energy calculation, thus ensuring efficient sampling along the whole reaction coordinate. In this way, umbrella sampling method allows forcing the exploration of regions of state space that would otherwise have insufficient sampling [Musiani and Giorgetti, 2017]. The applied bias potential can have any functional form, but often harmonic potentials are used for their simplicity. Furthermore, bias potential can be aimed either in one simulation or in different simulations called windows, whose distributions overlap. From the sampled distribution of the system along the reaction coordinate, the change in free energy in each window can be calculated [Saladino *et al.*, 2017]. The windows can also be combined by methods like the weighted histogram analysis method or umbrella integration. Moreover, the sampling in each window can be improved by replica exchange methods either by exchange between successive windows or by running additional simulations at higher temperatures. Then, a molecular dynamic simulation (MD) is performed at each of window [Liao, 2020]. Since umbrella sampling is one of the most powerful conformational sampling techniques, and the molecular dynamics simulations for the different windows can be run independently from each other allowing to add further windows to the system to improve convergence, umbrella sampling has demonstrated great successes in a huge number of studies about a wide range of biological systems including protein-protein interaction, ligand-protein binding, and DNA conformational change [Liao, 2020]. In particular, in this thesis, the simulation protocol was divided into two steps: a steered molecular dynamic (SMD) and an umbrella sampling (US) simulation. The SMD step was necessary to generate a series of configurations along the selected reaction coordinate, that is the separation event of the complexes. During this simulation, the subunits were pushed away one

from the other by applying a biasing potential to their centers of mass (COMs). COMs of subunits were oriented along *x*-direction of cartesian space. During steering/pulling simulations, a harmonic potential of 1000 kJ/mol nm^2 was applied only along *x*-direction with a pull rate of 0.005 nm/ps in order to obtain a COM displacement of 5 nm in 1 ns. The *x*-dimension of each simulation box were enlarged by 15.0 nm respect to the previous simulations and additional K^+ and Cl^- ions were added to obtain an ionic concentration of 100 mM. Frames representing a COM spacing of 0.1 nm, referred to as configurations, were extracted from pulling trajectories and were used as starting points for US simulations. US simulation was performed at 300 K and 1 atm for 20 ns for each configuration restraining it within a window corresponding to the chosen COM distance by applying harmonic potential of 1000 kJ/mol nm^2. All simulations were carried out using CHARMM36 as force field.

Potential of Mean Force (PMF) calculation

PMF was calculated from the umbrella histograms using the weighted histogram analysis method (WHAM) [Roux, 1995] implemented in GROMACS. For PMF calculation, the following settings have been used: 50 bins per 1 nm, 100 bootstraps to obtain an average bootstrapped PMF and error estimates. PMF was set to zero at the distance between COMs where the pull force drops to the minimum, which is 6.0 nm for Rap1-Rif2 system and 5.5 nm for DNA-Myb systems. Individual umbrella histograms were weighted with estimated integrated autocorrelation times (IACTs) smoothed along the reaction coordinate (*x*-direction) using gaussians with standard deviation $\sigma = 0.15$ nm [Jakubee and Vondrášek, 2019].

Molecular modeling

The structural models for $Ku70^{C85Y}$ mutant protein within the Ku70-Ku80 heterodimer were prepared starting from the crystal structure (PDB ID: 5Y58). PDB file was processed with MAESTRO (Schrödinger Release 2022-2: Maestro, Schrödinger, LLC, New York, NY, 2021) using the Protein Preparation Wizard tool [Sastry *et al.*, 2013] to add missing hydrogen atoms and assign proper bond orders, and with PRIME [Jacobson *et al.*, 2004] to fill in missing loops and missing side chain atoms. The mutation was generated in MAESTRO replacing the original side chains with the mutated residue tool. The regions in a range of 10 Å from the mutation were minimized using MACROMODEL (Schrödinger Release 2022-2: MacroModel, Schrödinger, LLC, New York, NY, 2021). Minimizations were carried on using AMBER force field [Weiner *et al.*, 1986] with implicit solvent, using PRCG method with maximum iteration of 2500 and a gradient convergence threshold of 0.05. The wild-type dimer structure (PDB ID: 5Y58) was submitted to Swarmdock, HDOCK, and ClusPro protein-protein docking servers [Torchala *et al.*, 2013; Kozakov *et al.*, 2017; Yan *et al.*, 2020] in order to establish the putative interfaces for tetramerization involving the vWA domain, which was previously reported for human Ku heterodimers and proposed to be conserved in yeast as well [Ribes-Zamora *et al.*, 2013]. The interfaces with best scoring were essentially two, where the α5 helix within the Ku70 vWA domain of one Ku70-Ku80 dimer would alternatively interact with: i) the opposite Ku70 vWA domain of the other Ku70-Ku80 dimer; ii) the C-terminal of Ku70 in the other dimer. Either interface was submitted as constraints for more refined complex modelling on HADDOCK 2.4 server [van Zundert *et al.*, 2016]. HADDOCK 2.4 built hundreds of models and clustered them, and the 20 top scoring clusters were further filtered for constraint adherence and for topological constraints (i.e., allowing the two DNA ends to be simultaneously approached by the DNA break repair machinery). The shown conformation (Figure 23D) was

chosen as it is comprised within the top three scoring clusters obtained by HADDOCK 2.4 server with the vWA vs vWA interface both for the wild type and the C85Y mutant.

Quantification and statistical analysis

Quantification and statistical analysis were performed using Microsoft Excel Professional 365 software or PRISM (GraphPad). Data are expressed as mean values ± standard deviation (s.d). P-values were determined by using unpaired two-tailed *t*-test. No statistical methods or criteria were used to estimate size or to include or exclude samples.

REFERENCES

Abraham MJ, Murtola T, Schulz R, Páll S, Smith JC, Hess B, Lindahl E (2015) GROMACS: High performance molecular simulations through multi-level parallelism from laptops to supercomputers. *Software X* **1-2**, 19-25.

Aguilera A, García-Muse T (2013) Causes of genome instability. *Annu Rev Genet* **47**, 1-32.

Ahnesorg P, Smith P, Jackson SP (2006) XLF interacts with the XRCC4-DNA ligase IV complex to promote nonhomologous end-joining. *Cell* **124**, 301-313.

Anbalagan S, Bonetti D, Lucchini G, Longhese MP (2011) Rif1 supports the function of the CST complex in yeast telomere capping. *PLoS Genet* **7**, e1002024.

Aravind L, Koonin EV (2001) Prokaryotic homologs of the eukaryotic DNA-end-binding protein Ku, novel domains in the Ku protein and prediction of a prokaryotic double-strand break repair system. *Genome Res* **11**, 1365-1374.

Audebert M, Salles B, Calsou P (2004) Involvement of poly(ADP-ribose) polymerase-1 and XRCC1/DNA ligase III in an alternative route for DNA double-strand breaks rejoining. *J Biol Chem* **279**, 55117-55126.

Aylon Y, Liefshitz B, Kupiec M (2004) The CDK regulates repair of double-strand breaks by homologous recombination during the cell cycle. *EMBO J* **23**, 4868-4875.

Azad GK, Tomar RS (2016) The multifunctional transcription factor Rap1: a regulator of yeast physiology. *Front Biosci* **21**, 918-930.

Bacal J, Moriel-Carretero M, Pardo B, Barthe A, Sharma S, Chabes A, Lengronne A, Pasero P (2018) Mrc1 and Rad9 cooperate to regulate initiation and elongation of DNA replication in response to DNA damage. *EMBO J* **37**, e99319.

Bakkenist CJ, Kastan MB (2003) DNA damage activates ATM through intermolecular autophosphorylation and dimer dissociation. *Nature* **421**, 499-506.

Bassing CH, Alt FW (2004) The cellular response to general and programmed DNA double strand breaks. *DNA Repair* **3**, 781-796.

Bennardo N, Cheng A, Huang N, Stark JM (2008) Alternative-NHEJ is a mechanistically distinct pathway of mammalian chromosome break repair. *PLoS Genet* **4**, e1000110.

Berkovich E, Monnat RJ Jr, Kastan MB (2007) Roles of ATM and NBS1 in chromatin structure modulation and DNA double-strand break repair. *Nat Cell Biol* **9**, 683-690.

Berti M, Vindigni A (2016) Replication stress: getting back on track. *Nat Struct Mol Biol* **23**, 103-109.

Bertocci B, De Smet A, Weill JC, Reynaud CA (2006) Nonoverlapping functions of DNA polymerases mu, lambda, and terminal deoxynucleotidyltransferase during immunoglobulin V(D)J recombination in vivo. *Immunity* **25**, 31-41.

Bertuch AA, Lundblad V (2003) The Ku heterodimer performs separable activities at double-strand breaks and chromosome termini. *Mol Cell Biol* **23**, 8202-8215.

Bhattacharya S, Asaithamby A (2017) Repurposing DNA repair factors to eradicate tumor cells upon radiotherapy. *Transl Cancer Res* **6** (Suppl 5), S822-S839.

Bi X, Wei SC, Rong YS (2004) Telomere protection without a telomerase; the role of ATM and Mre11 in Drosophila telomere maintenance. *Curr Biol* **14**, 1348-1353.

Bianchi A, Smith S, Chong L, Elias P, de Lange T (1997) TRF1 is a dimer and bends telomeric DNA. *EMBO J* **16**, 1785-1794.

Bianchi A, Stansel RM, Fairall L, Griffith JD, Rhodes D, de Lange T (1999) TRF1 binds a bipartite telomeric site with extreme spatial flexibility. *EMBO J* **18**, 5735-5744.

Bilaud T, Koering CE, Binet-Brasselet E, Ancelin K, Pollice A, Gasser SM, Gilson E (1996) The telobox, a Myb-related telomeric DNA binding motif found in proteins from yeast, plants and human. *Nucleic Acids Res* **24**, 1294-1303.

Blier PR, Griffith AJ, Craft J, Hardin JA (1993) Binding of Ku protein to DNA. Measurement of affinity for ends and demonstration of binding to nicks. *J Biol Chem* **268**, 7594-7601.

Bonetti D, Clerici M, Anbalagan S, Martina M, Lucchini G, Longhese MP (2010) Shelterin-like proteins and Yku inhibit nucleolytic processing of *Saccharomyces cerevisiae* telomeres. *PLoS Genet* **6**, e1000966.

Bonetti D, Clerici M, Manfrini N, Lucchini G, Longhese MP (2010) The MRX complex plays multiple functions in resection of Yku- and Rif2-protected DNA ends. *PLoS One* **5**, e14142.

Bonetti D, Colombo CV, Clerici M, Longhese MP (2018) Processing of DNA ends in the maintenance of genome stability. *Front Genet* **9**, 390.

Bonetti D, Martina M, Clerici M, Lucchini G, Longhese MP (2009) Multiple pathways regulate 3' overhang generation at *S. cerevisiae* telomeres. *Mol Cell* **35**, 70-81.

Bosotti R, Isacchi A, Sonnhammer EL (2000) FAT, a novel domain in PIK-related kinases. *Trends Biochem Sci* **25**, 225-227.

Bressan DA, Olivares HA, Nelms BE, Petrini JH (1998) Alteration of N-terminal phosphoesterase signature motifs inactivate *Saccharomyces cerevisiae* Mre11. *Genetics* **150**, 591-600.

Britton S, Chanut P, Delteil C, Barboule N, Frit P, Calsou P (2020) ATM antagonizes NHEJ proteins assembly and DNA-ends synapsis at single-ended DNA double strand breaks. *Nucleic Acids Res* **48**, 9710-9723.

Britton S, Coates J, Jackson SP (2013) A new method for high-resolution imaging of Ku foci to decipher mechanisms of DNA double-strand break repair. *J Cell Biol* **202**, 579-595.

Broccoli D, Smogorzewska A, Chong L, de Lange T (1997) Human telomeres contain two distinct Myb-related proteins, TRF1 and TRF2. *Nat Genet* **17**, 231-235.

Brouwer I, Sitters G, Candelli A, Heerema SJ, Heller I, de Melo AJ, Zhang H, Normanno D, Modesti M, Peterman EJ, Wuite GJ (2016) Sliding sleeves of XRCC4-XLF bridge DNA and connect fragments of broken DNA. *Nature* **535**, 566-569.

Cannavo E, Cejka P (2014) Sae2 promotes dsDNA endonuclease activity within Mre11-Rad50-Xrs2 to resect DNA breaks. *Nature* **514**, 122-125.

Cary RB, Chen F, Shen Z, Chen DJ (1998) A central region of Ku80 mediates interaction with Ku70 in vivo. *Nucleic Acids Res* **26**, 974-979.

Cary RB, Peterson SR, Wang J, Bear DG, Bradbury EM, Chen DJ (1997) DNA looping by Ku and the DNA-dependent protein kinase. *Proc Natl Acad Sci USA* **94**, 4267-4272.

Casari E, Gnugnoli M, Rinaldi C, Pizzul P, Colombo CV, Bonetti D, Longhese MP (2022) To Fix or not to fix: maintenance of chromosome ends versus repair of DNA double-strand breaks. *Cells* **11**, 3224.

Casari E, Gobbini E, Clerici M, Longhese MP (2021) Resection of a DNA double-strand break by alkaline gel electrophoresis and southern blotting. *Methods Mol Biol* **2153**, 33-45.

Casari E, Gobbini E, Gnugnoli M, Mangiagalli M, Clerici M, Longhese MP (2021) Dpb4 promotes resection of DNA double-strand breaks and checkpoint activation by acting in two different protein complexes. *Nat Commun* **12**, 4750.

Casari E, Rinaldi C, Marsella A, Gnugnoli M, Colombo CV, Bonetti D, Longhese MP (2019) Processing of DNA Double-Strand Breaks by the MRX complex in a chromatin context. *Front Mol Biosci* **6**, 43.

Cassani C, Gobbini E, Vertemara J, Wang W, Marsella A, Sung P, Tisi R, Zampella G, Longhese MP (2018) Structurally distinct Mre11 domains mediate MRX functions in resection, end-tethering and DNA damage resistance. *Nucleic Acids Res* **46**, 2990-3008.

Cassani C, Gobbini E, Wang W, Niu H, Clerici M, Sung P, Longhese MP (2016) Tel1 and Rif2 regulate MRX functions in end-tethering and repair of DNA double-strand breaks. *PLoS Biol* **14**, e1002387.

Cassani C, Vertemara J, Bassani M, Marsella A, Tisi R, Zampella G, Longhese MP (2019) The ATP-bound conformation of the Mre11-Rad50 complex is essential for Tel1/ATM activation. *Nucleic Acids Res* **47**, 3550-3567.

Cejka P (2015) DNA end resection, nucleases team up with the right partners to initiate homologous recombination. *J Biol Chem* **290**, 22931-22938.

Cejka P, Cannavo E, Polaczek P, Masuda-Sasa T, Pokharel S, Campbell JL, Kowalczykowski SC (2010) DNA end resection by Dna2-Sgs1-RPA and its stimulation by Top3-Rmi1 and Mre11-Rad50-Xrs2. *Nature* **467**, 112-116.

Chai W, Sfeir AJ, Hoshiyama H, Shay JW, Wright WE (2006) The involvement of the Mre11/Rad50/Nbs1 complex in the generation of G-overhangs at human telomeres. *EMBO Rep* **7**, 225-230.

Chan SW, Boule JB, Zakian VA (2008) Two pathways recruit telomerase to *Saccharomyces cerevisiae* telomeres. *PLoS Genet* **4**, e1000236.

Chang HHY, Pannunzio NR, Adachi N, Lieber MR (2017) Non-homologous DNA end joining and alternative pathways to double-strand break repair. *Nat Rev Mol Cell Biol* **18**, 495-506.

Chang HHY, Watanabe G, Gerodimos CA, Ochi T, Blundell TL, Jackson SP, Lieber MR (2016) Different DNA end configurations dictate which NHEJ components are most important for joining efficiency. *J Biol Chem* **291**, 24377-24389.

Chaplin AK, Blundell TL (2020) Structural biology of multicomponent assemblies in DNA double-strand-break repair through non-homologous end joining. *Curr Opin Struct Biol* **61**, 9-16.

Chaplin AK, Hardwick SW, Stavridi AK, Buehl CJ, Goff NJ, Ropars V, Liang S, De Oliveira TM, Chirgadze DY, Meek K, Charbonnier JB, Blundell TL (2021) Cryo-EM of NHEJ supercomplexes provides insights into DNA repair *Mol Cell* **81**, 3400-3409.

Chen S, Lee L, Naila T, Fishbain S, Wang A, Tomkinson AE, Lees-Miller SP, He Y (2021) Structural basis of long-range to short-range synaptic transition in NHEJ. *Nature* **593**, 294-298.

Chen Y, Rai R, Zhou ZR, Kanoh J, Ribeyre C, Yang Y, Zheng H, Damay P, Wang F, Tsujii H, Hiraoka Y, Shore D, Hu HY, Chang S, Lei M (2011) A conserved motif within RAP1 has diversified roles in telomere protection and regulation in different organisms. *Nat Struct Mol Biol* **18**, 213-221.

Chen YC, Teng SC, Wu KJ (2009) Phosphorylation of telomeric repeat binding factor 1 (TRF1) by Akt causes telomere shortening. *Cancer Invest* **27**, 24-28.

Chong L, van Steensel B, Broccoli D, Erdjument-Bromage H, Hanish J, Tempst P, de Lange T (1995) A human telomeric protein. *Science* **270**, 1663-1667.

Churikov D, Corda Y, Luciano P, Geli V (2013) Cdc13 at a crossroads of telomerase action. *Front Oncol* **3**, 39.

Ciccia A, Elledge SJ (2010) The DNA damage response, making it safe to play with knives. *Mol Cell* **40**, 179-204.

Clerici M, Mantiero D, Guerini I, Lucchini G, Longhese MP (2008) The Yku70-Yku80 complex contributes to regulate double-strand break processing and checkpoint activation during the cell cycle. *EMBO Rep* **9**, 810-818.

Clerici M, Mantiero D, Lucchini G, Longhese MP (2005) The *Saccharomyces cerevisiae* Sae2 protein promotes resection and bridging of double strand break ends. *J Biol Chem* **280**, 38631-38638.

Conrad MN, Wright JH, Wolf AJ, Zakian VA (1990) RAP1 protein interacts with yeast telomeres in vivo: overproduction alters telomere structure and decreases chromosome stability. *Cell* **63**, 739-750.

Cooper JP, Nimmo ER, Allshire RC, Cech TR (1997) Regulation of telomere length and function by a Myb-domain protein in fission yeast. *Nature* **385**, 744-747.

Daley JM, Palmbos PL, Wu D, Wilson TE (2005) Nonhomologous End Joining in yeast. *Annu Rev Genet* **39**, 431-451.

Daley JM, Wilson TE (2005) Rejoining of DNA double-strand breaks as a function of overhang length. *Mol Cell Biol* **25**, 896-906.

Davis AJ, Chen DJ (2013) DNA double strand break repair via non-homologous end-joining. *Transl Cancer Res* **2**, 130-143.

de Lange T (2018) Shelterin-mediated telomere protection. *Ann Rev Genet* **52**, 223-247.

de Villartay JP (2015) Congenital defects in V(D)J recombination. *Br Med Bull* **114**, 157-167.

de Villartay JP (2015) When natural mutants do not fit our expectations: the intriguing case of patients with XRCC4 mutations revealed by whole-exome sequencing. *EMBO Mol Med* **7**, 862-864.

de Vries E, van Driel W, Bergsma WG, Arnberg AC, van der Vliet PC (1989) HeLa nuclear protein recognizing DNA termini and translocating on DNA forming a regular DNAmultimeric protein complex. *J Mol Biol* **208**, 65-78.

DeFazio LG, Stansel RM, Griffith JD, Chu G (2002) Synapsis of DNA ends by DNA dependent protein kinase. *EMBO J* **21**, 3192-3200.

Del Vescovo V, De Sanctis V, Bianchi A, Shore D, Di Mauro E, Negri R (2004) Distinct DNA elements contribute to Rap1p affinity for its binding sites. *J Mol Biol* **338**, 877-893.

Deng C, Brown JA, You D, Brown JM (2005) Multiple endonucleases function to repair covalent topoisomerase I complexes in *Saccharomyces cerevisiae*. *Genetics* **170**, 591-600.

Deshpande RA, Williams GJ, Limbo O, Williams RS, Kuhnlein J, Lee JH, Classen S, Guenther G, Russell P, Tainer JA, Paull TT (2014) ATP-driven Rad50 conformations regulate DNA tethering, end resection, and ATM checkpoint signaling. *EMBO J* **33**, 482-500.

Dinkelmann M, Spehalski E, Stoneham T, Buis J, Wu Y, Sekiguchi JM, Ferguson DO (2009) Multiple functions of MRN in end-joining pathways during isotype class switching. *Nat Struct Mol Biol* **16**, 808-813.

Downs JA, Jackson SP (2004) A means to a DNA end: the many roles of Ku. *Nat Rev Mol Cell Biol* **5**, 367-378.

Downs JA, Lowndes NF, Jackson SP (2000) A role for *Saccharomyces cerevisiae* histone H2A in DNA repair. *Nature* **408**, 1001-1004.

Dudášová Z, Dudáš A, Chovanec M (2004) Non-homologous end-joining factors of *Saccharomyces cerevisiae*. *FEMS Microbiol Rev* **28**, 581-601.

Dueva R, Iliakis G (2013) Alternative pathways of non-homologous end joining (NHEJ) in genomic instability and cancer. *Translational cancer research* **2**, 163-177.

Elledge SJ (1996) Cell cycle checkpoints: preventing an identity crisis. *Science* **274**, 1664-1672.

Emerson CH, Bertuch AA (2016) Consider the workhorse: Nonhomologous end-joining in budding yeast. *Biochem Cell Biol* **94**, 396-406.

Errami A, Finnie NJ, Morolli B, Jackson SP, Lohman PH, Zdzienicka MZ (1998) Molecular and biochemical characterization of new X-ray-sensitive hamster cell mutants defective in Ku80. *Nucleic Acids Res* **26**, 4332-4338.

Falck J, Coates J, Jackson SP (2005) Conserved modes of recruitment of ATM, ATR and DNA-PKcs to sites of DNA damage. *Nature* **434**, 605-611.

Feeser EA, Wolberger C (2008) Structural and functional studies of the Rap1 C-terminus reveal novel separation-of-function mutants. *J Mol Biol* **380**, 520-531.

Feldmann EA, De Bona P, Galletto R (2015) The wrapping loop and Rap1 C-terminal (RCT) domain of yeast Rap1 modulate access to different DNA binding modes. *J Biol Chem* **290**, 11455-11466.

Feldmann EA, Galletto R (2014) The DNA-binding domain of yeast Rap1 interacts with double-stranded DNA in multiple binding modes. *Biochemistry* **53**, 7471-7483.

Feng L, Chen J (2012) The E3 ligase RNF8 regulates KU80 removal and NHEJ repair. *Nat Struct Mol Biol* **19**, 201-206.

Fisher TS, Taggart AKP, Zakian VA (2004). Cell cycle dependent regulation of yeast telomerase by Ku. *Nat Struct Mol Biol* **11**, 1198-1205.

Foster SS, Balestrini A, Petrini JH (2011) Functional interplay of the Mre11 nuclease and Ku in the response to replication-associated DNA damage. *Mol Cell Biol* **31**, 4379-4389.

Frank-Vaillant M, Marcand S (2001) NHEJ regulation by mating type is exercised through a novel protein, Lif2p, essential to the ligase IV pathway. *Genes Dev* **15**, 3005-3012.

Friedberg EC, Walker GC, Siede W, Wood RD, Schultz RA, Ellenberger T (2006) DNA repair and mutagenesis - 2nd edition. *DVM ASM Press* **19**, 711-739.

Gallardo F, Laterreur N, Cusanelli E, Querido E, Wellinger RJ, Chartrand P (2011) Live cell imaging of telomerase RNA dynamics reveals cell cycle-dependent clustering of telomerase at elongating telomeres. *Mol Cell* **44**, 819-827.

Gallardo F, Olivier C, Dandjinou AT, Wellinger RJ, Chartrand P (2008) TLC1 RNA nucleo-cytoplasmic trafficking links telomerase biogenesis to its recruitment to telomeres. *EMBO J* **27**, 748-757.

Garcia V, Phelps SE, Gray S, Neale MJ (2011) Bidirectional resection of DNA double-strand breaks by Mre11 and Exo1. *Nature* **479**, 241-244.

Gavande NS, VanderVere-Carozza PS, Hinshaw HD, Jalal SI, Sears CR, Pawelczak KS, Turchi JJ (2016) DNA repair targeted therapy: The past or future of cancer treatment? *Pharmacol Ther* **160**, 65-83.

Giannattasio M, Lazzaro F, Plevani P, Muzi-Falconi M (2005) The DNA damage checkpoint response requires histone H2B ubiquitination by Rad6-Bre1 and H3 methylation by Dot1. *J Biol Chem* **280**, 9879-9886.

Gilbert CS, Green CM, Lowndes NF (2001) Budding yeast Rad9 is an ATP-dependent Rad53 activating machine. *Mol Cell* **8**, 129-136.

Gobbini E, Cassani C, Vertemara J, Wang W, Mambretti F, Casari E, Sung P, Tisi R, Zampella G, Longhese MP (2018) The MRX complex regulates Exo1 resection activity by altering DNA end structure. *EMBO J* **37**, e98588.

Gobbini E, Cassani C, Villa M, Bonetti D, Longhese MP (2016) Functions and regulation of the MRX complex at DNA double-strand breaks. *Microb Cell* **3**, 329-337.

Gobbini E, Villa M, Gnugnoli M, Menin L, Clerici M, Longhese MP (2015) Sae2 function at DNA double-strand breaks is bypassed by dampening Tel1 or Rad53 activity. *PLoS Genet* **11**, e1005685.

Goodarzi AA, Yu Y, Riballo E, Douglas P, Walker SA, Ye R, Härer C, Marchetti C, Morrice N, Jeggo PA, Lees-Miller SP (2006) DNA-PK autophosphorylation facilitates Artemis endonuclease activity. *EMBO J* **25**, 3880-3889.

Gottschling DE, Aparicio OM, Billington BL, Zakian VA (1990) Position effect at *S. cerevisiae* telomeres: reversible repression of Pol II transcription. *Cell* **63**, 751-762.

Graham IR, Chambers A (1994) Use of a selection technique to identify the diversity of binding sites for the yeast RAP1 transcription factor. *Nucleic Acids Res* **22**, 124-130.

Graham TG, Walter JC, Loparo JJ (2016) Two-stage synapsis of DNA ends during nonhomologous end joining. *Mol Cell* **61**, 850-858.

Granata M, Lazzaro F, Novarina D, Panigada D, Puddu F, Abreu CM, Kumar R, Grenon M, Lowndes NF, Plevani P, Muzi-Falconi M (2010) Dynamics of Rad9 chromatin binding and checkpoint function are mediated by itsdimerization and are cell cycle-regulated by CDK1 activity. *PLoS Genet* **6**, e1001047.

Grawunder U, Wilm M, Wu X, Kulesza P, Wilson TE, Mann M, Lieber MR (1997) Activity of DNA ligase IV stimulated by complex formation with XRCC4 protein in mammalian cells. *Nature* **388**, 492-495.

Grenon M, Costelloe T, Jimeno S, O'Shaughnessy A, Fitzgerald J, Zgheib O, Degerth L, Lowndes NF (2007) Docking onto chromatin via the *Saccharomyces cerevisiae* Rad9 Tudor domain. *Yeast* **24**, 105-119.

Griffith AJ, Blier PR, Mimori T, Hardin JA (1992) Ku polypeptides synthesized in vitro assemble into complexes which recognize ends of double-stranded DNA. *J Biol Chem* **67**, 331-338.

Gu J, Li S, Zhang X, Wang LC, Niewolik D, Schwarz K, Legerski RJ, Zandi E, Lieber MR (2010) DNA-PKcs regulates a single-stranded DNA endonuclease activity of Artemis. *DNA Repair* **9**, 429-437.

Gu Y, Seidl KJ, Rathbun GA, Zhu C, Manis JP, van der Stoep N, Davidson L, Cheng HL, Sekiguchi JM, Frank K, Stanhope-Baker P, Schlissel MS, Roth DB, Alt FW (1997) Growth retardation and leaky SCID phenotype of Ku70-deficient mice. *Immunity* **7**, 653-665.

Hailemariam S, De Bona P, Galletto R, Hohl M, Petrini JH, Burgers PM (2019) The telomere-binding protein Rif2 and ATP-bound Rad50 have opposing roles in the activation of yeast Tel1ATM kinase. *J Biol Chem* **294**, 18846-18852.

Hammet A, Magill C, Heierhorst J, Jackson SP (2007) Rad9 BRCT domain interaction with phosphorylated H2AX regulates the G1 checkpoint in budding yeast. *EMBO Rep* **8**, 851-857.

Hanahan D (2022) Hallmarks of cancer: new dimensions. *Cancer Discov* **12**, 31-46.

Hardy CF, Sussel L, Shore D (1992) A RAP1-interacting protein involved in transcriptional silencing and telomere length regulation. *Genes Dev* **6**, 801-814.

Harrington JJ, Lieber MR (1994) Functional domains within FEN-1 and RAD2 define a family of structure-specific endonucleases: implications for nucleotide excision repair. *Gene Develop* **8**, 1344-1355.

Hefferin ML, Tomkinson AE (2005) Mechanism of DNA double-strand break repair by non-homologous end joining. *DNA Repair* **4**, 639-648.

Helena JM, Joubert AM, Grobbelaar S, Nolte EM, Nel M, Pepper MS, Coetzee M, Mercier AE (2018) Deoxyribonucleic acid damage and repair: capitalizing on our understanding of the mechanisms of maintaining genomic integrity for therapeutic purposes. *Int J Mol Sci* **19**, 1148.

Hirano Y, Fukunaga K, Sugimoto K (2009) Rif1 and Rif2 inhibit localization of Tel1 to DNA ends. *Mol Cell* **33**, 312-322.

Hoeijmakers JH (2009) DNA damage, aging, and cancer. *N Engl J Med* **361**, 1475-1485.

Huang H, Kahana A, Gottschling DE, Prakash L, Liebman SW (1997) The ubiquitinconjugating enzyme Rad6 (Ubc2) is required for silencing in Saccharomyces cerevisiae. *Mol Cell Biol* **17**, 6693-6699.

Huang J, MacKerell AD (2013) Jr CHARMM36 all-atom additive protein force field: validation based on comparison to NMR data. *J Comput Chem* **34**, 2135-2145.

Hughes TR, Evans SK, Weilbaecher RG, Lundblad V (2000) The Est3 protein is a subunit of yeast telomerase. *Curr Biol* **10**, 809-812.

Iglesias N, Redon S, Pfeiffer V, Dees M, Lingner J, Luke B (2011) Subtelomeric repetitive elements determine TERRA regulation by Rap1/Rif and Rap1/Sir complexes in yeast. *EMBO Rep* **12**, 587-593.

IJspeert H, Rozmus J, Schwarz K, Warren RL, van Zessen D, Holt RA, Pico-Knijnenburg I, Simons E, Jerchel I, Wawer A, Lorenz M, Patıroğlu T, Akar HH, Leite R, Verkaik NS, Stubbs AP, van Gent DC, van Dongen JJ, van der Burg M (2016) XLF deficiency results in reduced N-nucleotide addition during V(D)J recombination. *Blood* **128**, 650-659.

Ira G, Pellicioli A, Balijja A, Wang X, Fiorani S, Carotenuto W, Liberi G, Bressan D, Wan L, Hollingsworth NM, Haber JE, Foiani M (2004) DNA end resection, homologous recombination and DNA damage checkpoint activation require CDK1. *Nature* **431**, 1011-1017.

Iwasaki D, Hayashihara K, Shima H, Higashide M, Terasawa M, Gasser SM, Shinohara M (2016) The MRX complex ensures NHEJ fidelity through multiple pathways including Xrs2-FHA-dependent Tel1 activation. *PLoS Genet* **12**, e1005942.

Jackson SP, Bartek J (2009) The DNA-damage response in human biology and disease. *Nature* **461**, 1071-1078.

Jacobson MP, Pincus DL, Rapp CS, Day TJ, Honig B, Shaw DE, Friesner RA (2004) A hierarchical approach to all-atom protein loop prediction. *Proteins* **55**, 351-367.

Jain D, Cooper JP (2010). Telomeric strategies: means to an end. *Annu Rev Genet* **44**, 243-269.

Jakubec D, Vondrášek J (2019) Can all-atom molecular dynamics simulations quantitatively describe homeodomain-DNA binding equilibria. *J Chem Theory Comput* **15**, 2635-2648.

Javaheri A, Wysocki R, Jobin-Robitaille O, Altaf M, Côté J, Kron SJ (2006) Yeast G1 DNA damage checkpoint regulation by H2A phosphorylation is independent of chromatin remodeling. *Proc Natl Acad Sci USA* **103**, 13771-13776.

Jeggo PA, Pearl LH, Carr AM (2016) DNA repair, genome stability and cancer: a historical perspective. *Nat Rev Cancer* **16**, 35-42.

Kabir S, Sfeir A, de Lange T (2010) Taking apart Rap1: an adaptor protein with telomeric and non-telomeric functions. *Cell Cycle* **9**, 4061-4067.

Kaye JA, Melo JA, Cheung SK, Vaze MB, Haber JE, Toczyski DP (2004) DNA breaks promote genomic instability by impeding proper chromosome segregation. *Curr Biol* **14**, 2096-2106.

Kegel A, Sjöstrand JO, Aström SU (2001) Nej1p, a cell type-specific regulator of nonhomologous end joining in yeast. *Curr Biol* **11**, 1611-1617.

Kim JA, Kruhlak M, Dotiwala F, Nussenzweig A, Haber JE (2007) Heterochromatin is refractory to gamma-H2AX modification in yeast and mammals. *J Cell Biol* **178**, 209-218.

Kirkwood JG (1935) Statistical mechanics of fluid mixtures. *J Chem Phys* **3**, 300-313.

Kolodner RD, Putnam CD, Myung K (2002) Maintenance of genome stability in *Saccharomyces cerevisiae*. *Science* **297**, 552-557.

Kondo T, Wakayama T, Naiki T, Matsumoto K, Sugimoto K (2001) Recruitment of Mec1 and Ddc1 checkpoint proteins to double-strand breaks through distinct mechanisms. *Science* **294**, 867-870.

König P, Giraldo R, Chapman L, Rhodes D (1996) The crystal structure of the DNA-binding domain of yeast RAP1 in complex with telomeric DNA. *Cell* **85**, 125-136.

König P, Rhodes D (1997) Recognition of telomeric DNA. *Trends Biochem Sci* **22**, 43-47.

Kowalczykowski SC (2015) An overview of the molecular mechanisms of recombinational DNA repair. *Cold Spring Harb Perspect Biol* **7**, a016410.

Kozakov D, Hall DR, Xia B, Porter KA, Padhorny D, Yueh C, Beglov D, Vajda S (2017) The ClusPro web server for protein-protein docking. *Nat Protoc* **12**, 255-278.

Krejci L, Altmannova V, Spirek M, Zhao X (2012) Homologous recombination and its regulation. *Nucleic Acids Res* **40**, 5795-5818.

Kurtz S, Shore D (1991) RAP1 protein activates and silences transcription of mating-type genes in yeast. *Genes Dev* **5**, 616-628.

Kyrion G, Boakye KA, Lustig AJ (1992) C-terminal truncation of RAP1 results in the deregulation of telomere size, stability, and function in *Saccharomyces cerevisiae*. *Mol Cell Biol* **12**, 5159-5173.

Kyrion G, Liu K, Liu C, Lustig AJ (1993) RAP1 and telomere structure regulate telomere position effects in *Saccharomyces cerevisiae*. *Genes Dev* **7**, 1146-1159.

Lammens K, Bemeleit DJ, Möckel C, Clausing E, Schele A, Hartung S, Schiller CB, Lucas M, Angermüller C, Söding J, Strässer K, Hopfner KP (2011) The Mre11:Rad50 structure shows an ATP-dependent molecular clamp in DNA double-strand break repair. *Cell* **145**, 54-66.

Langerak P, Mejia-Ramirez E, Limbo O, Russell P (2011) Release of Ku and MRN from DNA ends by Mre11 nuclease activity and Ctp1 is required for

homologous recombination repair of double-strand breaks. *PLoS Genet* **7**, e1002271.

Lanz MC, Dibitetto D, Smolka MB (2019) DNA damage kinase signaling: checkpoint and repair at 30 years. *EMBO J* **38**, e101801.

Larrivée M, LeBel C, Wellinger RJ (2004). The generation of proper constitutive G-tails on yeast telomeres is dependent on the MRX complex. *Genes Dev* **18**, 1391-1396.

Lazzaro F, Sapountzi V, Granata M, Pellicioli A, Vaze M, Haber JE, Plevani P, Lydall D, Muzi-Falconi M (2008) Histone methyltransferase Dot1 and Rad9 inhibit single-stranded DNA accumulation at DSBs and uncapped telomeres. *EMBO J* **27**, 1502-1512.

Lee CS, Lee K, Legube G, Haber JE (2014) Dynamics of yeast histone H2A and H2B phosphorylation in response to a double-strand break. *Nat Struct Mol Biol* **21**, 103-109.

Lee JH, Paull TT (2005) ATM activation by DNA double-strand breaks through the Mre11-Rad50-Nbs1 complex. *Science* **308**, 551-554.

Lee JH, Paull TT (2021) Cellular functions of the protein kinase ATM and their relevance to human disease. *Nat Rev Mol Cell Biol* **22**, 796-814.

Lee K, Lee SE (2007) *Saccharomyces cerevisiae* Sae2- and Tel1-dependent single-strand DNA formation at DNA break promotes microhomology-mediated end joining. *Genetics* **176**, 2003-2014.

Lee K, Zhang Y, Lee SE (2008) *Saccharomyces cerevisiae* ATM orthologue suppresses break-induced chromosome translocations. *Nature* **454**, 543-546.

Lee SE, Moore JK, Holmes A, Umezu K, Kolodner RD, Haber JE (1998) *Saccharomyces* Ku70, Mre11/Rad50 and RPA proteins regulate adaptation to G2/M arrest after DNA damage. *Cell* **94**, 399-409.

Lemon LD, Morris DK, Bertuch AA (2019) Loss of Ku's DNA end binding activity affects telomere length via destabilizing telomere-bound Est1 rather than altering TLC1 homeostasis. *Sci Rep* **9**, 10607.

Lempiäinen H, Halazonetis TD (2009) Emerging common themes in regulation of PIKKs and PI3Ks. *EMBO J* **28**, 3067-3073.

Li B, Oestreich S, de Lange T (2000) Identification of human Rap1: implications for telomere evolution. *Cell* **101**, 471-483.

Li X, Tyler JK (2016) Nucleosome disassembly during human non-homologous end joining followed by concerted HIRA- and CAF-1-dependent reassembly. *eLife* **5**, e15129.

Liao Q (2020) Enhanced sampling and free energy calculations for protein simulations. *Prog Mol Biol Transl Sci* **170**, 177-213.

Lieb JD, Liu X, Botstein D, Brown PO (2001) Promoterspecific binding of Rap1 revealed by genome-wide maps of protein DNA association. *Nat Genet* **28**, 327-334.

Lieber MR (2010) The mechanism of double-strand DNA break repair by the non-homologous DNA end-joining pathway. *Annu Rev Biochem* **79**, 181-211.

Lim HS, Kim JS, Park YB, Gwon GH, Cho Y (2011) Crystal structure of the Mre11-Rad50-ATPγS complex: understanding the interplay between Mre11 and Rad50. *Genes Dev* **25**, 1091-1104.

Lin JJ, Zakian VA (1995) An in vitro assay for *Saccharomyces* telomerase requires *EST1*. *Cell* **81**, 1127-1135.

Lingner J, Hughes TR, Shevchenko A, Mann M, Lundblad V, Cech TR (1997) Reverse transcriptase motifs in the catalytic subunit of telomerase. *Science* **276**, 561-567.

Lisby M, Barlow JH, Burgess RC, Rothstein R (2004) Choreography of the DNA damage response: spatiotemporal relationships among checkpoint and repair proteins. *Cell* **118**, 699-713.

Liu C, Lustig AJ (1996) Genetic analysis of Rap1p/Sir3p interactions in telomeric and *HML* silencing in *Saccharomyces cerevisiae*. *Genetics* **143**, 81-93.

Liu C, Mao X, Lustig AJ (1994) Mutational analysis defines a C-terminal tail domain of *RAP1* essential for telomeric silencing in *Saccharomyces cerevisiae*. *Genetics* **138**, 1025-1040.

Liu Y, Sung S, Kim Y, Li F, Gwon G, Jo A, Kim AK, Kim T, Song OK, Lee SE, Cho Y (2016) ATP-dependent DNA binding, unwinding, and resection by the Mre11/Rad50 complex. *EMBO J* **35**, 743-58.

Lobachev K, Vitriol E, Stemple J, Resnick MA, Bloom K (2004) Chromosome fragmentation after induction of a double-strand break is an active process prevented by the RMX repair complex. *Curr Biol* **14**, 2107-2112.

Longhese MP, Bonetti D, Guerini I, Manfrini N, Clerici M (2009) DNA double-strand breaks in meiosis: checking their formation, processing and repair. *DNA Repair* **8**, 1127-1138.

Longhese MP, Paciotti V, Neecke H, Lucchini G (2000) Checkpoint proteins influence telomeric silencing and length maintenance in budding yeast. *Genetics* **155**, 1577-1591.

Lundblad V, Szostak JK (1989) A mutant with a defect in telomere elongation leads to senescence in yeast. *Cell* **57**, 633-643.

Lustig AJ, Kurtz S, Shore D (1990) Involvement of the silencer and UAS binding protein RAP1 in regulation of telomere length. *Science* **250**, 549-553.

Ma JL, Kim EM, Haber JE, Lee SE (2003) Yeast Mre11 and Rad1 proteins define a Ku-independent mechanism to repair double-strand breaks lacking overlapping end sequences. *Mol Cell Biol* **23**, 8820-8828.

Majka J, Niedziela-Majka A, Burgers PM (2006) The checkpoint clamp activates Mec1 kinase during initiation of the DNA damage checkpoint. *Mol Cell* **24**, 891-901.

Mallory JC, Petes TD (2000) Protein kinase activity of Tel1p and Mec1p, two *Saccharomyces cerevisiae* proteins related to the human ATM protein kinase. *Proc Natl Acad Sci USA* **97**, 13749-13754.

Manfrini N, Guerini I, Citterio A, Lucchini G, Longhese MP (2010) Processing of meiotic DNA double strand breaks requires cyclin-dependent kinase and multiple nucleases. *J Biol Chem* **285**, 11628-11637.

Mangiagalli M, Sarusi G, Kaleda A, Bar Dolev M, Nardone V, Vena VF, Braslavsky I, Lotti M, Nardini M (2018) Structure of a bacterial ice binding protein with two faces of interaction with ice. *FEBS J* **285**, 1653-1666.

Manis JP, Gu Y, Lansford R, Sonoda E, Ferrini R, Davidson L, Rajewsky K, Alt FW (1998) Ku70 is required for late B cell development and immunoglobulin heavy chain class switching. *J Exp Med* **187**, 2081-2089.

Marcand S, Gilson E, Shore D (1997) A protein-counting mechanism for telomere length regulation in yeast. *Science* **275**, 986-990.

Marcand S, Pardo B, Gratias A, Cahun S, Callebaut I (2008) Multiple pathways inhibit NHEJ at telomeres. *Genes Dev* **22**, 1153-1158.

Marsella A, Gobbini E, Cassani C, Tisi R, Cannavo E, Reginato G, Cejka P, Longhese MP (2021) Sae2 and Rif2 regulate MRX endonuclease activity at DNA double-strand breaks in opposite manners. *Cell Rep* **34**, 108906.

Martina M, Clerici M, Baldo V, Bonetti D, Lucchini G, Longhese MP (2012) A balance between Tel1 and Rif2 activities regulates nucleolytic processing and elongation at telomeres. *Mol Cell Biol* **32**, 1604-1617.

Matot B, Le Bihan YV, Lescasse R, Pérez J, Miron S, David G, Castaing B, Weber P, Raynal B, Zinn-Justin S, Gasparini S, Le Du MH (2012) The orientation of the C-terminal domain of the *Saccharomyces cerevisiae* Rap1 protein is determined by its binding to DNA. *Nucleic Acids Res* **40**, 3197-3207.

McKinnon PJ (2012) ATM and the molecular pathogenesis of ataxia telangiectasia. *Annu Rev Pathol* **7**, 303-321.

Meek K, Dang V, Lees-Miller SP (2008) DNA-PK: the means to justify the end? *Adv Immunonol* **99**, 33-58.

Mehta A, Haber JE (2014) Sources of DNA double-strand breaks and models of recombinational DNA repair. *Cold Spring Harb Perspect Biol* **6**, a016428.

Melo JA, Cohen J, Toczyski DP (2001) Two checkpoint complexes are independently recruited to sites of DNA damage in vivo. *Genes Dev* **15**, 2809-2821.

Mimitou EP, Symington LS (2008) Sae2, Exo1 and Sgs1 collaborate in DNA double-strand break processing. *Nature* **455**, 770-774.

Mimitou EP, Symington LS (2010) Ku prevents Exo1 and Sgs1-dependent resection of DNA ends in the absence of a functional MRX complex or Sae2. *EMBO J* **29**, 3358-3369.

Mimori T, Hardin JA (1986) Mechanism of interaction between Ku protein and DNA. *J Biol Chem* **261**, 10375-10379.

Miyake Y, Nakamura M, Nabetani A, Shimamura S, Tamura M, Yonehara S, Saito M, Ishikawa F (2009) RPA-like mammalian Ctc1-Stn1-Ten1 complex binds to single-stranded DNA and protects telomeres independently of the Pot1 pathway. *Mol Cell* **36**, 193-206.

Möckel C, Lammens K, Schele A, Hopfner KP (2012) ATP driven structural changes of the bacterial Mre11:Rad50 catalytic head complex. *Nucleic Acids Res* **40**, 914-927.

Moretti P, Freeman K, Coodly L, Shore D (1994) Evidence that a complex of SIR proteins interacts with the silencer and telomere-binding protein RAP1. *Genes Dev* **8**, 2257-2269.

Moretti P, Shore D (2001) Multiple interactions in Sir protein recruitment by Rap1p at silencers and telomeres in yeast. *Mol Cell Biol* **21**, 8082-8094.

Morin I, Ngo HP, Greenall A, Zubko MK, Morrice N, Lydall D (2008) Checkpoint-dependent phosphorylation of Exo1 modulates the DNA damage response. *EMBO J* **27**, 2400-2410.

Morris DK, Lundblad V (1997) Programmed translational frameshifting in a gene required for yeast telomere replication. *Curr Biol* **7**, 969-976.

Musiani F, Giorgetti A (2017) Protein aggregation and molecular crowding: perspectives from multiscale simulations. *Int Rev Cell Mol Biol* **329**, 49-77.

Nakada D, Matsumoto K, Sugimoto K (2003) ATM-related Tel1 associates with double-strand breaks through an Xrs2-dependent mechanism. *Genes Dev* **17**, 1957-1962.

Nakai W, Westmoreland J, Yeh E, Bloom K, Resnick MA (2011) Chromosome integrity at a double-strand break requires exonuclease 1 and MRX. *DNA Repair* **10**, 102-110.

Navadgi-Patil VM, Burgers PM (2009) A tale of two tails: activation of DNA damage checkpoint kinase Mec1/ATR by the 9-1-1 clamp and by Dpb11/TopBP1. *DNA Repair* (Amst) **8**, 996-1003.

Neale MJ, Pan J, Keeney S (2005) Endonucleolytic processing of covalent protein linked DNA double-strand breaks. *Nature* **436**, 1053-1057.

Negrini S, Gorgoulis VG, Halazonetis TD (2010) Genomic instability-an evolving hallmark of cancer. *Nat Rev Mol Cell Biol* **11**, 220-228.

Negrini S, Ribaud V, Bianchi A, Shore D (2007) DNA breaks are masked by multiple Rap1 binding in yeast: implications for telomere capping and telomerase regulation. *Genes Dev* **21**, 292-302.

Nimonkar AV, Genschel J, Kinoshita E, Polaczek P, Campbell JL, Wyman C, Modrich P, Kowalczykowski SC (2011) BLM-DNA2-RPA-MRN and EXO1-BLM-RPA-MRN constitute two DNA end resection machineries for human DNA break repair. *Genes Dev* **25**, 350-362.

Niu H, Chung WH, Zhu Z, Kwon Y, Zhao W, Chi P, Prakash R, Seong C, Liu D, Lu L, Ira G, Sung P (2010) Mechanism of the ATP-dependent DNA end-resection machinery from *Saccharomyces cerevisiae*. *Nature* **467**, 108-111.

Nugent CI, Hughes TR, Lue NF, Lundblad V (1996) Cdc13p: a single-strand telomeric DNA-binding protein with a dual role in yeast telomere maintenance. *Science* **274**, 249-252.

Nussenzweig A, Sokol K, Burgman P, Li L, Li GC (1997) Hypersensitivity of *Ku80*-deficient cell lines and mice to DNA damage: the effects of ionizing radiation on growth, survival, and development. *Proc Natl Acad Sci USA* **94**, 13588-13593.

O'Neil NJ, Bailey ML, Hieter P (2017) Synthetic lethality and cancer. *Nat Rev Genet* **18**, 613-623.

O'Driscoll M, Jackson AP, Jeggo PA (2006) Microcephalin: a causal link between impaired damage response signalling and microcephaly. *Cell Cycle* **5**, 2339-2344.

O'Driscoll M, Ruiz-Perez VL, Woods CG, Jeggo PA, Goodship JA (2003) A splicing mutation affecting expression of ataxia-telangiectasia and Rad3-related protein (ATR) results in Seckel syndrome. *Nat Genet* **33**, 497-501.

Oh J, Lee SJ, Rothstein R, Symington LS (2018) Xrs2 and Tel1 independently contribute to MR-mediated DNA tethering and replisome stability. *Cell Rep* **25**, 1681-1692.

Ono M, Tucker PW, Capra JD (1994) Production and characterization of recombinant human Ku antigen. *Nucleic Acids Res* **22**, 3918-3924.

Öz R, Wang JL, Guerois R, Goyal G, Sriram KK, Ropars V, Sharma R, Koca F, Charbonnier JB, Modesti M, Strick TR, Westerlund F (2021) Dynamics of Ku and bacterial non-homologous end-joining characterized using single DNA molecule analysis. *Nucleic Acids Res* **49**, 2629-2641.

Paciotti V, Lucchini G, Plevani P, Longhese MP (1998) Mec1p is essential for phosphorylation of the yeast DNA damage checkpoint protein Ddc1p, which physically interacts with Mec3p. *EMBO J* **17**, 4199-4209.

Pang D, Yoo S, Dynan WS, Jung M, Dritschilo A (1997) Ku proteins join DNA fragments as shown by atomic force microscopy. *Cancer Res* **57**, 1412-1415.

Pannunzio NR, Watanabe G, Lieber MR (2018) Nonhomologous DNA end-joining for repair of DNA double-strand breaks. *J Biol Chem* **293**, 10512-10523.

Pardo B, Marcand S (2005) Rap1 prevents telomere fusions by non-homologous end joining. *EMBO J* **24**, 3117-3127.

Patterson-Fortin J, D'Andrea AD (2020) Exploiting the Microhomology-Mediated End-Joining pathway in cancer therapy. *Cancer Res* **80**, 4593-4600.

Paull TT, Gellert M (1998) The 3' to 5' exonuclease activity of Mre11 facilitates repair of DNA double-strand breaks. *Mol Cell* **1**, 969-979.

Pellicioli A, Lucca C, Liberi G, Marini F, Lopes M, Plevani P, Romano A, Di Fiore PP, Foiani M (1999) Activation of Rad53 kinase in response to DNA damage and its effect in modulating phosphorylation of the lagging strand DNA polymerase. *EMBO J* **18**, 6561-6572.

Peterson SE, Stellwagen AE, Diede SJ, Singer MS, Haimberger ZW, Johnson CO, Tzoneva M, Gottschling DE (2001) The function of a stem-loop in telomerase RNA is linked to the DNA repair protein Ku. *Nat Genet* **27**, 64-67.

Pfander B, Diffley JF (2011) Dpb11 coordinates Mec1 kinase activation with cell cycle-regulated Rad9 recruitment. *EMBO J* **30**, 4897-4907.

Pizzul P, Casari E, Gnugnoli M, Rinaldi C, Corallo F, Longhese MP (2022) The DNA damage checkpoint: A tale from budding yeast. *Front Genet* **13**, 995163.

Poinsignon C, Moshous D, Callebaut I, de Chasseval R, Villey I, de Villartay JP (2004) The metallo-beta-lactamase/beta-CASP domain of Artemis constitutes the catalytic core for V(D)J recombination. *J Exp Med* **199**, 315-321.

Porter SE, Greenwell PW, Ritchie KB, Petes TD (1996) The DNA-binding protein Hdf1p (a putative Ku homologue) is required for maintaining normal telomere length in *Saccharomyces cerevisiae*. *Nucleic Acids Res* **24**, 582-585.

Postow L, Ghenoiu C, Woo EM, Krutchinsky AN, Chait BT, Funabiki H (2008) Ku80 removal from DNA through double strand break-induced ubiquitylation. *J Cell Biol* **182**, 467-479.

Ramsden DA, Gellert M (1998) Ku protein stimulates DNA end joining by mammalian DNA ligases: a direct role for Ku in repair of DNA double-strand breaks. *EMBO J* **17**, 609-614.

Rass E, Grabarz A, Plo I, Gautier J, Bertrand P, Lopez BS (2009) Role of Mre11 in chromosomal nonhomologous end joining in mammalian cells. *Nat Struct Mol Biol* **16**, 819-824.

Reginato G, Cannavo E, Cejka P (2017) Physiological protein blocks direct the Mre11-Rad50-Xrs2 and Sae2 nuclease complex to initiate DNA end resection. *Genes Dev* **31**, 2325-2330.

Reid DA, Keegan S, Leo-Macias A, Watanabe G, Strande NT, Chang HH, Oksuz BA, Fenyo D, Lieber MR, Ramsden DA, Rothenberg E (2015) Organization and dynamics of the nonhomologous end-joining machinery during DNA double-strand break repair. *Proc Natl Acad Sci USA* **112**, 2575-2584.

Ribes-Zamora A, Indiviglio SM, Mihalek I, Williams CL, Bertuch AA (2013) TRF2 interaction with Ku heterotetramerization interface gives insight into c-NHEJ prevention at human telomeres. *Cell Rep* **5**, 194-206.

Ribes-Zamora A, Mihalek I, Lichtarge O, Bertuch AA (2007) Distinct faces of the Ku heterodimer mediate DNA repair and telomeric functions. *Nat Struct Mol Biol* **14**, 301-307.

Rinaldi C, Pizzul P, Longhese MP, Bonetti D (2021) Sensing R-loop-associated DNA damage to safeguard genome stability. *Front Cell Dev Biol* **8**, 618157.

Ritchie KB, Petes TD (2000) The Mre11p/Rad50p/Xrs2p complex and the Tel1p function in a single pathway for telomere maintenance in yeast. *Genetics* **155**, 475-479.

Rivera-Calzada A, Spagnolo L, Pearl LH, Llorca O (2007) Structural model of full-length human Ku70-Ku80 heterodimer and its recognition of DNA and DNA-PKcs. *EMBO Rep* **8**, 56-62.

Roberts SA, Ramsden DA (2007) Loading of the nonhomologous end joining factor, Ku, on protein-occluded DNA ends. *J Biol Chem* **282**, 10605-10613.

Roos WP, Thomas AD, Kaina B (2016) DNA damage and the balance between survival and death in cancer biology. *Nat Rev Cancer* **16**, 20-33.

Rosinski JA, Atchley WR (1998) Molecular evolution of the Myb family of transcription factors: evidence for polyphyletic origin. *J Mol Evol* **46**, 74-83.

Rouse J, Jackson SP (2002) Interfaces between the detection, signaling, and repair of DNA damage. *Science* **297**, 547-51.

Roux B (1995) The calculation of the potential of mean force using computer simulations. *Comput Phys Commun* **91**, 275-282.

Saladino G, Estarellas C, Gervasio FL (2017) Recent progress in free energy methods. *Comprehensive Medicinal Chemistry III* **3.03.3.3**, 34-50.

San Filippo J, Sung P, Klein H (2008) Mechanism of eukaryotic homologous recombination. *Annu Rev Biochem* **77**, 229-257.

Sanchez Y, Bachant J, Wang H, Hu F, Liu D, Tetzlaff M, Elledge SJ (1999) Control of the DNA damage checkpoint by Chk1 and Rad53 protein kinases through distinct mechanisms. *Science* **286**, 1166-1171.

Sartori AA, Lukas C, Coates J, Mistrik M, Fu S, Bartek J, Baer R, Lukas J, Jackson SP (2007) Human CtIP promotes DNA end resection. *Nature* **450**, 509-514.

Sastry GM, Adzhigirey M, Day T, Annabhimoju R, Sherman WJ (2013) Protein and ligand preparation: parameters, protocols, and influence on virtual screening enrichments. *Comput Aided Mol Des* **27**, 221-234.

Savitsky K, Sfez S, Tagle DA, Ziv Y, Sartiel A, Collins FS, Shiloh Y, Rotman G (1995) The complete sequence of the coding region of the ATM gene reveals similarity to cell cycle regulators in different species. *Hum Mol Genet* **4**, 2025-2032.

Schiller JT, Lowy DR (2014) Virus infection and human cancer: an overview. *Recent Results Cancer Res* **193**, 1-10.

Seifert FU, Lammens K, Stoehr G, Kessler B, Hopfner KP (2016) Structural mechanism of ATP-dependent DNA binding and DNA end bridging by eukaryotic Rad50. *EMBO J* **35**, 759-772.

Sharif H, Li Y, Dong Y, Dong L, Wang WL, Mao Y, Wu H (2017) Cryo-EM structure of the DNA-PK holoenzyme. *Proc Natl Acad Sci USA* **114**, 7367-7372.

Shi T, Bunker RD, Mattarocci S, Ribeyre C, Faty M, Gut H, Scrima A, Rass U, Rubin SM, Shore D, Thomä NH (2013) Rif1 and Rif2 shape telomere function and architecture through multivalent Rap1 interactions. *Cell* **153**, 340-353.

Shibata A, Moiani D, Arvai AS, Perry J, Harding SM, Genois MM, Maity R, van Rossum-Fikkert S, Kertokalio A, Romoli F, Ismail A, Ismalaj E, Petricci E, Neale MJ, Bristow RG, Masson JY, Wyman C, Jeggo PA, Tainer JA (2014) DNA double-strand break repair pathway choice is directed by distinct MRE11 nuclease activities. *Mol Cell* **53**, 7-18.

Shim EY, Chung WH, Nicolette ML, Zhang Y, Davis M, Zhu Z, Paull TT, Ira G, Lee SE (2010) *Saccharomyces cerevisiae* Mre11/Rad50/Xrs2 and Ku proteins regulate association of Exo1 and Dna2 with DNA breaks. *EMBO J* **29**, 3370-3380.

Shimada K, Pasero P, Gasser SM (2002) ORC and the intra-S-phase checkpoint: a threshold regulates Rad53p activation in S phase. *Genes Dev*. **16**, 3236-3252.

Shore D, Nasmyth K (1987) Purification and cloning of a DNA binding protein from yeast that binds to both silencer and activator elements. *Cell* **51**, 721-732.

Shroff R, Arbel-Eden A, Pilch D, Ira G, Bonner WM, Petrini JH, Haber JE, Lichten M (2004) Distribution and dynamics of chromatin modification induced by a defined DNA double-strand break. *Curr Biol* **14**, 1703-1711.

Siebenmorgen T, Zacharias M (2019) Evaluation of predicted protein-protein complexes by binding free energy simulations. *J Chem Theory Comput* **15**, 2071-2086.

Singer MS, Gottschling DE (1994) *TLC1*: template RNA component of the *Saccharomyces cerevisiae* telomerase. *Science* **266**, 404-409.

Singer MS, Kahana A, Wolf AJ, Meisinger LL, Peterson SE, Goggin C, Mahowald M, Gottschling DE (1998) Identification of high-copy disruptors of telomeric silencing in *Saccharomyces cerevisiae*. *Genetics* **150**, 613-632.

Spagnolo L, Rivera-Calzada A, Pearl LH, Llorca O (2006) Three-dimensional structure of the human DNA-PKcs/Ku70/Ku80 complex assembled on DNA and its implications for DNA DSB repair. *Mol Cell* **22**, 511-519.

Srinivas US, Tan BWQ, Vellayappan BA, Jeyasekharan AD (2019) ROS and the DNA damage response in cancer. *Redox Biol*. **25**, 101084.

Stellwagen AE, Haimberger ZW, Veatch JR, Gottschling DE (2003) Ku interacts with telomerase RNA to promote telomere addition at native and broken chromosome ends. *Genes Dev* **17**, 2384-2395.

Stinson BM, Loparo JJ (2021) Repair of DNA double-strand breaks by the non-homologous end joining pathway. *Annu Rev Biochem* **90**, 137-164.

Sturzenegger A, Burdova K, Kanagaraj R, Levikova M, Pinto C, Cejka P, Janscak P (2014) DNA2 cooperates with the WRN and BLM RecQ helicases to mediate long-range DNA end resection in human cells. *J Biol Chem* **289**, 27314-27326.

Sung H, Ferlay J, Siegel RL, Laversanne M, Soerjomataram I, Jemal A, Bray F (2021) Global cancer statistics 2020: GLOBOCAN estimates of incidence and mortality worldwide for 36 cancers in 185 countries. *CA Cancer J Clin* **71**, 209-249.

Sussel L, Shore D (1991) Separation of transcriptional activation and silencing functions of the RAP1-encoded repressor/activator protein 1: isolation of viable mutants affecting both silencing and telomere length. *Proc Nat Acad Sci USA* **88**, 7749-7753.

Syed A, Tainer JA (2018) The MRE11-RAD50-NBS1 complex conducts the orchestration of damage signaling and outcomes to stress in DNA replication and repair. *Annu Rev Biochem* **87**, 263-294.

Symington LS, Gautier J (2011) Double-strand break end resection and repair pathway choice. *Annu Rev Genet* **45**, 247-271.

Taylor AMR, Rothblum-Oviatt C, Ellis NA, Hickson ID, Meyer S, Crawford TO, Smogorzewska A, Pietrucha B, Weemaes C, Stewart GS (2019) Chromosome instability syndromes. *Nat Rev Dis Primers* **5**, 64.

Taylor HO, O'Reilly M, Leslie AG, Rhodes D (2000) How the multifunctional yeast Rap1p discriminates between DNA target sites: a crystallographic analysis. *J Mol Biol* **303**, 693-707.

Tercero JA, Longhese MP, Diffley JF (2003) A central role for DNA replication forks in checkpoint activation and response. *Mol Cell* **11**, 1323-1336.

Toh GW, Lowndes NF (2003) Role of the *Saccharomyces cerevisiae* Rad9 protein in sensing and responding to DNA damage. *Biochem Soc Trans* **31**, 242-246.

Toh GW, O'Shaughnessy AM, Jimeno S, Dobbie IM, Grenon M, Maffini S, O'Rorke A, Lowndes NF (2006) Histone H2A phosphorylation and H3 methylation are required for a novel Rad9 DSB repair function following checkpoint activation. *DNA Repair* **5**, 693-703.

Torchala M, Moal IH, Chaleil RA, Fernandez-Recio J, Bates PA (2013) SwarmDock: a server for flexible protein-protein docking. *Bioinformatics* **29**, 807-809.

Tornow J, Zeng X, Gao W, Santangelo GM (1993) GCR1, a transcriptional activator in *Saccharomyces cerevisiae*, complexes with RAP1 and can function without its DNA binding domain. *EMBO J* **12**, 2431-2437.

Trujillo KM, Yuan SS, Lee EY, Sung P (1998) Nuclease activities in a complex of human recombination and DNA repair factors Rad50, Mre11, and p95. *J Biol Chem* **273**, 21447-21450.

Tseng HM, Tomkinson AE (2002) A physical and functional interaction between yeast Pol4 and Dnl4-Lif1 links DNA synthesis and ligation in nonhomologous end joining. *J Biol Chem* **277**, 45630-45637.

Tsukuda T, Fleming AB, Nickoloff JA, Osley MA (2005) Chromatin remodelling at a DNA double-strand break site in *Saccharomyces cerevisiae*. *Nature* **438**, 379-383.

Usui T, Petrini JH, Morales M (2006) Rad50S alleles of the Mre11 complex: questions answered and questions raised. *Exp Cell Res* **312**, 2694-2699.

Valencia M, Bentele M, Vaze MB, Herrmann G, Kraus E, Lee SE, Schär P, Haber JE (2001) NEJ1 controls non-homologous end joining in *Saccharomyces cerevisiae*. *Nature* **414**, 666-669.

van Leeuwen F, Gafken PR, Gottschling DE (2002) Dot1p modulates silencing in yeast by methylation of the nucleosome core. *Cell* **109**, 745-756.

van Zundert GCP, Rodrigues JPGLM, Trellet M, Schmitz C, Kastritis PL, Karaca E, Melquiond ASJ, van Dijk M, de Vries SJ, Bonvin AMJJ (2016) The HADDOCK2.2 web server: user-friendly integrative modeling of biomolecular complexes. *J Mol Biol* **428**, 720-725.

Vermaas JV, Trebesch N, Mayne CG, Thangapandian S, Shekhar M, Mahinthichaichan P, Baylon JL, Jiang T, Wang Y, Muller MP, Shinn E, Zhao Z, Wen PC, Tajkhorshid E (2016) Microscopic characterization of membrane transporter function by in silico modeling and simulation. *Methods Enzymol* **578**, 373-428.

Villa M, Cassani C, Gobbini E, Bonetti D, Longhese MP (2016) Coupling end resection with the checkpoint response at DNA double-strand breaks. *Cell Mol Life Sci* **73**, 3655-3663.

Vodenicharov MD, Laterreur N, Wellinger RJ (2010) Telomere capping in non-dividing yeast cells requires Yku and Rap1. *EMBO J* **29**, 3007-3019.

Volk T, Pannicke U, Reisli I, Bulashevska A, Ritter J, Björkman A, Schäffer AA, Fliegauf M, Sayar EH, Salzer U, Fisch P, Pfeifer D, Di Virgilio M, Cao H, Yang F, Zimmermann K, Keles S, Caliskaner Z, Güner SÜ, Schindler D, Hammarström L, Rizzi M, Hummel M, Pan-Hammarström Q, Schwarz K, Grimbacher B (2015) DCLRE1C (ARTEMIS) mutations causing phenotypes ranging from atypical severe combined immunodeficiency to mere antibody deficiency. *Hum Mol Genet* **24**, 7361-7372.

Walker JR, Corpina RA, Goldberg J (2001) Structure of the Ku heterodimer bound to DNA and its implications for double-strand break repair. *Nature* **412**, 607-614.

Wang H, Rosidi B, Perrault R, Wang M, Zhang L, Windhofer F, Iliakis G (2005) DNA ligase III as a candidate component of backup pathways of nonhomologous end joining. *Cancer Res* **65**, 4020-4030.

Wang JL, Duboc C, Wu Q, Ochi T, Liang S, Tsutakawa SE, Lees-Miller SP, Nadal M, Tainer JA, Blundell TL, Strick TR (2018) Dissection of DNA double-strand-break repair using novel single-molecule forceps. *Nat Struct Mol Biol* **25**, 482-487.

Wang W, Daley JM, Kwon Y, Krasner DS, Sung P (2017) Plasticity of the Mre11-Rad50-Xrs2-Sae2 nuclease ensemble in the processing of DNA-bound obstacles. *Genes Dev* **31**, 2331-2336.

Weiner SJ, Kollman PA, Nguyen DT, Case DA (1986) An all atom force field for simulations of proteins and nucleic acids. *J Comput Chem* **7**, 230-252.

Wellinger RJ, Zakian VA (2012) Everything you ever wanted to know about *Saccharomyces cerevisiae* telomeres: beginning to end. *Genetics*. **191**, 1073-1105.

Weterings E, Verkaik NS, Brüggenwirth HT, Hoeijmakers JH, van Gent DC (2003) The role of DNA dependent protein kinase in synapsis of DNA ends. *Nucleic Acids Res* **31**, 7238-7246.

Williams GJ, Hammel M, Radhakrishnan SK, Ramsden D, Lees-Miller SP, Tainer JA (2014) Structural insights into NHEJ: Building up an integrated picture of the dynamic DSB repair super complex, one component and interaction at a time. *DNA Repair* **17**, 110-120.

Williams GJ, Williams RS, Williams JS, Moncalian G, Arvai AS, Limbo O, Guenther G, SilDas S, Hammel M, Russell P, Tainer JA (2011) ABC ATPase signature helices in Rad50 link nucleotide state to Mre11 interface for DNA repair. *Nat Struct Mol Biol* **18**, 423-431.

Williams JM, Ouenzar F, Lemon LD, Chartrand P, Bertuch AA (2014) The principal role of Ku in telomere length maintenance is promotion of Est1 association with telomeres. *Genetics* **197**, 1123-1136.

Wotton D, Shore D (1997) A novel Rap1p-interacting factor, Rif2p, cooperates with Rif1p to regulate telomere length in *Saccharomyces cerevisiae*. *Genes Dev* **11**, 748-760.

Wu D, Topper LM, Wilson TE (2008) Recruitment and dissociation of nonhomologous end joining proteins at a DNA double-strand break in *Saccharomyces cerevisiae*. *Genetics* **178**, 1237-1249.

Wu P, Takai H, de Lange T (2012) Telomeric 3′ overhangs derive from resection by Exo1 and Apollo and fill-in by POT1b-associated CST. *Cell* **150**, 39-52.

Wu X, Lieber MR (1996) Protein-protein and protein-DNA interaction regions within the DNA end-binding protein Ku70-Ku80. *Mol Cell Biol* **16**, 5186-5193.

Wysocki R, Javaheri A, Allard S, Sha F, Coté J, Kron SJ (2005) Role of Dot1-dependent histone H3 methylation in G1 and S phase DNA damage checkpoint functions of Rad9. *Mol Cell Biol* **25**, 8430-8443.

Xie A, Kwok A, Scully R (2009) Role of mammalian Mre11 in classical and alternative nonhomologous end joining. *Nat Struct Mol Biol* **16**, 814-818.

Yan Y, Tao H, He J, Huang SY (2020) The HDOCK server for integrated protein-protein docking. *Nat Protoc* **15**, 1829-1852.

Yaneva M, Kowalewski T, Lieber MR (1997) Interaction of DNA-dependent protein kinase with DNA and with Ku: biochemical and atomic-force microscopy studies. *EMBO J* **16**, 5098-50112.

You Z, Chahwan C, Bailis J, Hunter T, Russell P (2005) ATM activation and its recruitment to damaged DNA require binding to the C terminus of Nbs1. *Mol Cell Biol* **25**, 5363-5379.

Yu X, Gabriel A (2003) Ku-dependent and Ku-independent end-joining pathways lead to chromosomal rearrangements during double-strand break repair in *Saccharomyces cerevisiae*. *Genetics* **163**, 843-856.

Zahid S, Seif El Dahan M, Iehl F, Fernandez-Varela P, Le Du MH, Ropars V, Charbonnier JB (2021) The multifaceted roles of Ku70/80. *Int J Mol Sci* **22**, 4134.

Zhao B, Watanabe G, Morten MJ, Reid D, Rothenberg E, Lieber MR (2019) The essential elements for the noncovalent association of two DNA ends during NHEJ synapsis. *Nat Commun* **10**, 3588.

Zhao Y, McIntosh KB, Rudra D, Schawalder S, Shore D, Warner JR (2006) Fine-structure analysis of ribosomal protein gene transcription. *Mol Cell Biol* **26**, 4853-4862.

Zheng L, Alhossary AA, Kwoh CK, Mu Y (2019) Molecular dynamics and simulation. *Encyclopedia of Bioinformatics and Computational Biology* **2**, 550-566.

Zhu Z, Chung WH, Shim EY, Lee SE, Ira G (2008) Sgs1 helicase and two nucleases Dna2 and Exo1 resect DNA double-strand break ends. *Cell* **134**, 981-994.

Zierhut C, Diffley JF (2008) Break dosage, cell cycle stage and DNA replication influence DNA double strand break response. *EMBO J* **27**, 1875-1885.

Zou L, Elledge SJ (2003) Sensing DNA damage through ATRIP recognition of RPA-ssDNA complexes. *Science* **300**, 1542-1548.

APPENDIX

Cells

2022 Oct 14; 11(20) 3224

doi: 10.3390/cells11203224

To fix or not to fix: maintenance of chromosome ends versus repair of DNA double-strand breaks

Erika Casari[1], Marco Gnugnoli[1], **Carlo Rinaldi**[1],

Paolo Pizzul[1], Chiara Vittoria Colombo[1], Diego Bonetti[1],

Maria Pia Longhese[1*]

[*] Corresponding Author

[1] Dipartimento di Biotecnologie e Bioscienze, Università degli Studi di Milano-Bicocca, Milano, 20126, Italy

Frontiers in Genetics

2022 Sep 15; 8:618157

doi: 10.3389//fgene.2022.995163

The DNA damage checkpoint: a tale from budding yeast

Paolo Pizzul[1], Erika Casari[1], Marco Gnugnoli[1],

Carlo Rinaldi[1], Flavio Corallo[1], Maria Pia Longhese[1*]

[*] Corresponding Author

[1] Dipartimento di Biotecnologie e Bioscienze, Università degli Studi di Milano-Bicocca, Milano, 20126, Italy

Frontiers in
Cell and Developmental Biology

2021 Jan 11; 8:618157

doi: 10.3389/fcell.2020.618157

Sensing R-loop-associated DNA damage to safeguard genome stability

Carlo Rinaldi[1], Paolo Pizzul[1], Maria Pia Longhese[1],

Diego Bonetti[1*]

[*] Corresponding Author

[1] Dipartimento di Biotecnologie e Bioscienze, Università degli Studi di Milano-Bicocca, Milano, 20126, Italy

CONTRIBUTIONS TO THE STUDIES

- ***The Ku complex promotes DNA end-bridging and this function is antagonized by Tel1/ATM kinase***

  MPL conceived the study, and supervised and coordinated the work. CR and MPL designed the experiments. CR performed the screen and identified the five *ku70* alleles including *ku70-C85Y*; he also perfomed drop tests shown in Figs. 20 and 24, the telomere length analysis shown in Fig. 20, DSB resection and relative analysis shown in Fig. 21, the ChIP analysis and western blot shown in Figs. 21, 23, 24, end-tethering experiments shown in Figs. 22 and 24, and the coimmunoprecipitation shown in Fig. 23. PP performed drop tests shown in Figs. 21 and 22; he contributed to perform telomere length analysis shown in Fig. 20 and DSB resection shown in Fig. 21. EC contributed to perform coimmunoprecipitation shown in Fig. 23. RT performed computational analyses and interpretation, she also performed the construction of structural models shown in Figs. 20 and 23. CR and MPL analysed the data, wrote the manuscript, and realized the working model shown in Fig 25. CR, PP, EC, and MPL revised the text.

- ***DNA binding modes influence Rap1 activity in the regulation of telomere length and MRX functions at DNA ends***

  MPL conceived the study, and supervised and coordinated the work. DB and MPL designed the experiments. DB performed the screen by identifying *rif2* and *rap1* alleles; he also performed telomere length analysis shown in Figs. 9, 10, 15, 18, the coimmunoprecipitation shown in Fig. 10, the ChIP analysis and western blot shown in Figs. 12, 13, 14, 15, 18, end-tethering experiments shown in Figs. 12 and 14, and the colony color assay shown in Fig. 18. CR performed drop tests shown in Figs. 9 and 10. CR contributed to identify the *rif2* alleles; he also contributed to perform telomere length analysis shown in Figs. 9 and 10, the ChIP analysis and western blot shown in Figs. 12 and 13, and the coimmunoprecipitation shown in Fig. 10. MN performed drop tests shown in Figs. 14 and 15; he contributed to performed the screen by identifying *rap1* alleles, the ChIP analysis and western blot shown in Figs. 14 and 15, and telomere length analysis shown in Fig. 15. PP performed drop tests shown in Fig. 18; he contributed to performed end-tethering experiments shown in Figs. 12 and 14, the ChIP analysis shown in Fig. 18, telomere length analysis shown in Fig. 18, the colony color assay shown in Fig. 18. DB, CR, and PP performed EMSA shown in Fig. 16. JV, RT, and GZ performed computational analyses and interpretation shown in Figs. 10, 11, 16 and 17. RT realized structurual models shown in Figs. 10 and 16. DB and MPL analysed the data, wrote the manuscript and realized the working model shown in Fig. 19. DB, CR, PP, and MPL revised the text.

- ***The DNA damage checkpoint: a tale from budding yeast***

  MPL conceived the idea. PP, EC, and MPL wrote the manuscript. MG, CR, and FC revised and edited the manuscript.

- ***To fix or not to fix: maintenance of chromosome ends versus repair of DNA double-strand breaks***

  MPL conceived the idea. MPL, EC, and MG wrote the original draft. CR, PP, CVC, and DB revised and edited the manuscript.

- ***Sensing R-loop-associated DNA damage to safeguard genome stability***

  DB and MPL conceived the idea. CR and DB wrote the manuscript. DB, CR, and MPL revised and edited the manuscript. CR and PP created the figures. All authors contributed to the article and approved the submitted version.